# Nonlinear Uncertainty Propagation In Space Trajectories

Sunil K. Malhotra

Thesis in Partial Fulfillment of the
Requirements for the Degree of
Mechanical Engineer

May 15, 1992

*California Institute of Technology , Pasadena , California 91125*

**Acknowledgement**

The author extends sincere thanks to his advisor, Dr. Thomas K. Caughey, who provided support and guidance throughout the following work.

## Abstract

This thesis addresses the problem of nonlinear uncertainty propagation in space trajectories. This problem can be specifically stated as follows: Given the initial orbital state of a spacecraft trajectory as random variables, what is the orbital state at some later time?

This problem is currently encountered by mission designers at institutions such as the Jet Propulsion Laboratory. Before an expensive space probe is irretrievably launched, extensive trajectory analyses are conducted to determine the amount of fuel needed to correct for trajectory errors. This involves propagation of uncertainties in the trajectories.

The current method for uncertainty propagation involves linearizing about the nominal trajectory to obtain a state transition matrix used to map the covariance matrix to a later orbital state. This method neglects nonlinear effects.

Two new algorithms were developed to account for nonlinear effects in the propagation of uncertainties in space trajectories. The first utilized simplifying assumptions to obtain analytic expressions for the probabilistic quantities describing the final orbital state. This algorithm provided good trend information but lacked precision. The second algorithm utilized Gaussian quadrature techniques to numerically compute the desired quantities. While requiring significant computational effort, this algorithm provided high precision.

Example trajectories were analyzed to compare the results from the new algorithms to those from the current method. Nonlinear effects were shown to influence both the mean and the variance results.

# Table of Contents

CHAPTER I - INTRODUCTION

A. Problem Origin in Current Mission Analysis 1
B. Uncertainty Models 2
C. Meaning of Probabilistic Quantities 3

CHAPTER II - SPACE TRAJECTORY MATHEMATICS

A. Classical Conic Trajectory Calculations 6
B. Variational Planetary Equations For Numerical Integration 12

CHAPTER III - ANALYTIC SOLUTIONS

A. Intermediate Solutions From Conic Algorithm 14
B. Further Solutions For Conic Variables 35

CHAPTER IV - LINEAR APPROXIMATION SOLUTIONS

A. Historical Background of the Linear Approximation Method 38
B. Detailed Exposition of the Linear Approximation Method 38
C. Impact of Linearization on Accuracy 40

CHAPTER V - COMPLETE NUMERICAL SOLUTIONS

A. General Explanation of Gaussian Quadrature Methods 43
B. Gauss-Legendre Quadrature For Constant Density Functions 44
C. Gauss-Hermitian Quadrature For Gaussian Density Functions 44
D. Dependent Gaussian Distributed Variables 45
E. Comments on the Application of Romberg Integration Methods 46

CHAPTER VI - COMPUTER DEMONSTRATIONS OF ALGORITHMS

A. Demonstration of the Analytic Solution Algorithm 48
B. Demonstration of the Romberg Integration Algorithm 48
C. Demonstration of the Gauss-Legendre Quadrature Algorithm 48
D. Demonstration of the Gauss-Hermitian Quadrature Algorithm 49
E. Demonstration of the Linear Approximation Algorithm 49
F. Comparison of the Analytic Algorithm With the Quadrature Algorithm 49
G. Comparison of the Gaussian Distribution With the Constant Distribution 50
H. Comparison of the Linear Approximation Algorithm With the Quadrature Algorithm 50
I. Example Analysis of a Hyperbolic Trajectory 50
J. Comparison Between Elliptic and Hyperbolic Trajectory Analyses 51
K. Example Analysis With Dependent Variables 51

CHAPTER VII - CONCLUSIONS 53

REFERENCES 54

APPENDIX A - GRAPHS A - 1

# I. Introduction

This first chapter serves to introduce the reader to the problem addressed in this thesis. Simply stated, this problem is the determination of a spacecraft's orbital state at a specific time given probabilistic initial conditions. The necessity of this determination derives from mission design analyses performed currently at institutions such as the Jet Propulsion Laboratory. The sources of uncertainty are discussed along with models for describing these uncertainties. The probabilistic quantities of mean and variance are discussed both qualitatively and quantitatively to provide a foundation for understanding the developments contained in this thesis.

The following mathematical conventions will be used throughout this thesis.

$\underline{r}$ = vector

$r_1$ = first element of vector r

r = scalar

## A. Problem Origin in Current Mission Analysis

This thesis addresses the problem of uncertainty propagation in space trajectories. This problem can be specifically stated as follows: Given the initial orbital state of a spacecraft trajectory as random variables, what is the orbital state at some later time?

This question is currently asked by mission designers at institutions such as the Jet Propulsion Laboratory. Before an expensive space probe is irretrievably launched, extensive trajectory analyses are conducted [1]. The results of these analyses are a nominal trajectory for launch targetting purposes as well as numerous maneuvers along the trajectory to correct for launch errors and uncertainties in navigation.

The sources of trajectory errors from launch are numerous. The launch vehicle engines may give different thrusts than expected. The guidance system on the launch vehicle may contain errors itself from gyroscope drift and other sources. Finally, unforseen perturbations may occur during the separation of the spacecraft from the launch vehicle.

Uncertainty is also introduced from the navigation algorithms themselves. The orbital state of the spacecraft is determined from antennae sightings from Earth. Numerical methods are used to minimize the differences between each sighting; however, the existence of the differences is evidence of the uncertainty in the sightings.

## B. Uncertainty Models

The uncertainty from sources described above must be modelled with some analytic probability distribution function. This will enable calculations to be made according to standard probability theory. A probability distribution function provides all necessary information about the nature of the random variable.

The difficulty in modelling uncertainty as an analytical function is that actual uncertainties are difficult to estimate. The processes leading to uncertainty are often nonlinear and, therefore, are difficult to predict. Typically, multiple cases are simulated to determine the extent of variation in the process. The conditions of the simulation may not exactly match actual conditions.

Even if the possible extent of variation is understood, it is difficult to assign a distribution function to the data. Real systems rarely exhibit behavior which is exactly modelled by analytical functions. The engineer must usually choose a function closest to reality and then let conservative allowances account for any differences.

With respect to space trajectories, engineers typically use Gaussian distributions to model uncertainties. One reason for this is that the Gaussian distribution decreases away from the mean. This satisfies the engineer's intuition. However, the main reason it is used is because the ease with which it lends itself in linear theory. As will be further explained, linear assumptions result in simple calculations for Gaussian distributions. New numerical algorithms presented in this thesis are valid for any distribution choice.

A disadvantage of the Gaussian distribution is the unrealistic finite probability existing at great distances from the mean. Consider the mathematical representation of the Gaussian distribution shown below.

$$p(x) = \frac{1}{\sqrt{2\pi}\,\sigma_x} \exp\left(-\frac{(x-\mu_x)^2}{2\sigma_x^2}\right), \quad -\infty < x < +\infty \tag{1}$$

$p(x)$ = probability density function of x

$\sigma_x$ = variance of x

$\mu_x$ = mean of x

Clearly, no matter how large the variable x becomes, the distribution function still retains a finite value. This does not accurately portray the real system which has bounds in the range of errors.

As mentioned above, new numerical algorithms presented in this thesis accept any distributions. Therefore, a distribution used may have finite bounds. One such example used extensively in this thesis is the uniform distribution.

$$p(x) = \begin{cases} \frac{1}{2\kappa}, & -\kappa < x < +\kappa \\ 0, & |x| > \kappa \end{cases} \tag{2}$$

This distribution function maintains a constant probability density value up to a bound, at which point it returns a value of zero.

Other distribution functions can be found in any standard probability reference [2]. They include Beta, Gamma, and Cauchy functions.

### C. Meaning of Probabilistic Quantities

Engineers interpret the random variables through quantities known as the mean and variance. An understanding of these is especially important since the results of the numerical algorithms presented in this thesis are given in these quantities. In fact, when the full nonlinearities of the problem are considered, as will be explained later, there is no analytic function to represent the distribution and engineers must correctly interpret the mean and variance for proper analysis.

The mean is more commonly known as the average. It represents the expected output of the system. Engineers will usually designate the mean trajectory as the nominal trajectory and plan the mission according to it. Clearly it is the most important result of probability theory. As will be explained later, the mean can be significantly affected by nonlinear considerations, which is an important point of this thesis. Mathematically, the mean is calculated according to the equation below.

$$\mu_y = \int_{-\infty}^{+\infty} f(x)\, p(x)\, dx \qquad (3)$$

$$y = f(x)$$

This equation will be central to the numerical algorithms presented later.

The engineers would also like to know how closely the distribution surrounds the mean. Consider Figure 1-1 below. Notice how in Case 1 the distribution is much more spread out than in Case 2.

Figure 1-1

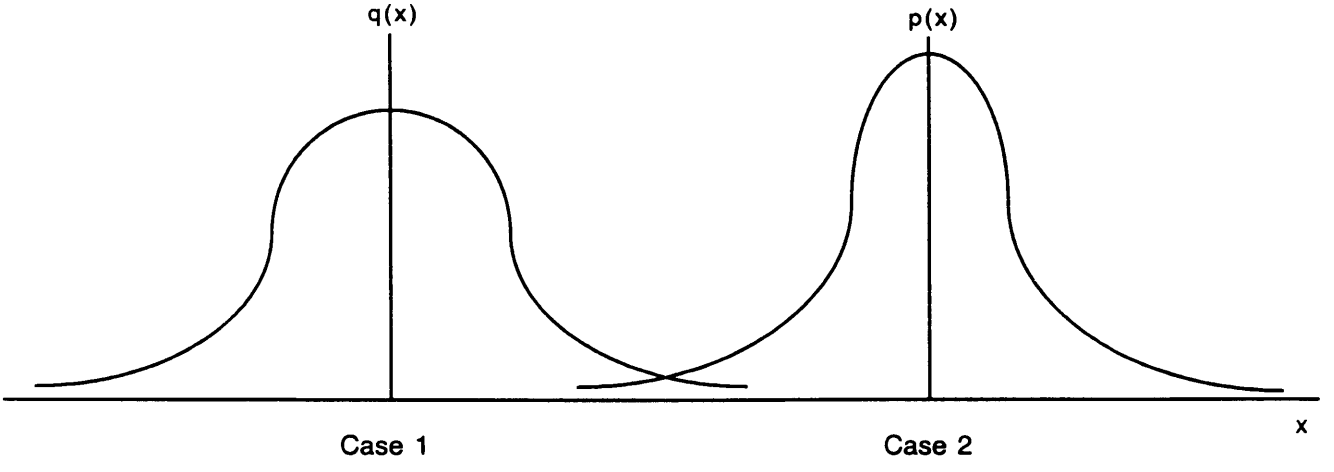


If they represented the distribution of trajectories, the spacecraft would have to carry more fuel in Case 1 to correct for deviations from the nominal trajectory. Clearly the engineers need to have some measure of this variation from the mean.

The probabilistic quantity which tells engineers how the distribution varies from the mean is called the variance. It is given by the following equation.

$$\sigma_y^2 = \int_{-\infty}^{+\infty} (\, f(x) - \mu_y \,)^2\, p(x)\, dx \qquad (4)$$

This equation will also be central to the numerical algorithms presented later.

In conclusion, engineers utilize both the mean and the variance in their analysis of a trajectory. The mean is the nominal trajectory around which the mission will be designed. The variance tells how spread out the distribution is about the mean so that the range of variation can be understood.

# II. Space Trajectory Mathematics

The solution of the problem addressed in this thesis is the calculation of the integrals for mean and variance presented in the previous chapter. This requires the mathematical relationship between the orbital state and the initial conditions and time of flight. The purpose of this chapter is to describe this relationship in detail so that the specifics can be drawn on later in the presentation of the results of this thesis. Both the classical formulation and the numerical integration method using Gauss' variational equations will be described.

## A. Classical Conic Trajectory Calculations

The equations for classical conic trajectories represent the only existing analytical relationships between orbital elements at different times. This is possible because of several assumptions that reduce the general trajectory problem down to what is known as "The Two-Body Problem". As the name suggests, we only consider two objects, specifically the spacecraft and the planet around which it orbits. The spacecraft mass is considered negligible with respect to the planet, which is a good assumption. The planet is assumed perfectly symmetric. Finally, there are no other forces acting on the system other than the gravitational force between the planet and the spacecraft.

The results of this simplified model is an implicit analytic relationship between an orbital state and the initial state after some flight time. The step-by-step calculation procedure follows in this section. Note that all of the relationships that can be derived from this model are not presented. The reader can refer to a standard astrodynamics text for these details [3].

In the algorithms used in this thesis, the initial orbital state is assumed to be known in a planet-based fixed Cartesian coordinate system. In this system, the orbital state consists of a position vector and a velocity vector. We write the position and velocity vectors as follows.

$$\underline{r} = r_1\,\underline{e}_1 + r_2\,\underline{e}_2 + r_3\,\underline{e}_3 \tag{5}$$

$$\underline{v} = v_1\,\underline{e}_1 + v_2\,\underline{e}_2 + v_3\,\underline{e}_3 \tag{6}$$

The first quantities calculated are the angular momentum vector $\underline{h}$, the nodal vector $\underline{n}$, and the eccentricity vector $\underline{e}$. The equations for these fundamental vectors are below.

$$\underline{h} = \underline{r} \times \underline{v} \tag{7}$$

$$\underline{n} = \underline{e}_3 \times \underline{h} \tag{8}$$

$$\underline{e} = \frac{1}{\eta}\left( \left( v^2 - \frac{\eta}{r} \right) \underline{r} - (\underline{r} \cdot \underline{v})\, \underline{v} \right) \tag{9}$$

$\eta$ = planet gravitational parameter

$$v = | \underline{v} | \tag{10}$$

$$r = | \underline{r} | \tag{11}$$

These vectors are illustrated in Figure 2-1 below.

Figure 2-1

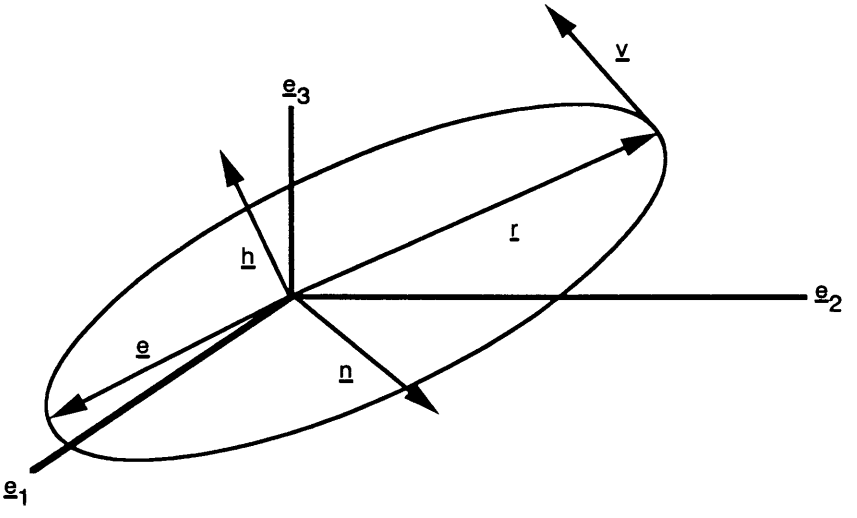


The magnitudes of these vectors are also important and will be used in several equations below.

$$e = | \underline{e} | \tag{12}$$

$$n = | \underline{n} | \tag{13}$$

$$h = | \underline{h} | \tag{14}$$

The next group of quantities to be calculated are known as the classical orbital elements. They represent various geometric characteristics of the spacecraft trajectory. Both the names and the mathematical definitions of these elements are now presented.

p = semi-latus rectum

$$p = \frac{h^2}{\eta} \tag{15}$$

i = inclination

$$i = \cos^{-1}\left(\frac{h_3}{h}\right) \tag{16}$$

$\Omega$ = longitude of the ascending node

$$\Omega = \cos^{-1}\left(\frac{n_3}{n}\right) \tag{17}$$

$\omega$ = argument of the periapsis

$$\omega = \cos^{-1}\left(\frac{\mathbf{n}\cdot\mathbf{e}}{ne}\right) \tag{18}$$

$\nu$ = true anomaly

$$\nu = \cos^{-1}\left(\frac{\mathbf{e}\cdot\mathbf{r}}{er}\right) \tag{19}$$

a = semi-major axis

$$a = \frac{p}{1-e^2} \tag{20}$$

Time-of-flight must now be brought into the algorithm. This is done through geometric conversion of the flight time into area swept out in the conic section of the trajectory. Certain new relationships must be developed to enable this. Consider the elliptical trajectory in Figure 2-2 below. Note the new variable E called the eccentric anomaly. This is calculated according to the following equation.

$$E = \cos^{-1}\left(\frac{ae + r\cos\nu}{a}\right) \tag{21}$$

Given an initial eccentric anomaly, the time of flight to the final desired position, and the number of complete orbits passed during the flight, an implicit equation for the final position eccentric anomaly can be developed. This equation appears below.

$$t - t_o = \sqrt{\frac{a^3}{\eta}}\left[\,2k\pi + (e - e\sin E) - (E_o - e\sin E_o)\,\right] \tag{22}$$

$t$ = time at the final spacecraft position

$t_o$ = time at the initial spacecraft position

$k$ = number of complete orbits passed during flight

$E$ = eccentric anomaly of final spacecraft position

$E_o$ = eccentric anomaly of initial spacecraft position

The algorithm must solve this equation for the eccentric anomaly of the final spacecraft position. Since this variable is implicitly defined, numerical methods must be used to find the solution. This lack of explicit solutions for the eccentric anomaly will be an obstacle to fully analytic stochastic solutions, as explained in the next chapter.

Figure 2-2

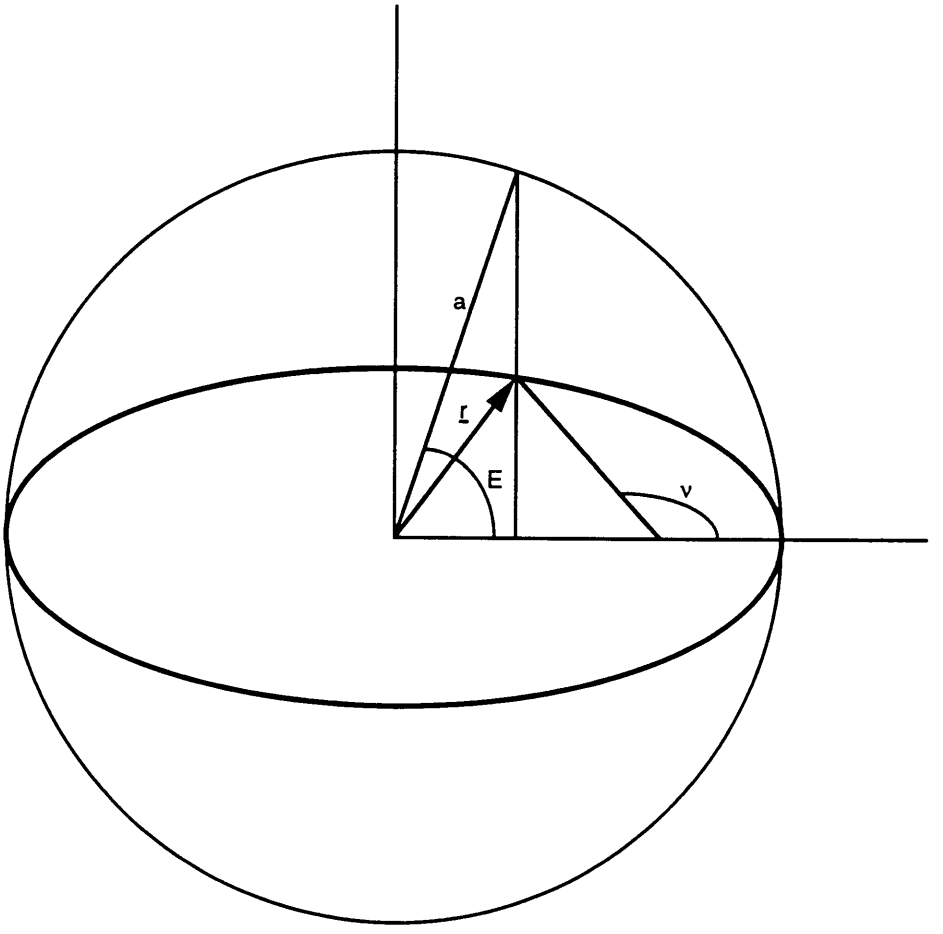

An analogous equation for hyperbolic trajectories also exists. Instead of the eccentric anomaly used for elliptical trajectories, the hyperbolic eccentric anomaly is used. It also has geometric significance. Its mathematical definition is as follows.

$$F = \ln [\, y + \sqrt{y^2-1}\, ] \tag{23}$$

$$y = \frac{e + \cos \nu}{1 + e \cos \nu} \tag{24}$$

Similar to the above case, if given the hyperbolic eccentric anomaly of the initial spacecraft position and the time of flight, the hyperbolic eccentric anomaly of the final spacecraft position can be calculated. This is done with the following equation.

$$t - t_o = \sqrt{\frac{(-a^3)}{\eta}} [\, (\, e \sinh F - F\, ) - (\, e \sinh F_o - F_o\, )\, ] \tag{25}$$

$F$ = hyperbolic eccentric anomaly of initial spacecraft position

$F_o$ = hyperbolic eccentric anomaly of final spacecraft position

This implicit equation is solved with numerical methods.

At this point, the algorithm has the value of the eccentric anomaly for the final spacecraft position. The same equations that enabled the calculation of this eccentric anomaly from the true anomaly can be reversed now to calculate the true anomaly of the final spacecraft position. Note that the eccentricity of the orbit remains constant.

The algorithm's objective is to compute the Cartesian-based position and velocity vectors. The next step in doing this is to compute the position and velocity in the Perifocal system. Figure 2-3 illustrating this coordinate system with respect to the orbit is shown below. The position and velocity vectors are calculated according to the following equation.

$$\underline{r} = r \cos \nu\, \underline{P} + r \sin \nu\, \underline{Q} \tag{26}$$

$$r = \frac{p}{1 + e \cos \nu} \tag{27}$$

$$\underline{v} = \sqrt{\frac{\eta}{p}} [\, -\sin \nu\, \underline{P} + (\, e + \cos \nu\, )\, \underline{Q}\, ] \tag{28}$$

Figure 2-3

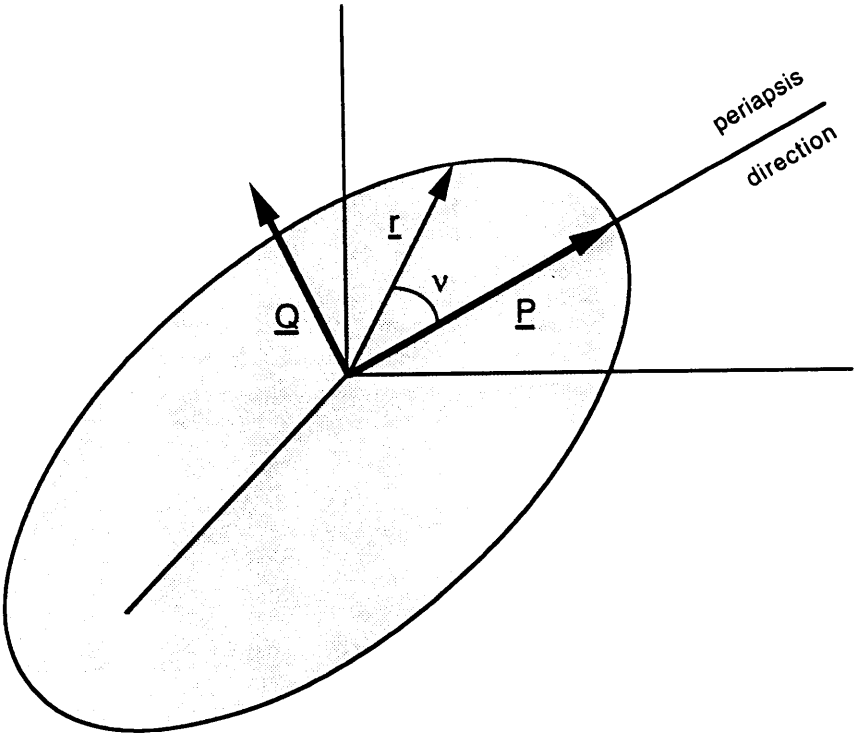


The last step in calculating the final spacecraft position and velocity vectors is to rotate the Perifocal system-based vectors to a Cartesian planet-based system. The rotation is accomplished as follows.

$$\underline{r}_c = R\,\underline{r}_p \tag{29}$$

$\underline{r}_c$ = position (velocity) vector in planet-based system

$\underline{r}_p$ = position (velocity) vector in Perifocal system

R = 3x3 rotation matrix

The rotation matrix R has the following elements.

$$R_{11} = \cos\Omega\cos\omega - \sin\Omega\sin\omega\cos i \tag{30}$$

$$R_{12} = -\cos\Omega\sin\omega - \sin\Omega\cos\omega\cos i \tag{31}$$

$$R_{13} = \sin\Omega\sin i \tag{32}$$

$$R_{21} = \sin \Omega \cos \omega + \cos \Omega \sin \omega \cos i \tag{33}$$

$$R_{22} = -\sin \Omega \sin \omega + \cos \Omega \cos \omega \cos i \tag{34}$$

$$R_{23} = -\cos \Omega \sin i \tag{35}$$

$$R_{31} = \sin \omega \sin i \tag{36}$$

$$R_{32} = \cos \omega \sin i \tag{37}$$

$$R_{33} = \cos i \tag{38}$$

## B. Variational Planetary Equations For Numerical Integration

In order to develop the analytic algorithm above, it was necessary to make some very severe restrictions. No perturbations from the two-body model are allowed. This is not sufficient for modern space navigation. Engineers currently account for nonspherical planets, solar pressure, third-body gravitational influences, and many other perturbations from the simplified models. The equations that allow the inclusion of these perturbations are for the derivatives of the orbital elements with respect to time. Numerical integration schemes utilize these derivatives to compute the trajectory step by step.

The orbital element derivative equations were derived using the technique of variation of parameters by Lagrange and improved by Gauss [4]. These equations can appear in several forms through various coordinate transformations. The set shown below is representative. Most of the orbital elements have been defined earlier. Perturbations enter the equations through acceleration terms.

$a_r$ = acceleration in the radial vector direction
$a_\theta$ = acceleration in the direction of motion $\perp$ to the radial vector
$a_h$ = acceleration in the angular momentum vector direction

Three new quantities should be defined before the variational equations are presented.

M = mean anomaly

$$M = E - e \sin E \tag{39}$$

f = mean true anomaly

$$\tan \frac{f}{2} = \sqrt{\frac{1+e}{1-e}} \tan \frac{E}{2} \tag{40}$$

$b$ = semiminor axis

$$b = | a^2 ( 1 - e^2 ) | \tag{41}$$

Gauss' form of the planetary variational equations can now be presented.

$$\frac{d\Omega}{dt} = \frac{r \sin \theta}{h \sin i} a_h \tag{42}$$

$$\frac{di}{dt} = \frac{r \cos \theta}{h} a_h \tag{43}$$

$$\frac{d\omega}{dt} = \frac{1}{eh} [ - p \cos f a_r + ( p + r ) \sin f a_\theta ] - \frac{r \sin \theta \cos i}{h \sin i} a_h \tag{44}$$

$$\frac{da}{dt} = \frac{2 a^2}{h} ( e \sin f a_r + \frac{p}{r} a_\theta ) \tag{45}$$

$$\frac{de}{dt} = \frac{1}{h} \{ p \sin f a_r + [ ( p + r ) \cos f + re ] a_\theta \} \tag{46}$$

$$\frac{dM}{dt} = n + \frac{b}{ahe} [ ( p \cos f - 2 re ) a_r - ( p + r ) \sin f a_\theta ] \tag{47}$$

The variational equations can be integrated from some initial spacecraft orbital state to an orbital state at a later time by any one of many numerical integration algorithms, such as Runga-Kutta methods. The reader can find detailed explanations in specific reference books on that subject [5].

# III. Analytic Solutions

As the reader will recall, the objective of this thesis is to compute the mean and variance of the elements of the final spacecraft state. This is done via integrals described in Chapter 1. The purpose of this chapter is to present analytic solutions to these integrals. Utilizing the analytic conic algorithm for computing trajectories, several intermediate results can be determined. Furthermore, specific analytic relationships exist between many orbital quantities allowing probabilistic integral computation.

## A. Intermediate Solutions From Conic Algorithm

The ultimate objective is to compute the mean and variance of the orbital elements after some flight time from uncertain initial conditions. Although this will be numerically possible in later chapters, an analytic solution is impossible. In the conic algorithm, an implicit equation occurs for a variable which makes it impossible to analytically compute an integral. Furthermore, although each step in the algorithm is reasonable, after substituting them into each other to obtain the final nonlinear, algebraically complex expression, the integral is unknown.

It is possible to compute the mean and variance from step to step by assuming for each calculation that the input variables are independent and described with a uniform probability density function. These relationships may assist the engineer in understanding the probabilistic relationships between orbital elements.

The remainder of this section is devoted to presenting the probabilistic relationships between the steps in the conic trajectory algorithm. Readers may have a need compute the relationships between quantities not presented here. Those may be calculated in an analogous method as that which follows.

The first quantity is the angular momentum vector. The procedure for calculating the mean and variance of the first element of the angular momentum vector will be illustrated to demonstrate the procedure used for all of the calculations in this section. The calculation of the mean is as follows.

$$\mu_{h_1} = \int_{LL1}^{UL1} \int_{LL2}^{UL2} \int_{LL3}^{UL3} \int_{LL4}^{UL4} \frac{( r_2 v_3 - r_3 v_2 )}{16 \delta^2 \epsilon^2} \, dv_2 \, dv_3 \, dr_2 \, dr_3 \tag{48}$$

$$\mu_{h_1} = \mu_{r_2} \mu_{v_3} - \mu_{r_3} \mu_{v_2} \tag{49}$$

$$UL1 = \mu_{r_2} + \delta$$
$$UL2 = \mu_{r_3} + \delta$$
$$UL3 = \mu_{v_2} + \epsilon$$
$$UL4 = \mu_{v_3} + \epsilon$$

$$LL1 = \mu_{r_2} - \delta$$
$$LL2 = \mu_{r_3} - \delta$$
$$LL3 = \mu_{v_2} - \epsilon$$
$$LL4 = \mu_{v_3} - \epsilon$$

$\mu_{h_1}$ = angular momentum vector first element mean
$\delta$ = distribution limit of all position vector elements
$\epsilon$ = distribution limit of all velocity vector elements

The remaining results for the angular momentum vector element means are presented below.

$$\mu_{h_2} = \mu_{r_3} \mu_{v_1} - \mu_{r_1} \mu_{v_3} \tag{50}$$

$$\mu_{h_3} = \mu_{r_2} \mu_{v_3} - \mu_{r_3} \mu_{v_2} \tag{51}$$

The angular momentum vector element variances are presented below.

$$\sigma^2_{h_1} = \tfrac{2}{9} \delta^2 \epsilon^2 + \tfrac{1}{3} \mu^2_{r_2} \epsilon^2 + \tfrac{1}{3} \mu^2_{r_3} \epsilon^2 + \tfrac{1}{3} \mu^2_{v_2} \delta^2 + \tfrac{1}{3} \mu^2_{v_3} \delta^2 \tag{52}$$

$$\sigma^2_{h_2} = \tfrac{2}{9} \delta^2 \epsilon^2 + \tfrac{1}{3} \mu^2_{r_1} \epsilon^2 + \tfrac{1}{3} \mu^2_{r_3} \epsilon^2 + \tfrac{1}{3} \mu^2_{v_1} \delta^2 + \tfrac{1}{3} \mu^2_{v_3} \delta^2 \tag{53}$$

$$\sigma^2_{h_3} = \tfrac{2}{9} \delta^2 \epsilon^2 + \tfrac{1}{3} \mu^2_{r_2} \epsilon^2 + \tfrac{1}{3} \mu^2_{r_1} \epsilon^2 + \tfrac{1}{3} \mu^2_{v_2} \delta^2 + \tfrac{1}{3} \mu^2_{v_1} \delta^2 \tag{54}$$

The nodal vector element means are presented below.

$$\mu_{n_1} = -\mu_{h_2} \tag{55}$$

$$\mu_{n_2} = \mu_{h_1} \tag{56}$$

The nodal vector element variances are presented below.

$$\sigma^2_{n_1} = \sigma^2_{h_2} \tag{57}$$

$$\sigma^2_{n_2} = \sigma^2_{h_1} \tag{58}$$

The eccentricity vector equations are algebraically complex and require some simplifying assumptions. These involve computing the probabilistic quantities of intermediate expressions within the equations. They are computed below.

$$y = r_1^2 + r_2^2 + r_3^2 \tag{59}$$

$$\mu_y = \delta^2 + \mu^2_{r_1} + \mu^2_{r_2} + \mu^2_{r_3} \tag{60}$$

$$\sigma^2_y = \frac{19}{15}\,\delta^4 + \frac{10}{3}\,\delta^2\,[\,\mu^2_{r_1} + \mu^2_{r_2} + \mu^2_{r_3}\,] + \mu^4_{r_1} + \mu^4_{r_2} + \mu^4_{r_3}$$

$$+ 2\,[\,\mu^2_{r_1}\,\mu^2_{r_2} + \mu^2_{r_1}\,\mu^2_{r_3} + \mu^2_{r_2}\,\mu^2_{r_3}\,] - \mu^2_y \tag{61}$$

$$F = y^{\frac{1}{2}} \tag{62}$$

$$\mu_F = \left(\frac{1}{3L_y}\right)[\,(\,\mu_y + L_y\,)^{\frac{3}{2}} - (\,\mu_y - L_y\,)^{\frac{3}{2}}\,] \tag{63}$$

$$\sigma^2_F = \mu_y - \mu^2_F \tag{64}$$

$L_y$ = probability distribution limit of y

The mean eccentricity vector elements are presented below.

$$\mu_{e_1} = \frac{2\epsilon^2\mu_{r_1}}{3\eta} - \frac{\mu_{r_2}\,\mu_{v_1}\,\mu_{v_2}}{\eta} + \frac{\mu_{r_1}\,\mu_{v_2}^2}{\eta} - \frac{\mu_{r_3}\,\mu_{v_1}\,\mu_{v_3}}{\eta} + \frac{\mu_{r_1}\,\mu_{v_3}^2}{\eta}$$
$$- \frac{\mu_{r_1}}{2L_F}\log\left(\frac{\mu_F + L_F}{\mu_F - L_F}\right) \tag{65}$$

$$\mu_{e_2} = \frac{2\epsilon^2\mu_{r_2}}{3\eta} - \frac{\mu_{r_1}\,\mu_{v_1}\,\mu_{v_2}}{\eta} + \frac{\mu_{r_2}\,\mu_{v_1}^2}{\eta} - \frac{\mu_{r_3}\,\mu_{v_2}\,\mu_{v_3}}{\eta} + \frac{\mu_{r_2}\,\mu_{r_3}^2}{\eta}$$
$$- \frac{\mu_{r_2}}{2L_F}\log\left(\frac{\mu_F + L_F}{\mu_F - L_F}\right) \tag{66}$$

$$\mu_{e_3} = \frac{2\epsilon^2\mu_{r_3}}{3\eta} - \frac{\mu_{r_2}\,\mu_{v_3}\,\mu_{v_2}}{\eta} + \frac{\mu_{r_3}\,\mu_{v_2}^2}{\eta} - \frac{\mu_{r_1}\,\mu_{v_1}\,\mu_{v_3}}{\eta} + \frac{\mu_{r_3}\,\mu_{v_1}^2}{\eta}$$
$$- \frac{\mu_{r_3}}{2L_F}\log\left(\frac{\mu_F + L_F}{\mu_F - L_F}\right) \tag{67}$$

The eccentricity vector variances are presented below.

$$\sigma_{e_1}^2 = \frac{\delta^2}{6\,(\mu_F - L_F)\,L_F} - \frac{\delta^2}{6\,(\mu_F + L_F)\,L_F} + \frac{\mu_{r_1}^2}{2\,(\mu_F - L_F)\,L_F} - \frac{\mu_{r_1}^2}{2\,(\mu_F + L_F)\,L_F}$$
$$+ \frac{38\delta^2\epsilon^4}{135\eta^2} + \frac{28\mu_{r_1}^2\epsilon^4}{45\eta^2} + \frac{\epsilon^4\mu_{r_2}^2}{9\eta^2} + \frac{\epsilon^4\mu_{r_3}^2}{9\eta^2} + \frac{2\delta^2\epsilon^2\mu_{v_1}^2}{9\eta^2}$$
$$+ \frac{\epsilon^2\mu_{r_2}^2\mu_{v_1}^2}{3\eta^2} + \frac{\epsilon^2\mu_{r_3}^2\mu_{v_1}^2}{3\eta^2} - \frac{2\epsilon^2\mu_{r_1}\mu_{r_2}\mu_{v_1}\mu_{v_2}}{3\eta^2}$$
$$- \frac{2\epsilon^2\mu_{r_1}\mu_{r_2}\mu_{v_1}\mu_{v_2}}{\eta^2} + \frac{(\delta\,\epsilon\,\mu_{v_2})^2}{\eta^2} + \frac{8(\epsilon\,\mu_{r_1}\mu_{v_2})^2}{3\eta^2} + \frac{(\epsilon\,\mu_{r_2}\mu_{v_2})^2}{3\eta^2}$$
$$+ \frac{(\delta\,\mu_{v_1}\mu_{v_2})^2}{3\eta^2} + \frac{(\mu_{r_2}\mu_{v_1}\mu_{v_2})^2}{\eta^2} - \frac{2\mu_{r_1}\mu_{r_2}\mu_{v_1}\mu_{v_2}^3}{\eta^2} + \frac{\delta^2\mu_{v_2}^4}{3\eta^2}$$
$$+ \frac{\mu_{r_1}^2\mu_{v_2}^4}{\eta^2} - \frac{8\epsilon^2\,\mu_{r_1}\mu_{r_3}\mu_{v_1}\mu_{v_3}}{3\eta^2} + \frac{2\epsilon^2\mu_{r_2}\mu_{r_3}\mu_{v_2}\mu_{v_3}}{3\eta^2}$$
$$+ \frac{2\mu_{r_2}\mu_{r_3}\mu_{v_1}^2\mu_{v_2}\mu_{v_3}}{\eta^2} - \frac{2\mu_{r_1}\mu_{r_3}\mu_{v_1}\mu_{v_2}^2\mu_{v_3}}{\eta^2} + \frac{(\delta\,\epsilon\,\mu_{v_3})^2}{\eta^2}$$
$$+ \frac{8(\epsilon\,\mu_{r_1}\mu_{v_3})^2}{3\eta^2} + \frac{(\epsilon\,\mu_{r_3}\mu_{v_3})^2}{3\eta^2} + \frac{(\delta\,\mu_{v_1}\mu_{v_3})^2}{3\eta^2} + \frac{(\mu_{r_3}\mu_{v_1}\mu_{v_3})^2}{\eta^2}$$

$$
\begin{aligned}
&- \frac{2\mu_{r_1}\mu_{r_2}\mu_{v_1}\mu_{v_2}\mu_{v_3}^2}{\eta^2} + \frac{2(\delta\ \mu_{v_2}\mu_{v_3})^2}{3\eta^2} + \frac{2(\mu_{r_1}\mu_{v_2}\mu_{v_3})^2}{\eta^2} \\
&- \frac{2\mu_{r_1}\mu_{r_3}\mu_{v_1}\mu_{v_3}^3}{\eta^2} + \frac{\delta^2\mu_{v_3}^4}{3\eta^2} + \frac{\mu_{r_1}^2\mu_{v_3}^4}{\eta^2} + \frac{2\delta^2\epsilon^2\log(\mu_F - L_F)}{9\ L_F\eta} \\
&+ \frac{2\epsilon^2\mu_{r_1}^2\log(\mu_F - L_F)}{3\ L_F\eta} - \frac{\mu_{r_1}\mu_{r_2}\mu_{v_1}\mu_{v_2}\log(\mu_F - L_F)}{L_F\eta} + \frac{\delta^2\mu_{v_2}^2\log(\mu_F - L_F)}{3\ L_F\eta} \\
&+ \frac{(\mu_{r_1}\mu_{v_2})^2\log(\mu_F - L_F)}{L_F\eta} - \frac{\mu_{r_1}\mu_{r_3}\mu_{v_1}\mu_{v_3}\log(\mu_F - L_F)}{L_F\eta} + \frac{\delta^2\mu_{v_3}^2\log(\mu_F - L_F)}{3\ L_F\eta} \\
&+ \frac{(\mu_{r_1}\mu_{v_3})^2\log(\mu_F - L_F)}{L_F\eta} - \frac{2\delta^2\epsilon^2\log(\mu_F + L_F)}{9\ L_F\eta} - \frac{2\epsilon^2\mu_{r_1}^2\log(\mu_F + L_F)}{3\ L_F\eta} \\
&+ \frac{\mu_{r_1}\mu_{r_2}\mu_{v_1}\mu_{v_2}\log(\mu_F + L_F)}{L_F\eta} - \frac{\delta^2\mu_{v_2}^2\log(\mu_F + L_F)}{3\ L_F\eta} - \frac{(\mu_{r_1}\mu_{v_2})^2\log(\mu_F + L_F)}{L_F\eta} \\
&+ \frac{\mu_{r_1}\mu_{r_3}\mu_{v_1}\mu_{v_3}\log(\mu_F + L_F)}{L_F\eta} - \frac{\delta^2\mu_{v_3}^2\log(\mu_F + L_F)}{3\ L_F\eta} - \frac{(\mu_{r_1}\mu_{v_3})^2\log(\mu_F + L_F)}{L_F\eta} \\
&- \mu_{e_1}^2
\end{aligned}
\tag{68}
$$

$$
\begin{aligned}
\sigma_{e_2}^2 = {} & \frac{\delta^2}{6\ (\mu_F - L_F)\ L_F} - \frac{\delta^2}{6\ (\mu_F + L_F)\ L_F} + \frac{\mu_{r_2}^2}{2\ (\mu_F - L_F)\ L_F} - \frac{\mu_{r_2}^2}{2\ (\mu_F + L_F)\ L_F} \\
&+ \frac{38\delta^2\epsilon^4}{135\eta^2} + \frac{28\ \mu_{r_2}^2\epsilon^4}{45\eta^2} + \frac{\epsilon^4\mu_{r_1}^2}{9\eta^2} + \frac{\epsilon^4\mu_{r_3}^2}{9\eta^2} + \frac{2\delta^2\epsilon^2\mu_{v_2}^2}{9\eta^2} \\
&+ \frac{\epsilon^2\mu_{r_1}^2\mu_{v_2}^2}{3\eta^2} + \frac{\epsilon^2\mu_{r_3}^2\mu_{v_2}^2}{3\eta^2} - \frac{2\epsilon^2\mu_{r_1}\mu_{r_2}\mu_{v_1}\mu_{v_2}}{3\eta^2} \\
&- \frac{2\epsilon^2\mu_{r_1}\mu_{r_2}\mu_{v_1}\mu_{v_2}}{\eta^2} + \frac{(\delta\ \epsilon\ \mu_{v_1})^2}{\eta^2} + \frac{8(\epsilon\ \mu_{r_2}\mu_{v_2})^2}{3\eta^2} + \frac{(\epsilon\ \mu_{r_1}\mu_{v_1})^2}{3\eta^2} \\
&+ \frac{(\delta\ \mu_{v_1}\mu_{v_2})^2}{3\eta^2} + \frac{(\mu_{r_1}\mu_{v_1}\mu_{v_2})^2}{\eta^2} - \frac{2\mu_{r_1}\mu_{r_2}\mu_{v_2}\mu_{v_1}^3}{\eta^2} + \frac{\delta^2\mu_{v_1}^4}{3\eta^2} \\
&+ \frac{\mu_{r_2}^2\mu_{v_1}^4}{\eta^2} - \frac{8\epsilon^2\ \mu_{r_2}\mu_{r_3}\mu_{v_2}\mu_{v_3}}{3\eta^2} + \frac{2\epsilon^2\mu_{r_1}\mu_{r_3}\mu_{v_1}\mu_{v_3}}{3\eta^2} \\
&+ \frac{2\mu_{r_1}\mu_{r_3}\mu_{v_2}^2\mu_{v_1}\mu_{v_3}}{\eta^2} - \frac{2\mu_{r_2}\mu_{r_3}\mu_{v_2}\mu_{v_1}^2\mu_{v_3}}{\eta^2} + \frac{(\delta\ \epsilon\ \mu_{v_3})^2}{\eta^2} \\
&+ \frac{8(\epsilon\ \mu_{r_2}\mu_{v_3})^2}{3\eta^2} + \frac{(\epsilon\ \mu_{r_3}\mu_{v_3})^2}{3\eta^2} + \frac{(\delta\ \mu_{v_2}\mu_{v_3})^2}{3\eta^2} + \frac{(\mu_{r_3}\mu_{v_2}\mu_{v_3})^2}{\eta^2} \\
&- \frac{2\mu_{r_1}\mu_{r_2}\mu_{v_1}\mu_{v_2}\mu_{v_3}^2}{\eta^2} + \frac{2(\delta\ \mu_{v_1}\mu_{v_3})^2}{3\eta^2} + \frac{2(\mu_{r_2}\mu_{v_1}\mu_{v_3})^2}{\eta^2}
\end{aligned}
$$

$$
\begin{aligned}
&- \frac{2\mu_{r_2}\mu_{r_3}\mu_{v_2}\mu_{v_3}^3}{\eta^2} + \frac{\delta^2\mu_{v_3}^4}{3\eta^2} + \frac{\mu_{r_2}^2\mu_{v_3}^4}{\eta^2} + \frac{2\delta^2\epsilon^2\log(\mu_F - L_F)}{9\ L_F\eta} \\
&+ \frac{2\epsilon^2\mu_{r_2}^2\log(\mu_F - L_F)}{3\ L_F\eta} - \frac{\mu_{r_1}\mu_{r_2}\mu_{v_1}\mu_{v_2}\log(\mu_F - L_F)}{L_F\eta} + \frac{\delta^2\mu_{v_1}^2\log(\mu_F - L_F)}{3\ L_F\eta} \\
&+ \frac{(\mu_{r_2}\mu_{v_1})^2\log(\mu_F - L_F)}{L_F\eta} - \frac{\mu_{r_2}\mu_{r_3}\mu_{v_2}\mu_{v_3}\log(\mu_F - L_F)}{L_F\eta} + \frac{\delta^2\mu_{v_3}^2\log(\mu_F - L_F)}{3\ L_F\eta} \\
&+ \frac{(\mu_{r_2}\mu_{v_3})^2\log(\mu_F - L_F)}{L_F\eta} - \frac{2\delta^2\epsilon^2\log(\mu_F + L_F)}{9\ L_F\eta} - \frac{2\epsilon^2\mu_{r_2}^2\log(\mu_F + L_F)}{3\ L_F\eta} \\
&+ \frac{\mu_{r_1}\mu_{r_2}\mu_{v_1}\mu_{v_2}\log(\mu_F + L_F)}{L_F\eta} - \frac{\delta^2\mu_{v_1}^2\log(\mu_F + L_F)}{3\ L_F\eta} - \frac{(\mu_{r_2}\mu_{v_1})^2\log(\mu_F + L_F)}{L_F\eta} \\
&+ \frac{\mu_{r_2}\mu_{r_3}\mu_{v_2}\mu_{v_3}\log(\mu_F + L_F)}{L_F\eta} - \frac{\delta^2\mu_{v_3}^2\log(\mu_F + L_F)}{3\ L_F\eta} - \frac{(\mu_{r_2}\mu_{v_3})^2\log(\mu_F + L_F)}{L_F\eta} \\
&- \mu_{e_2}^2
\end{aligned}
\tag{69}
$$

$$
\begin{aligned}
\sigma_{e_3}^2 = {} & \frac{\delta^2}{6\ (\mu_F - L_F)\ L_F} - \frac{\delta^2}{6\ (\mu_F + L_F)\ L_F} + \frac{\mu_{r_3}^2}{2\ (\mu_F - L_F)\ L_F} - \frac{\mu_{r_3}^2}{2\ (\mu_F + L_F)\ L_F} \\
&+ \frac{38\delta^2\epsilon^4}{135\eta^2} + \frac{28\ \mu_{r_3}^2\epsilon^4}{45\eta^2} + \frac{\epsilon^4\mu_{r_2}^2}{9\eta^2} + \frac{\epsilon^4\mu_{r_1}^2}{9\eta^2} + \frac{2\delta^2\epsilon^2\mu_{v_3}^2}{9\eta^2} \\
&+ \frac{\epsilon^2\mu_{r_2}^2\mu_{v_3}^2}{3\eta^2} + \frac{\epsilon^2\mu_{r_1}^2\mu_{v_3}^2}{3\eta^2} - \frac{2\epsilon^2\mu_{r_3}\mu_{r_2}\mu_{v_3}\mu_{v_2}}{3\eta^2} \\
&- \frac{2\epsilon^2\mu_{r_3}\mu_{r_2}\mu_{v_3}\mu_{v_2}}{\eta^2} + \frac{(\delta\ \epsilon\ \mu_{v_2})^2}{\eta^2} + \frac{8(\epsilon\ \mu_{r_3}\mu_{v_2})^2}{3\eta^2} + \frac{(\epsilon\ \mu_{r_2}\mu_{v_2})^2}{3\eta^2} \\
&+ \frac{(\delta\ \mu_{v_3}\mu_{v_2})^2}{3\eta^2} + \frac{(\mu_{r_2}\mu_{v_3}\mu_{v_2})^2}{\eta^2} - \frac{2\mu_{r_3}\mu_{r_2}\mu_{v_3}v_2^3}{\eta^2} + \frac{\delta^2\mu_{v_2}^4}{3\eta^2} \\
&+ \frac{\mu_{r_3}^2\mu_{v_2}^4}{\eta^2} - \frac{8\epsilon^2\ \mu_{r_1}\mu_{r_3}\mu_{v_1}\mu_{v_3}}{3\eta^2} + \frac{2\epsilon^2\mu_{r_2}\mu_{r_1}\mu_{v_1}\mu_{v_2}}{3\eta^2} \\
&+ \frac{2\mu_{r_2}\mu_{r_1}\mu_{v_3}^2\mu_{v_1}\mu_{v_2}}{\eta^2} - \frac{2\mu_{r_1}\mu_{r_3}\mu_{v_3}\mu_{v_2}^2\mu_{v_1}}{\eta^2} + \frac{(\delta\ \epsilon\ \mu_{v_1})^2}{\eta^2} \\
&+ \frac{8(\epsilon\ \mu_{r_3}\mu_{v_1})^2}{3\eta^2} + \frac{(\epsilon\ \mu_{r_1}\mu_{v_1})^2}{3\eta^2} + \frac{(\delta\ \mu_{v_3}\mu_{v_1})^2}{3\eta^2} + \frac{(\mu_{r_1}\mu_{v_1}\mu_{v_3})^2}{\eta^2} \\
&- \frac{2\mu_{r_3}\mu_{r_2}\mu_{v_3}\mu_{v_2}\mu_{v_1}^2}{\eta^2} + \frac{2(\delta\ \mu_{v_2}\mu_{v_1})^2}{3\eta^2} + \frac{2(\mu_{r_3}\mu_{v_2}\mu_{v_1})^2}{\eta^2} \\
&- \frac{2\mu_{r_1}\mu_{r_3}\mu_{v_3}\mu_{v_1}^3}{\eta^2} + \frac{\delta^2\mu_{v_1}^4}{3\eta^2} + \frac{\mu_{r_3}^2\mu_{v_1}^4}{\eta^2} + \frac{2\delta^2\epsilon^2\log(\mu_F - L_F)}{9\ L_F\eta}
\end{aligned}
$$

$$+ \frac{2\epsilon^2\mu_{r_3}^2\log(\mu_F - L_F)}{3\ L_F\eta} - \frac{\mu_{r_3}\mu_{r_2}\mu_{v_3}\mu_{v_2}\log(\mu_F - L_F)}{L_F\eta} + \frac{\delta^2\mu_{v_2}^2\log(\mu_F - L_F)}{3\ L_F\eta}$$

$$+ \frac{(\mu_{r_3}\mu_{v_2})^2\log(\mu_F - L_F)}{L_F\eta} - \frac{\mu_{r_3}\mu_{r_1}\mu_{v_1}\mu_{v_3}\log(\mu_F - L_F)}{L_F\eta} + \frac{\delta^2\mu_{v_1}^2\log(\mu_F - L_F)}{3\ L_F\eta}$$

$$+ \frac{(\mu_{r_3}\mu_{v_1})^2\log(\mu_F - L_F)}{L_F\eta} - \frac{2\delta^2\epsilon^2\log(\mu_F + L_F)}{9\ L_F\eta} - \frac{2\epsilon^2\mu_{r_3}^2\log(\mu_F + L_F)}{3\ L_F\eta}$$

$$+ \frac{\mu_{r_3}\mu_{r_2}\mu_{v_3}\mu_{v_2}\log(\mu_F + L_F)}{L_F\eta} - \frac{\delta^2\mu_{v_2}^2\log(\mu_F + L_F)}{3\ L_F\eta} - \frac{(\mu_{r_3}\mu_{v_2})^2\log(\mu_F + L_F)}{L_F\eta}$$

$$+ \frac{\mu_{r_1}\mu_{r_3}\mu_{v_1}\mu_{v_3}\log(\mu_F + L_F)}{L_F\eta} - \frac{\delta^2\mu_{v_1}^2\log(\mu_F + L_F)}{3\ L_F\eta} - \frac{(\mu_{r_3}\mu_{v_1})^2\log(\mu_F + L_F)}{L_F\eta}$$

$$- \mu_{e_3}^2 \tag{70}$$

The semi-latus rectum mean and variance follow.

$$\mu_p = \tfrac{1}{\eta}\left[\ \mu_{h_1}^2 + \mu_{h_2}^2 + \mu_{h_3}^2 + \tfrac{1}{3}\left(\ L_{h_1}^2 + L_{h_2}^2 + L_{h_3}^2\ \right)\ \right] \tag{71}$$

$$\sigma_p^2 = \frac{4}{3\eta^2}\left[\ \mu_{h_1}^2 L_{h_1}^2 + \mu_{h_2}^2 L_{h_2}^2 + \mu_{h_3}^2 L_{h_3}^2 + \tfrac{1}{15}\left(\ L_{h_1}^4 + L_{h_2}^4 + L_{h_3}^4\ \right)\ \right] \tag{72}$$

The eccentricity magnitude mean and variance follow.

$$y = e_1^2 + e_2^2 + e_3^2 \tag{73}$$

$$\mu_y = \tfrac{1}{3}\left(\ L_{e_1}^2 + L_{e_2}^2 + L_{e_3}^2\ \right) + \mu_{e_1}^2 + \mu_{e_2}^2 + \mu_{e_3}^2 \tag{74}$$

$$\sigma_y^2 = \tfrac{4}{3}\left[\ \mu_{e_1}^2 L_{e_1}^2 + \mu_{e_2}^2 L_{e_2}^2 + \mu_{e_3}^2 L_{e_3}^2\ \right] + \tfrac{4}{45}\left(\ L_{e_1}^4 + L_{e_2}^4 + L_{e_3}^4\ \right) \tag{75}$$

$$e = y^{\frac{1}{2}} \tag{76}$$

$$\mu_e = \left(\ \frac{1}{3L_y}\ \right)\left[\ \left(\ \mu_y + L_y\ \right)^{\frac{3}{2}} - \left(\ \mu_y - L_y\ \right)^{\frac{3}{2}}\ \right] \tag{77}$$

$$\sigma_e^2 = \mu_y - \mu_e^2 \tag{78}$$

The semi-major axis mean and variance follow.

$$z = 1 - e^2 \tag{79}$$

$$\mu_z = 1 - \mu_e^2 - \tfrac{1}{3}L_e^2 \tag{80}$$

$$\sigma_z^2 = \tfrac{4}{45}\left( \mu_e^2 L_e^2 + L_e^4 \right) \tag{81}$$

$$\mu_a = \frac{\mu_p}{2L_z} \log\left( \frac{\mu_z + L_z}{\mu_z - L_z} \right) \tag{82}$$

$$\sigma_a^2 = \frac{\mu_p^2}{2L_z(\mu_z - L_z)} + \frac{L_p^2}{6L_z(\mu_z - L_z)} - \frac{\mu_p^2}{2L_z(\mu_z + L_z)} - \frac{L_p^2}{6L_z(\mu_z + L_z)} - \mu_a^2 \tag{83}$$

The angular momentum magnitude mean and variance follow.

$$y = h_1^2 + h_2^2 + h_3^2 \tag{84}$$

$$\mu_y = \tfrac{1}{3}\left( L_{h_1}^2 + L_{h_2}^2 + L_{h_3}^2 \right) + \mu_{h_1}^2 + \mu_{h_2}^2 + \mu_{h_3}^2 \tag{85}$$

$$\sigma_y^2 = \tfrac{4}{3}\left[ \mu_{h_1}^2 L_{h_1}^2 + \mu_{h_2}^2 L_{h_2}^2 + \mu_{h_3}^2 L_{h_3}^2 \right] + \tfrac{4}{45}\left( L_{h_1}^4 + L_{h_2}^4 + L_{h_3}^4 \right) \tag{86}$$

$$h = y^{\frac{1}{2}} \tag{87}$$

$$\mu_h = \left( \frac{1}{3L_y} \right)\left[ \left( \mu_y + L_y \right)^{\frac{3}{2}} - \left( \mu_y - L_y \right)^{\frac{3}{2}} \right] \tag{88}$$

$$\sigma_h^2 = \mu_y - \mu_h^2 \tag{89}$$

The nodal vector magnitude mean and variance follow.

$$y = n_1^2 + n_2^2 + n_3^2 \tag{90}$$

$$\mu_y = \frac{1}{3}\left( L_{n_1}^2 + L_{n_2}^2 + L_{n_3}^2 \right) + \mu_{n_1}^2 + \mu_{n_2}^2 + \mu_{n_3}^2 \tag{91}$$

$$\sigma_y^2 = \frac{4}{3}\left[ \mu_{n_1}^2 L_{n_1}^2 + \mu_{n_2}^2 L_{n_2}^2 + \mu_{n_3}^2 L_{n_3}^2 \right] + \frac{4}{45}\left( L_{n_1}^4 + L_{n_2}^4 + L_{n_3}^4 \right) \tag{92}$$

$$n = y^{\frac{1}{2}} \tag{93}$$

$$\mu_n = \left( \frac{1}{3L_y} \right)\left[ \left( \mu_y + L_y \right)^{\frac{3}{2}} - \left( \mu_y - L_y \right)^{\frac{3}{2}} \right] \tag{94}$$

$$\sigma_n^2 = \mu_y - \mu_n^2 \tag{95}$$

The mean and variance of the cosine of the inclination follow.

$$\mu_{cin} = \frac{\mu_{h_3}}{2L_h} \log\left( \frac{\mu_h + L_h}{\mu_h - L_h} \right) \tag{96}$$

$$\sigma_{cin}^2 = \frac{\mu_{h_3}^2}{2L_h(\mu_h - L_h)} + \frac{L_{h_3}^2}{6L_h(\mu_h - L_h)} - \frac{\mu_{h_3}^2}{2L_h(\mu_h + L_h)} - \frac{L_{h_3}^2}{6L_h(\mu_h + L_h)} - \mu_{cin}^2 \tag{97}$$

The mean and variance of the sine of the inclination follow.

$$y = h_1^2 + h_2^2 \tag{98}$$

$$\mu_y = \frac{1}{3}\left( L_{h_1}^2 + L_{h_2}^2 \right) + \mu_{h_1}^2 + \mu_{h_2}^2 \tag{99}$$

$$\sigma_y^2 = \frac{4}{3}\left[ \mu_{h_1}^2 L_{h_1}^2 + \mu_{h_2}^2 L_{h_2}^2 \right] + \frac{4}{45}\left( L_{h_1}^4 + L_{h_2}^4 \right) \tag{100}$$

$$z = y^{\frac{1}{2}} \tag{101}$$

$$\mu_z = \left( \frac{1}{3L_y} \right)\left[ \left( \mu_y + L_y \right)^{\frac{3}{2}} - \left( \mu_y - L_y \right)^{\frac{3}{2}} \right] \tag{102}$$

$$\sigma_z^2 = \mu_y - \mu_z^2 \tag{103}$$

$$\mu_{sin} = \frac{\mu_z}{2L_h} \log\left( \frac{\mu_h + L_h}{\mu_h - L_h} \right) \tag{104}$$

$$\sigma_{sin}^2 = \frac{\mu_z^2}{2L_h(\mu_h - L_h)} + \frac{L_z^2}{6L_h(\mu_h - L_h)} - \frac{\mu_z^2}{2L_h(\mu_h + L_h)}$$

$$- \frac{L_z^2}{6L_h(\mu_h + L_h)} - \mu_{sin}^2 \tag{105}$$

The mean and variance of the cosine of the longitude of the ascending node follow.

$$\mu_{com} = \frac{\mu_{n_1}}{2L_n} \log\left( \frac{\mu_n + L_n}{\mu_n - L_n} \right) \tag{106}$$

$$\sigma_{com}^2 = \frac{\mu_{n_1}^2}{2L_n(\mu_n - L_n)} + \frac{L_{n_1}^2}{6L_n(\mu_n - L_n)} - \frac{\mu_{n_1}^2}{2L_n(\mu_n + L_n)}$$

$$- \frac{L_{n_1}^2}{6L_n(\mu_n + L_n)} - \mu_{com}^2 \tag{107}$$

The mean and variance of the sine of the longitude of the ascending node follow.

$$\mu_{som} = \frac{\mu_{n_2}}{2L_n} \log\left( \frac{\mu_n + L_n}{\mu_n - L_n} \right) \tag{108}$$

$$\sigma_{som}^2 = \frac{\mu_{n_2}^2}{2L_n(\mu_n - L_n)} + \frac{L_{n_2}^2}{6L_n(\mu_n - L_n)} - \frac{\mu_{n_2}^2}{2L_n(\mu_n + L_n)}$$

$$- \frac{L_{n_2}^2}{6L_n(\mu_n + L_n)} - \mu_{som}^2 \tag{109}$$

The mean and variance of the cosine of the argument of periapsis follow.

$$y = n_1 e_1 + n_2 e_2 + n_3 e_3 \tag{110}$$

$$\mu_y = \mu_{n_1}\mu_{e_1} + \mu_{n_2}\mu_{e_2} + \mu_{n_3}\mu_{e_3} \tag{111}$$

$$\sigma_y^2 = \tfrac{1}{3}\left( L_{e_1}^2\mu_{n_1}^2 + L_{e_2}^2\mu_{n_2}{}^2 + L_{n_1}^2\mu_{e_1}^2 + L_{n_2}^2\mu_{e_2}^2 \right)$$

$$+ \tfrac{1}{9}\left( L_{e_1}^2 L_{n_1}^2 + L_{e_2}^2 L_{n_2}^2 \right) \tag{112}$$

$$z = ne \tag{113}$$

$$\mu_z = \mu_n \mu_e \tag{114}$$

$$\sigma_z^2 = \tfrac{1}{3} \left( L_e^2 \mu_n^2 + L_n^2 \mu_e^2 \right) + \tfrac{1}{9} L_e^2 L_n^2 \tag{115}$$

$$\mu_{cw} = \frac{\mu_y}{2L_z} \log\left( \frac{\mu_z + L_z}{\mu_z - L_z} \right) \tag{116}$$

$$\sigma_{cw}^2 = \frac{\mu_y^2}{2L_z(\mu_z - L_z)} + \frac{L_y^2}{6L_z(\mu_z - L_z)} - \frac{\mu_y^2}{2L_z(\mu_z + L_z)} - \frac{L_y^2}{6L_z(\mu_z + L_z)} - \mu_{cw}^2 \tag{117}$$

The mean and variance of the cosine of the true anomaly follow.

$$y = r_1 e_1 + r_2 e_2 + r_3 e_3 \tag{118}$$

$$\mu_y = \mu_{r_1} \mu_{e_1} + \mu_{r_2} \mu_{e_2} + \mu_{r_3} \mu_{e_3} \tag{119}$$

$$\sigma_y^2 = \tfrac{1}{3} \left( L_{e_1}^2 \mu_{r_1}^2 + L_{e_2}^2 \mu_{r_2}^2 + L_{r_1}^2 \mu_{e_1}^2 + L_{r_2}^2 \mu_{e_2}^2 \right) + \tfrac{1}{9} \left( L_{e_1}^2 L_{r_1}^2 + L_{e_2}^2 L_{r_2}^2 \right) \tag{120}$$

$$z = re \tag{121}$$

$$\mu_z = \mu_r \mu_e \tag{122}$$

$$\sigma_z^2 = \tfrac{1}{3} \left( L_e^2 \mu_r^2 + L_r^2 \mu_e^2 \right) + \tfrac{1}{9} L_e^2 L_r^2 \tag{123}$$

$$\mu_{cv} = \frac{\mu_y}{2L_z} \log\left( \frac{\mu_z + L_z}{\mu_z - L_z} \right) \tag{124}$$

$$\sigma_{cv}^2 = \frac{\mu_y^2}{2L_z(\mu_z - L_z)} + \frac{L_y^2}{6L_z(\mu_z - L_z)} - \frac{\mu_y^2}{2L_z(\mu_z + L_z)} - \frac{L_y^2}{6L_z(\mu_z + L_z)} - \mu_{cv}^2 \tag{125}$$

The mean and variance of the sine of the argument of periapsis follow.

$$x_1 = n_2 e_3 \tag{126}$$

$$x_2 = -n_1 e_3 \tag{127}$$

$$x_3 = n_1 e_2 - n_2 e_1 \tag{128}$$

$$\mu_{x_1} = \mu_{n_2}\mu_{e_3} \tag{129}$$

$$\mu_{x_2} = -\mu_{n_1}\mu_{e_3} \tag{130}$$

$$\mu_{x_3} = \mu_{n_1}\mu_{e_2} - \mu_{n_2}\mu_{e_1} \tag{131}$$

$$\sigma^2_{x_1} = \tfrac{1}{3}\left( L^2_{n_2}\mu^2_{e_3} + \mu^2_{n_2}L^2_{e_3} \right) + \tfrac{1}{9} L^2_{n_2}L^2_{e_3} \tag{132}$$

$$\sigma^2_{x_2} = \tfrac{1}{3}\left( L^2_{n_1}\mu^2_{e_3} + \mu^2_{n_1}L^2_{e_3} \right) + \tfrac{1}{9} L^2_{n_1}L^2_{e_3} \tag{133}$$

$$\sigma^2_{x_3} = \tfrac{1}{3}\left( L^2_{n_2}\mu^2_{e_1} + \mu^2_{n_1}L^2_{e_2} + L^2_{n_1}\mu^2_{e_2} + \mu^2_{n_2}L^2_{e_1} \right) + \tfrac{1}{9}\left( L^2_{n_1}L^2_{e_2} + L^2_{n_2}L^2_{e_1} \right) \tag{134}$$

$$y = x_1^2 + x_2^2 + x_3^2 \tag{135}$$

$$\mu_y = \tfrac{1}{3}\left( L^2_{x_1} + L^2_{x_2} + L^2_{x_3} \right) + \mu^2_{x_1} + \mu^2_{x_2} + \mu^2_{x_3} \tag{136}$$

$$\sigma^2_y = \tfrac{4}{3}\left[ \mu^2_{x_1}L^2_{x_1} + \mu^2_{x_2}L^2_{x_2} + \mu^2_{x_3}L^2_{x_3} \right] + \tfrac{4}{45}\left( L^4_{x_1} + L^4_{x_2} + L^4_{x_3} \right) \tag{137}$$

$$x = y^{\frac{1}{2}} \tag{138}$$

$$\mu_x = \left( \frac{1}{3L_y} \right)\left[ \left( \mu_y + L_y \right)^{\frac{3}{2}} - \left( \mu_y - L_y \right)^{\frac{3}{2}} \right] \tag{139}$$

$$\sigma^2_x = \mu_y - \mu^2_x \tag{140}$$

$$z = ne \tag{141}$$

$$\mu_z = \mu_n \mu_e \tag{142}$$

$$\sigma_z^2 = \tfrac{1}{3}\left( L_e^2 \mu_n^2 + L_n^2 \mu_e^2 \right) + \tfrac{1}{9} L_e^2 L_n^2 \tag{143}$$

$$\mu_{sw} = \frac{\mu_x}{2L_z} \log\left( \frac{\mu_z + L_z}{\mu_z - L_z} \right) \tag{144}$$

$$\sigma_{sw}^2 = \frac{\mu_x^2}{2L_z(\mu_z - L_z)} + \frac{L_x^2}{6L_z(\mu_z - L_z)} - \frac{\mu_x^2}{2L_z(\mu_z + L_z)} - \frac{L_x^2}{6L_z(\mu_z + L_z)} - \mu_{sw}^2 \tag{145}$$

The mean and variance of the sine of the true anomaly follow.

$$x_1 = e_2 r_3 - e_3 r_2 \tag{146}$$

$$x_2 = e_3 r_1 - e_1 r_3 \tag{147}$$

$$x_3 = e_1 r_2 - e_2 r_1 \tag{148}$$

$$\mu_{x_1} = \mu_{e_2} \mu_{r_3} - \mu_{e_3} \mu_{r_2} \tag{149}$$

$$\mu_{x_2} = \mu_{e_3} \mu_{r_1} - \mu_{e_1} \mu_{r_3} \tag{150}$$

$$\mu_{x_3} = \mu_{e_1} \mu_{r_2} - \mu_{e_2} \mu_{r_1} \tag{151}$$

$$\sigma_{x_1}^2 = \tfrac{1}{3}\left( L_{e_2}^2 \mu_{r_3}^2 + \mu_{e_2}^2 L_{r_3}^2 + L_{e_3}^2 \mu_{r_2}^2 + \mu_{e_3}^2 L_{r_2}^2 \right) + \tfrac{1}{9}\left( L_{e_2}^2 L_{r_3}^2 + L_{e_3}^2 L_{r_2}^2 \right) \tag{152}$$

$$\sigma_{x_2}^2 = \tfrac{1}{3}\left( L_{e_3}^2 \mu_{r_1}^2 + \mu_{e_3}^2 L_{r_1}^2 + L_{e_1}^2 \mu_{r_3}^2 + \mu_{e_1}^2 L_{r_3}^2 \right) + \tfrac{1}{9}\left( L_{e_3}^2 L_{r_1}^2 + L_{e_1}^2 L_{r_3}^2 \right) \tag{153}$$

$$\sigma_{x_3}^2 = \tfrac{1}{3}\left( L_{r_2}^2 \mu_{e_1}^2 + \mu_{r_1}^2 L_{e_2}^2 + L_{r_1}^2 \mu_{e_2}^2 + \mu_{r_2}^2 L_{e_1}^2 \right) + \tfrac{1}{9}\left( L_{r_1}^2 L_{e_2}^2 + L_{r_2}^2 L_{e_1}^2 \right) \tag{154}$$

$$y = x_1^2 + x_2^2 + x_3^2 \tag{155}$$

$$\mu_y = \frac{1}{3}\left( L_{x_1}^2 + L_{x_2}^2 + L_{x_3}^2 \right) + \mu_{x_1}^2 + \mu_{x_2}^2 + \mu_{x_3}^2 \tag{156}$$

$$\sigma_y^2 = \frac{4}{3}\left[ \mu_{x_1}^2 L_{x_1}^2 + \mu_{x_2}^2 L_{x_2}^2 + \mu_{x_3}^2 L_{x_3}^2 \right] + \frac{4}{45}\left( L_{x_1}^4 + L_{x_2}^4 + L_{x_3}^4 \right) \tag{157}$$

$$x = y^{\frac{1}{2}} \tag{158}$$

$$\mu_x = \left( \frac{1}{3L_y} \right)\left[ \left( \mu_y + L_y \right)^{\frac{3}{2}} - \left( \mu_y - L_y \right)^{\frac{3}{2}} \right] \tag{159}$$

$$\sigma_x^2 = \mu_y - \mu_x^2 \tag{160}$$

$$z = re \tag{161}$$

$$\mu_z = \mu_r \mu_e$$

$$\sigma_z^2 = \frac{1}{3}\left( L_e^2 \mu_r^2 + L_r^2 \mu_e^2 \right) + \frac{1}{9} L_e^2 L_r^2 \tag{162}$$

$$\mu_{sv} = \frac{\mu_x}{2L_z} \log\left( \frac{\mu_z + L_z}{\mu_z - L_z} \right) \tag{163}$$

$$\sigma_{sv}^2 = \frac{\mu_x^2}{2L_z(\mu_z - L_z)} + \frac{L_x^2}{6L_z(\mu_z - L_z)} - \frac{\mu_x^2}{2L_z(\mu_z + L_z)} - \frac{L_x^2}{6L_z(\mu_z + L_z)} - \mu_{sv}^2 \tag{164}$$

The mean and variance of the cosine of the eccentric anomaly follow.

$$y = e + \cos(\nu) \tag{165}$$

$$\mu_y = \mu_e + \mu_{cv} \tag{166}$$

$$\sigma_y^2 = \frac{1}{3} L_e^2 + \frac{1}{3} L_{cv}^2 \tag{167}$$

$$z = 1 + e\cos(\nu) \tag{168}$$

$$\mu_z = 1 + \mu_e \mu_{cv} \tag{169}$$

$$\sigma_z^2 = \frac{1}{3}\left( L_{cv}^2 \mu_e^2 + \mu_{cv}^2 L_e^2 \right) + \frac{1}{9} L_{cv}^2 L_e^2 \tag{170}$$

$$\mu_{ceo} = \frac{\mu_y}{2L_z} \log\left( \frac{\mu_z + L_z}{\mu_z - L_z} \right) \tag{171}$$

$$\sigma^2_{ceo} = \frac{\mu_y^2}{2L_z(\mu_z - L_z)} + \frac{L_y^2}{6L_z(\mu_z - L_z)} - \frac{\mu_y^2}{2L_z(\mu_z + L_z)} - \frac{L_y^2}{6L_z(\mu_z + L_z)} - \mu^2_{ceo} \tag{172}$$

The mean and variance of the eccentric anomaly follow.

$$\mu_{eo} = \frac{1}{2L_{ceo}} [ (\mu_{ceo} + L_{ceo}) \cos^{-1}(\mu_{ceo} + L_{ceo}) - (\mu_{ceo} - L_{ceo}) \cos^{-1}(\mu_{ceo} - L_{ceo}) - \sqrt{1 - (\mu_{ceo} + L_{ceo})^2} + \sqrt{1 - (\mu_{ceo} - L_{ceo})^2} ] \tag{173}$$

$$\sigma^2_{eo} = \frac{1}{2L_{ceo}} [ (\mu_{ceo} + L_{ceo}) \{ \cos^{-1}(\mu_{ceo} + L_{ceo}) \}^2 - (\mu_{ceo} - L_{ceo}) ( \cos^{-1}(\mu_{ceo} - L_{ceo}) )^2 - 2 (\mu_{ceo} + L_{ceo}) + 2 (\mu_{ceo} - L_{ceo}) - 2\sqrt{1 - (\mu_{ceo} + L_{ceo})^2} \cos^{-1}(\mu_{ceo} + L_{ceo}) + \sqrt{1 - (\mu_{ceo} - L_{ceo})^2} \cos^{-1}(\mu_{ceo} - L_{ceo}) ] \tag{174}$$

The mean and variance of the mean anomaly follow.

$$M = E - e \sin E \tag{175}$$

$$\mu_{mo} = \mu_{eo} + \frac{\mu_e}{2L_{eo}} [ \cos(\mu_{eo} + L_{eo}) - \cos(\mu_{eo} - L_{eo}) ] \tag{176}$$

$$\sigma^2_{mo} = \mu^2_{eo} + \frac{1}{3} L^2_{eo} - \frac{\mu_e}{2L_{eo}} [ \sin(\mu_{eo} + L_{eo}) - \sin(\mu_{eo} - L_{eo}) - (\mu_{eo} + L_{eo}) \cos(\mu_{eo} + L_{eo}) + (\mu_{eo} - L_{eo}) \cos(\mu_{eo} - L_{eo}) ] + \left(\frac{\mu_e^2}{2L_{eo}} + \frac{L_e^2}{6L_{eo}}\right) [ .5(\mu_{eo} + L_{eo}) - .5(\mu_{eo} - L_{eo}) - .25 \sin\{2(\mu_{eo} + L_{eo})\} + .25 \sin\{2(\mu_{eo} - L_{eo})\} ] \tag{177}$$

The progress through the analytic trajectory algorithm has now reached Kepler's Equation. This is an implicit equation for the eccentric anomaly given an initial mean anomaly and flight time. The mean and variance of this final eccentric anomaly can be found using numerical techniques following some preliminary analysis. The final mean anomaly calculations are below. The final eccentric anomaly will be calculated from these results.

$$aa = t\left(\frac{\eta}{a^3}\right)^{\frac{1}{2}} \tag{178}$$

$$\mu_{aa} = -\frac{t\sqrt{\eta}}{L_a\sqrt{\mu_a+L_a}} + \frac{t\sqrt{\eta}}{L_a\sqrt{\mu_a-L_a}} \tag{179}$$

$$\sigma^2_{aa} = -\frac{t^2\eta}{4L_a}\left(\frac{1}{(\mu_a+L_a)^2} - \frac{1}{(\mu_a-L_a)^2}\right) \tag{180}$$

$$M_n = aa - 2k\pi + M_o \tag{181}$$

$M_n$ = final mean anomaly

$M_o$ = initial mean anomaly

$$\mu_{mn} = \mu_{aa} - 2k\pi + \mu_{mo} \tag{182}$$

$$\sigma^2_{mn} = \frac{1}{3}\left(L^2_{aa} + L^2_{mo}\right) \tag{183}$$

The final eccentric anomaly mean, $\mu_{en}$, and its uncertainty limit, $L_{en}$, can be found numerically using the Newton-Raphson method for nonlinear systems of equations. The two functional relations to be zeroed are given below.

$$f_1 = -\mu_{mn} + \mu_{en} + \frac{\mu_e}{2L_{en}}\left[\cos(\mu_{en}+L_{en}) - \cos(\mu_{en}-L_{en})\right] \tag{184}$$

$$\begin{aligned} f_2 = \Bigg( & \mu^2_{en} + \frac{L^2_{en}}{3} - \frac{\mu_e}{2L_{en}}\left[\sin(\mu_{en}+L_{en}) - \sin(\mu_{en}-L_{en}) - (\mu_{en}+L_{en})\cos(\mu_{en}+L_{en})\right. \\ & \left. + (\mu_{en}-L_{en})\cos(\mu_{en}-L_{en})\right] + \frac{1}{2L_{en}}\left(\mu^2_e+\frac{L^2_e}{3}\right)\left[.5\,(\mu_{en}+L_{en}) - .5\,(\mu_{en}-L_{en})\right. \\ & \left. - .25\sin(2\mu_{en}+2L_{en}) + .25\sin(2\mu_{en}-2L_{en})\right] - \left\{\mu_{en} + \frac{\mu_e}{2L_{en}}\left[\cos(\mu_{en}+L_{en})\right.\right. \\ & \left.\left. - \cos(\mu_{en}-L_{en})\right]\right\}^2\Bigg)^{\frac{1}{2}}\sqrt{3} - L_{mn} \end{aligned} \tag{185}$$

The partials used in the numerical search are provided below.

$$\frac{\partial f_1}{\partial \mu_{en}} = 1 + \mu_e \left[ \sin(\mu_{en}-L_{en}) - \sin(\mu_{en}+L_{en}) \right] / 2\, L_{en} \tag{186}$$

$$\frac{\partial f_1}{\partial L_{en}} = -\mu_e \left[ -\sin(\mu_{en}-L_{en}) - \sin(\mu_{en}+L_{en}) \right] / 2\, L_{en}$$

$$-\mu_e \left[ -\cos(\mu_{en}-L_{en}) + \cos(\mu_{en}+L_{en}) \right] / 2\, L_{en}^2 \tag{187}$$

$$z_1 = 2\mu_{en} - \frac{\mu_e}{2L_{en}} \{ \cos(\mu_{en}-L_{en}) - \cos(\mu_{en}+L_{en}) - (\mu_{en}-L_{en}) \sin(\mu_{en}-L_{en})$$

$$+ (\mu_{en}+L_{en}) \sin(\mu_{en}+L_{en}) - \cos(\mu_{en}-L_{en}) + \cos(\mu_{en}+L_{en}) \}$$

$$+ \frac{(\mu_e^2+L_e^2/3)}{2L_{en}} \left[ .5 \cos(2\mu_{en}-2L_{en}) - .5 \cos(2\mu_{en}+2L_{en}) \right] \tag{188}$$

$$z_2 = \frac{(\mu_{en}-L_{en})^2 + (\mu_{en}+L_{en})^2}{2L_{en}} - \frac{(\mu_{en}^2+L_{en}^2/3)}{L_{en}}$$

$$+ \frac{\mu_e}{2L_{en}^2} \left[ (\mu_{en}-L_{en}) \cos(\mu_{en}-L_{en}) \right.$$

$$\left. - (\mu_{en}+L_{en}) \cos(\mu_{en}+L_{en}) - \sin(\mu_{en}-L_{en}) + \sin(\mu_{en}+L_{en}) \right]$$

$$- \frac{(\mu_e^2+L_e^2/3)}{2L_{en}} \left[ L_{en} + .25 \sin(2\mu_{en}-2L_{en}) - .25 \sin(2\mu_{en}+2L_{en}) \right]$$

$$- \frac{\mu_e}{2L_{en}} \left[ (\mu_{en}-L_{en}) \sin(\mu_{en}-L_{en}) - (\mu_{en}+L_{en}) \sin(\mu_{en}+L_{en}) \right]$$

$$+ \frac{(\mu_e^2+L_e^2/3)}{2L_{en}} \left[ 1 - .5 \cos(2\mu_{en}-2L_{en}) - .5 \cos(2\mu_{en}+2L_{en}) \right] \tag{189}$$

$$\frac{\partial f_2}{\partial \mu_{en}} = \frac{.5}{f_2+L_{mn}} \left[ 3z_1 - 6\,(f_1 + \mu_{mn}) \frac{\partial f_1}{\partial \mu_{en}} \right] \tag{190}$$

$$\frac{\partial f_2}{\partial L_{en}} = \frac{.5}{f_2+L_{mn}} \left[ 3z_2 - 6\,(f_1 + \mu_{mn}) \frac{\partial f_1}{\partial L_{en}} \right] \tag{191}$$

The mean and variance of the cosine of the new eccentric anomaly follow.

$$\mu_{cen} = \frac{1}{2L_{en}} \left[ -\sin(\mu_{en}-L_{en}) + \sin(\mu_{en}+L_{en}) \right] \tag{192}$$

$$\sigma^2_{cen} = \frac{1}{2L_{en}} [\ L_{en} + .25 \sin(2\mu_{en}+2L_{en}) - .25 \sin(2\mu_{en}-2L_{en})\ ] - \mu^2_{cen} \tag{193}$$

The mean and variance of the cosine of the new true anomaly follow.

$$y = -e + \cos(E_n) \tag{194}$$

$$\mu_y = -\mu_e + \mu_{cen} \tag{195}$$

$$\sigma^2_y = \tfrac{1}{3} L^2_e + \tfrac{1}{3} L^2_{cen} \tag{196}$$

$$z = 1 - e\cos(E_n) \tag{197}$$

$$\mu_z = 1 - \mu_e\mu_{cen} \tag{198}$$

$$\sigma^2_z = \tfrac{1}{3} ( L^2_{cen}\mu^2_e + \mu^2_{cen}L^2_e ) + \tfrac{1}{9} L^2_{cen}L^2_e \tag{199}$$

$$\mu_{cvn} = \frac{\mu_y}{2L_z} \log\left( \frac{\mu_z + L_z}{\mu_z - L_z} \right) \tag{200}$$

$$\sigma^2_{cvn} = \frac{\mu^2_y}{2L_z(\mu_z-L_z)} + \frac{L^2_y}{6L_z(\mu_z-L_z)} - \frac{\mu^2_y}{2L_z(\mu_z+L_z)} - \frac{L^2_y}{6L_z(\mu_z+L_z)} - \mu^2_{cvn} \tag{201}$$

The mean and variance of the new true anomaly follow.

$$\mu_{vn} = \frac{1}{2L_{cvn}} [\ -(\mu_{cvn}-L_{cvn}) \cos^{-1}(\mu_{cvn}-L_{cvn}) + (\mu_{cvn}+L_{cvn}) \cos^{-1}(\mu_{cvn}+L_{cvn}) - \sqrt{1-(\mu_{cvn}+L_{cvn})^2} + \sqrt{1-(\mu_{cvn}-L_{cvn})^2}\ ] \tag{202}$$

$$\sigma^2_{vn} = \frac{1}{2L_{cvn}} [\ -(\mu_{cvn}-L_{cvn}) \{\cos^{-1}(\mu_{cvn}-L_{cvn})\}^2 + (\mu_{cvn}+L_{cvn}) \{\cos^{-1}(\mu_{cvn}+L_{cvn})\}^2 - L_{cvn} - 2\sqrt{1-(\mu_{cvn}+L_{cvn})^2} \cos^{-1}(\mu_{cvn}+L_{cvn}) + 2\sqrt{1-(\mu_{cvn}-L_{cvn})^2} \cos^{-1}(\mu_{cvn}-L_{cvn})\ ] - \mu^2_{vn} \tag{203}$$

The mean and variance of the sine of the new true anomaly follow.

$$\mu_{svn} = \frac{1}{2L_{vn}} [\ \cos(\mu_{vn}-L_{vn}) - \sin(\mu_{vn}+L_{vn})\ ] \tag{204}$$

$$\sigma^2_{svn} = \frac{1}{2L_{vn}} [\ L_{vn} - .25\ \sin(2\mu_{vn}+2L_{vn}) + .25\ \sin(2\mu_{vn}-2L_{vn})\ ] - \mu^2_{svn} \tag{205}$$

The mean and variance of the new radial distance follow.

$$z = 1 + e\cos(\nu_n) \tag{206}$$

$$\mu_z = 1 + \mu_e\mu_{cvn} \tag{207}$$

$$\sigma^2_z = \tfrac{1}{3}\ (\ L^2_{cvn}\mu^2_e + \mu^2_{cvn}L^2_e\ ) + \tfrac{1}{9}\ L^2_{cvn}L^2_e \tag{208}$$

$$\mu_{rr} = \frac{\mu_p}{2L_z} \log\left( \frac{\mu_z + L_z}{\mu_z - L_z} \right) \tag{209}$$

$$\sigma^2_{rr} = \frac{\mu^2_p}{2L_z(\mu_z-L_z)} + \frac{L^2_p}{6L_z(\mu_z-L_z)} - \frac{\mu^2_p}{2L_z(\mu_z+L_z)} - \frac{L^2_p}{6L_z(\mu_z+L_z)} - \mu^2_{rr} \tag{210}$$

The mean and variance of the perifocal position vector follow.

$$\mu_{rp_1} = \mu_{rr}\ \mu_{cvn} \tag{211}$$

$$\mu_{rp_2} = \mu_{rr}\ \mu_{svn} \tag{212}$$

$$\sigma^2_{rp_1} = \tfrac{1}{3}\ (\ L^2_{rr}\mu^2_{cvn} + L^2_{cvn}\mu^2_{rr}\ ) + \tfrac{1}{9}\ L^2_{cvn}L^2_{rr} \tag{213}$$

$$\sigma^2_{rp_2} = \tfrac{1}{3}\ (\ L^2_{rr}\mu^2_{svn} + L^2_{svn}\mu^2_{rr}\ ) + \tfrac{1}{9}\ L^2_{svn}L^2_{rr} \tag{214}$$

The mean and variance of the perifocal velocity vector follow.

$$\mu_{vp_1} = \frac{\sqrt{\eta}\ \mu_{svn}\ (\sqrt{\mu_p+L_p} - \sqrt{\mu_p-L_p})}{L_p} \tag{215}$$

$$\mu_{vp_2} = \frac{\sqrt{\eta}\ (\mu_{cvn} + \mu_e)\ (\sqrt{\mu_p+L_p} - \sqrt{\mu_p-L_p})}{L_p} \tag{216}$$

$$\sigma^2_{vp_1} = \frac{\eta}{2L_p} \log\left(\frac{\mu_p + L_p}{\mu_p - L_p}\right) (\mu^2_{svn} + L^2_{svn}/3) - \mu^2_{vp_1} \tag{217}$$

$$\sigma^2_{vp_2} = \frac{\eta}{2L_p} \log\left(\frac{\mu_p + L_p}{\mu_p - L_p}\right) (\mu^2_e + L^2_e/3) - \mu^2_{vp_2}$$
$$+ \frac{\eta}{2L_p} \log\left(\frac{\mu_p + L_p}{\mu_p - L_p}\right) (\mu^2_{cvn} + L^2_{cvn}/3) + \frac{\eta}{L_p} \log\left(\frac{\mu_p + L_p}{\mu_p - L_p}\right) \mu_e \mu_{cvn} \tag{218}$$

The mean and variance of the Cartesian-based final position vector follow. Those for the velocity vector are identical with these with position information replaced with corresponding velocity information.

$$\mu_{rn_1} = \mu_{rp_1}\mu_{com}\mu_{cw} - \mu_{rp_1}\mu_{som}\mu_{sw}\mu_{cin} - \mu_{rp_2}\mu_{com}\mu_{sw}$$
$$- \mu_{rp_2}\mu_{som}\mu_{cw}\mu_{cin} \tag{219}$$

$$\mu_{rn_2} = \mu_{rp_1}\mu_{som}\mu_{cw} + \mu_{rp_1}\mu_{com}\mu_{sw}\mu_{cin} - \mu_{rp_2}\mu_{som}\mu_{sw}$$
$$+ \mu_{rp_2}\mu_{com}\mu_{cw}\mu_{cin} \tag{220}$$

$$\sigma^2_{rn_1} = (\mu^2_{rp_1} + L^2_{rp_1}/3)\,(\mu^2_{com} + L^2_{com}/3)\,(\mu^2_{cw} + L^2_{cw}/3)$$
$$- 2\,(\mu^2_{rp_1} + L^2_{rp_1}/3)\,\mu_{som}\mu_{com}\mu_{cw}\mu_{sw}\mu_{cin}$$
$$- 2\,(\mu^2_{com} + L^2_{com}/3)\,\mu_{rp_1}\mu_{rp_2}\mu_{cw}\mu_{sw}$$
$$- 2\,(\mu^2_{cw} + L^2_{cw}/3)\,\mu_{som}\mu_{com}\mu_{rp_1}\mu_{rp_2}\mu_{cin}$$
$$+ (\mu^2_{rp_1} + L^2_{rp_1}/3)\,(\mu^2_{som} + L^2_{som}/3)\,(\mu^2_{sw} + L^2_{sw}/3)\,(\mu^2_{cin} + L^2_{cin}/3)$$
$$+ 2\,(\mu^2_{sw} + L^2_{sw}/3)\,\mu_{som}\mu_{com}\mu_{rp_1}\mu_{rp_2}\mu_{cin}$$
$$+ 2\,(\mu^2_{som} + L^2_{som}/3)\,\mu_{sw}\mu_{cw}\mu_{rp_1}\mu_{rp_2}\,(\mu^2_{cin} + L^2_{cin}/3)$$
$$+ (\mu^2_{rp_2} + L^2_{rp_2}/3)\,(\mu^2_{com} + L^2_{com}/3)\,(\mu^2_{sw} + L^2_{sw}/3)$$
$$+ 2\,(\mu^2_{rp_2} + L^2_{rp_2}/3)\,\mu_{som}\mu_{com}\mu_{cw}\mu_{sw}\mu_{cin}$$

$$+ (\mu_{rp_2}^2 + L_{rp_2}^2/3)\,(\mu_{som}^2 + L_{som}^2/3)\,(\mu_{cw}^2 + L_{cw}^2/3)\,(\mu_{cin}^2 + L_{cin}^2/3)$$

$$- \mu_{rp_1}^2 \tag{221}$$

$$\sigma_{rn_2}^2 = (\mu_{rp_1}^2 + L_{rp_1}^2/3)\,(\mu_{som}^2 + L_{som}^2/3)\,(\mu_{cw}^2 + L_{cw}^2/3)$$

$$+ 2\,(\mu_{rp_1}^2 + L_{rp_1}^2/3)\,\mu_{som}\mu_{com}\mu_{cw}\mu_{sw}\mu_{cin}$$

$$- 2\,(\mu_{som}^2 + L_{som}^2/3)\,\mu_{rp_1}\mu_{rp_2}\mu_{cw}\mu_{sw}$$

$$+ 2\,(\mu_{cw}^2 + L_{cw}^2/3)\,\mu_{som}\mu_{com}\mu_{rp_1}\mu_{rp_2}\mu_{cin}$$

$$+ (\mu_{rp_1}^2 + L_{rp_1}^2/3)\,(\mu_{com}^2 + L_{com}^2/3)\,(\mu_{sw}^2 + L_{sw}^2/3)\,(\mu_{cin}^2 + L_{cin}^2/3)$$

$$- 2\,(\mu_{sw}^2 + L_{sw}^2/3)\,\mu_{som}\mu_{com}\mu_{rp_1}\mu_{rp_2}\mu_{cin}$$

$$+ 2\,(\mu_{com}^2 + L_{com}^2/3)\,\mu_{sw}\mu_{cw}\mu_{rp_1}\mu_{rp_2}\,(\mu_{cin}^2 + L_{cin}^2/3)$$

$$+ (\mu_{rp_2}^2 + L_{rp_2}^2/3)\,(\mu_{som}^2 + L_{som}^2/3)\,(\mu_{sw}^2 + L_{sw}^2/3)$$

$$- 2\,(\mu_{rp_2}^2 + L_{rp_2}^2/3)\,\mu_{som}\mu_{com}\mu_{cw}\mu_{sw}\mu_{cin}$$

$$+ (\mu_{rp_2}^2 + L_{rp_2}^2/3)\,(\mu_{com}^2 + L_{com}^2/3)\,(\mu_{cw}^2 + L_{cw}^2/3)\,(\mu_{cin}^2 + L_{cin}^2/3)$$

$$- \mu_{rp_2}^2 \tag{222}$$

$$\sigma_{rn_3}^2 = (\mu_{rp_1}^2 + L_{rp_1}^2/3)\,(\mu_{sin}^2 + L_{sin}^2/3)\,(\mu_{sw}^2 + L_{sw}^2/3)$$

$$+ 2\,(\mu_{sin}^2 + L_{sin}^2/3)\,\mu_{rp_1}\mu_{rp_2}\mu_{cw}\mu_{sw}$$

$$(\mu_{rp_2}^2 + L_{rp_2}^2/3)\,(\mu_{sin}^2 + L_{sin}^2/3)\,(\mu_{cw}^2 + L_{cw}^2/3) \tag{223}$$

The analytic computation of the probabilistic quantities of the conic trajectory algorithm are now complete. Example applications and comparisons with numerical results will be presented in a later chapter of this thesis.

## B. Further Solutions For Conic Variables

There are several relationships existing between conic trajectory variables that are not used in the trajectory propagation algorithm presented above. These lead to additional analytic probabilistic relationships. The input variables are again assumed to be independent with uniform probability distribution functions.

The periapse radius is a function of the eccentricity and semi-major axis.

$$r_p = a\,(\,1 - e\,) \tag{224}$$

$$\mu_{r_p} = \mu_a\,(\,1 - \mu_e\,) \tag{225}$$

$$\sigma^2_{r_p} = \tfrac{1}{3}\,(\,L_a^2 - 2\mu_e L_a^2 + \mu_e^2 L_a^2 + \mu_a^2 L_e^2\,) + \tfrac{1}{9} L_a^2 L_e^2 \tag{226}$$

The results for the apoapse radius are similar.

$$r_a = a\,(\,1 + e\,) \tag{227}$$

$$\mu_{r_a} = \mu_a\,(\,1 + \mu_e\,) \tag{228}$$

$$\sigma^2_{r_a} = \tfrac{1}{3}\,(\,L_a^2 + 2\mu_e L_a^2 + \mu_e^2 L_a^2 + \mu_a^2 L_e^2\,) + \tfrac{1}{9} L_a^2 L_e^2 \tag{229}$$

The angular momentum is a function of the radius and velocity at either the periapsis or the apoapsis.

$$h = r_p v_p = r_a v_a \tag{230}$$

$$\mu_h = \mu_{r_p}\mu_{v_p} = \mu_{r_a}\mu_{v_a} \tag{231}$$

$$\sigma^2_h = \tfrac{1}{3}\,(\,L^2_{r_p}\mu^2_{v_p} + L^2_{v_p}\mu^2_{r_p}\,) \tag{232}$$

$$v_p = \frac{h}{r_p} \tag{233}$$

$$\mu_{v_p} = \frac{\mu_h}{2L_{r_p}} \log\left( \frac{\mu_{r_p} + L_{r_p}}{\mu_{r_p} - L_{r_p}} \right) \tag{234}$$

$$\sigma^2_{v_p} = \frac{\mu_h^2}{2L_{r_p}(\mu_{r_p} - L_{r_p})} + \frac{L_h^2}{6L_{r_p}(\mu_{r_p} - L_{r_p})} - \frac{\mu_h^2}{2L_{r_p}(\mu_{r_p} + L_{r_p})} - \frac{L_h^2}{6L_{r_p}(\mu_{r_p} + L_{r_p})} - \mu^2_{v_p} \tag{235}$$

The semi-major axis can be expressed as a function of the periapse and apoapse radii.

$$a = \frac{1}{2} ( r_p + r_a ) \tag{236}$$

$$\mu_a = \frac{1}{2} ( \mu_{r_p} + \mu_{r_a} ) \tag{237}$$

$$\sigma^2_a = \frac{1}{12} ( L^2_{r_a} + L^2_{r_p} ) \tag{238}$$

The period of an elliptical orbit is a function of the semi-major axis.

$$TP = \frac{2\pi}{\sqrt{\eta}} a^{\frac{3}{2}} \tag{239}$$

$$\mu_{TP} = \frac{2\pi}{5\sqrt{\eta}} \left( [ 2\mu_a - \frac{\mu_a^2}{L_a} - L_a ] \sqrt{\mu_a - L_a} + [ 2\mu_a + \frac{\mu_a^2}{L_a} + L_a ] \sqrt{\mu_a + L_a} \right) \tag{240}$$

$$\sigma^2_{TP} = \frac{4\pi^2}{\eta} \left( \mu_a^3 + \mu_a L_a^2 \right) - \mu^2_{TP} \tag{241}$$

The velocity of a circular orbit is inversely proportional to the square root of the radius.

$$v_{cs} = \sqrt{\frac{\eta}{r_{cs}}} \tag{242}$$

$$\mu_{v_{cs}} = \frac{L_{r_{cs}} + \mu_{r_{cs}}}{L_{r_{cs}}} \sqrt{\frac{\eta}{\mu_{r_{cs}} + L_{r_{cs}}}} - \frac{L_{r_{cs}} - \mu_{r_{cs}}}{L_{r_{cs}}} \sqrt{\frac{\eta}{\mu_{r_{cs}} - L_{r_{cs}}}} \tag{243}$$

$$\sigma^2_{v_{cs}} = \frac{\eta}{2L_{r_{cs}}} \log ( \mu_{r_{cs}} + L_{r_{cs}}) - \frac{\eta}{2L_{r_{cs}}} \log ( \mu_{r_{cs}} - L_{r_{cs}} ) - \mu^2_{r_{cs}} \tag{244}$$

The escape velocity from an elliptical orbit has similar relations.

$$v_{es} = \sqrt{\frac{2\eta}{r_{es}}} \tag{245}$$

$$\mu_{v_{es}} = \frac{L_{r_{es}} + \mu_{r_{es}}}{L_{r_{es}}} \sqrt{\frac{2\eta}{\mu_{r_{es}} + L_{r_{es}}}} - \frac{L_{r_{es}} - \mu_{r_{es}}}{L_{r_{es}}} \sqrt{\frac{2\eta}{\mu_{r_{es}} - L_{r_{es}}}} \tag{246}$$

$$\sigma^2_{v_{es}} = \frac{\eta}{L_{r_{es}}} \log ( \mu_{r_{es}} + L_{r_{es}}) - \frac{\eta}{L_{r_{es}}} \log ( \mu_{r_{es}} - L_{r_{es}} ) - \mu^2_{r_{es}} \tag{247}$$

The analytic solutions provided in this chapter were based on simplifying assumptions that render them inadequate for many practical applications. If the user were to use the results to find the final state of the trajectory, he would have to assume variable independence and constant probability distribution for each step. Specifically, the probability distribution limit would be found from the covariance result through the following equation.

$$L^2 = 3\,\sigma^2 \tag{248}$$

This is not fully realistic. Furthermore, the conic algorithm can not adapt to non-perfect trajectory situations where perturbations exist. These errors will be evident in a later chapter where example results are compared with numerical ones.

# IV. Linear Approximation Solutions

This chapter presents the only method of propagating uncertainty through a trajectory known prior to the work of this thesis. It involves linearizing about a numerically propagated trajectory for each integration step and then mapping a Gaussian covariance matrix with linear techniques. The details of this method will be presented along with comments on the method's neglect of nonlinear effects.

## A. Historical Background of the Linear Approximation Method

Navigational data is gathered by a spacecraft by various optical sightings of stars and other heavenly bodies. As can be expected, errors exist in these instruments. A "best" estimate of the spacecraft trajectory state is typically found by minimizing the errors between many sightings using algorithms such as least squares and maximum likelihood estimation [6].

These estimation methods are linear. The output is given as the expected values and a covariance matrix for a Gaussian distribution. The need for mission planners is to propagate that matrix and the mean state to some later point along the trajectory.

The current method of linearizing about a nominal trajectory was developed at least three decades ago and continues to be used today. The earliest references from the Massachusetts Institute of Technology [7] utilize linear theory developed by Kalman [8] in 1960. These techniques were used for both hypothetical studies of Mars and Venus missions as well as analysis of the Apollo translunar trajectory [9].

This linear theory appeared in unmanned spaceflight analysis in the early sixties as well [10]. The same document from the Jet Propulsion Laboratory that first explained the linearized method is still passed on today to newly hired engineers. The reasons for this long-standing success is because of the difficulty in explicitly analyzing the trajectory nonlinearity.

## B. Detailed Exposition of the Linear Approximation Method

The linear approximation method can be summarized very quickly. The mean trajectory state is propagated numerically through integration of either the equations of motion or the variational equations. The covariance matrix is mapped step-to-step with a state transition matrix based on the mean trajectory state at each step.

The mean trajectory state is often called the nominal state because the covariance matrix has no affect on its propagation. More specifically, this mean state is propagated in the same way as if there were no uncertainty in the first place. This is done through numerical integration of the equations of motion or the variational equations described in an earlier chapter. This propagation method is able to include all possible perturbative effects not included in the analytic conic algorithm such as solar pressure, non-spherical planets, and third-body gravitational influences. This method models the trajectory environment very accurately.

The covariance matrix is a 6x6 matrix of the correlations between the orbital elements, as shown below.

$$\left[ \quad \sigma^2 \quad \right]$$

$s_i$ = ith element of the state vector consisting of position and velocity

$\sigma_{ij}^2$ = covariance of the ith and jth elements of the state vector s

It consists of the covariances of the position and velocity elements with respect to each other. Furthermore, each element is assumed to have a Gaussian distribution.

From linear system theory, the covariance matrix is mapped from one state in the integration process to the next state with a transition matrix as follows.

$$\left[ \quad \sigma^2 \quad \right]_{i+1} = \left[ T_{i,i+1} \right] \left[ \quad \sigma^2 \quad \right]_i \left[ T_{i,i+1} \right]^T \tag{249}$$

$\left[ \quad \sigma^2 \quad \right]_i$ = covariance matrix for the ith integration step state

$\left[ T_{i,i+1} \right]$ = transition matrix from the ith state to the (i+1)th state

The transition matrix consists of the partials of each state element with respect to each other. These quantities are available from either analytic sources such as the variational equations or numerical methods where a finite difference is used to approximate an infinitesimal difference.

Note that the probabilistic integrals described in the first chapter need not be explicitly

computed. The mean state is found independent of any knowledge of uncertainty by simply propagating the mean initial conditions as a single trajectory. The final covariance matrix is computed by mapping the initial covariance matrix linearly with a state transition matrix. This involves simple arithmetic procedures.

## C. Impact of Linearization on Accuracy

The linearization assumption used in the above algorithm leads to easy use. Propagation of the mean state without regard to uncertainty magnitudes is as simple as propagating a single trajectory. The propagation of the covariance matrix is equally simple. It is mapped with a transition matrix from step to step in the numerical integration process of propagating the mean state. Note that the Gaussian distributed elements remain Gaussian distributed because of the linearization.

**Figure 4-1**

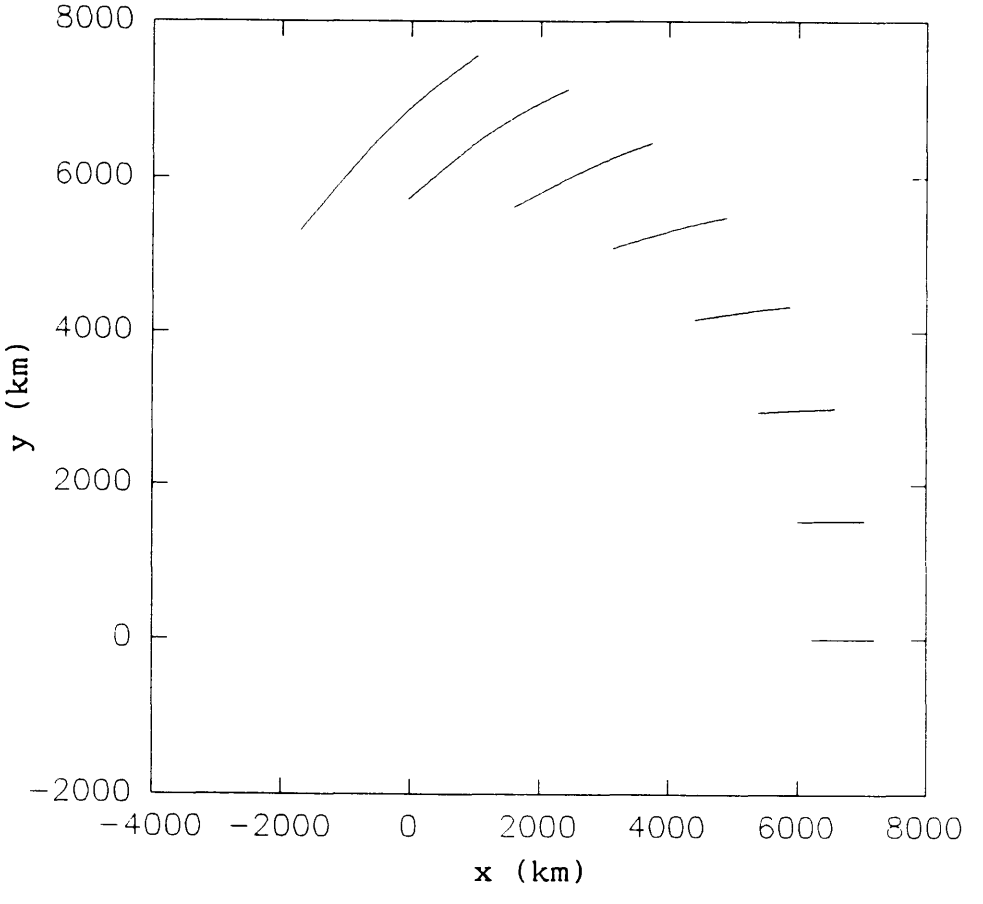

The first sacrifice of linearization is the necessity for Gaussian distributions. The unrealistic nature of this distribution can be demonstrated by considering the infinite limits that it has. Certainly there is some limit beyond which the trajectory cannot exist. Furthermore, the distribution shape may not be accurate for any number of reasons particular to each trajectory. This algorithm is inflexible with regard to distribution choice.

This linearized algorithm maintains the distribution as Gaussian. In actuality, nonlinear effects distort the initial distribution as the trajectory is propagated, as illustrated in Figure 4-1 above where the initial radial distance is uncertain. The trajectories in the distribution closest to the gravitational center curve more than those farther away. This nonlinear effect means that an initial Gaussian distribution will generally no longer be Gaussian after being propagated along a trajectory. This non-Gaussian distribution will have different moments than that given by the Gaussian result.

Another result of the linear assumption is that the mean is independent of the uncertainty magnitudes. It is propagated without regard to the rest of the distribution. If nonlinear effects are not ignored, then the distribution size and shape affect the mean. For example, suppose that the distribution consists of just two trajectories initially aligned along a radial line as shown in Figure 4-2 below. The initial mean is just the trajectory halfway between them. Consider the propagation of these two trajectories. As before, the trajectory closest to the gravitational center bends the most. The propagation of the initial mean trajectory according to the linearized method is compared with the actual mean of the two propagated distribution trajectories. As seen in Figure 4-2, the initial mean trajectory diverges from the actual mean trajectory.

The conditions under which nonlinearities have the greatest impact can be seen in the two-body equation of motion shown below.

$$\ddot{\underline{r}} + \frac{\eta}{r^3}\underline{r} = 0 \tag{250}$$

Clearly, the nonlinear term in this equation becomes less significant as the distance from the gravitational center becomes greater. Empirical demonstration of this fact is included in this thesis in a later chapter. Clearly the linear approximation method is more accurate for hyperbolic trajectories away from a planet than for elliptical trajectories or planetary flyby cases.

**Figure 4-2**

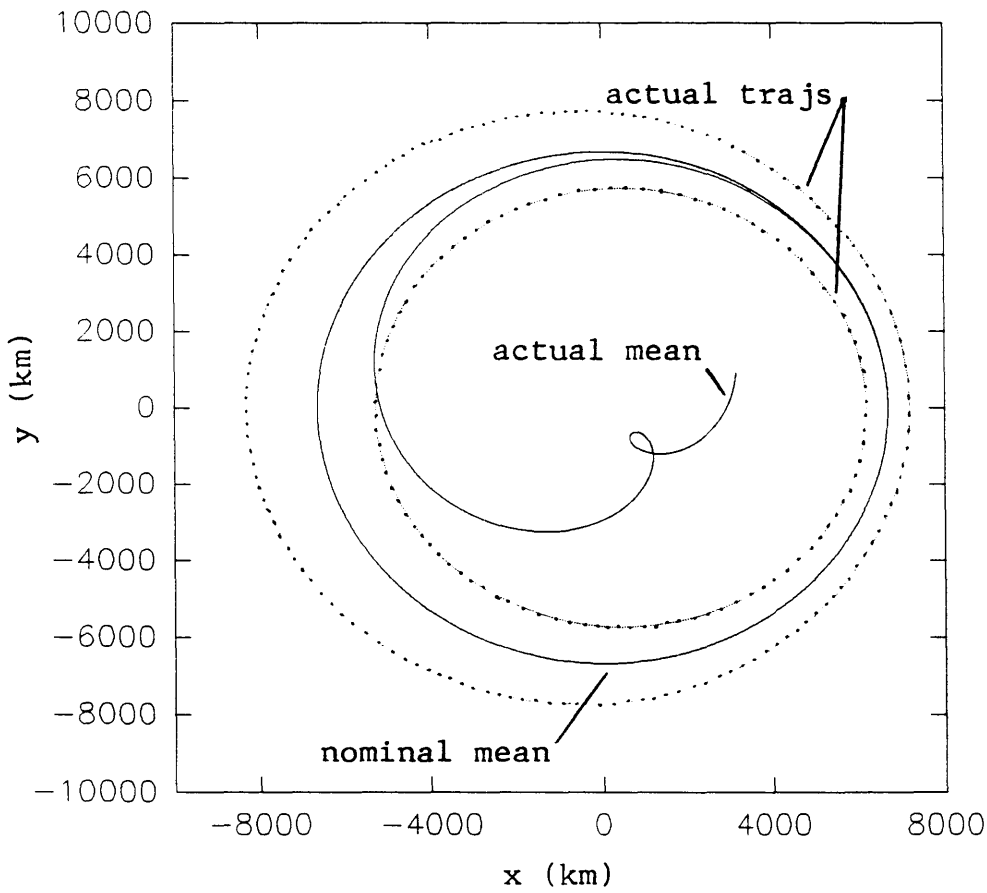
10000
8000
6000
4000
2000
0
−2000
−4000
−6000
−8000
−10000
y (km)
−8000
−4000
0
4000
8000
x (km)
actual trajs
actual mean
nominal mean

# V. Complete Numerical Solutions

The difficulty in computing the exact mean and variance integrals from the first chapter has been made very clear. In fact, the lack of an explicit trajectory solution requires numerical approaches from the very start. Therefore, possibly the only way to get the exact solutions is through numerical methods.

The purpose of this chapter is to demonstrate the application of Gaussian quadrature techniques to the integrals of concern, an approach that has never been tried previously with space trajectories. The case of dependent orbital elements is addressed.

## A. General Explanation of Gaussian Quadrature Methods

Gaussian quadrature techniques are used to compute integrals [11]. Typically, the integral is represented and computed as follows.

$$\int_b^a G(x)\, f(x)\, dx \approx \sum_{i=1}^{N} w_i\, f(x_i) \tag{251}$$

Note that the integral is converted into a finite weighted sum. For our purposes, f(x) is the trajectory algorithm. It may be either the conic algorithm or the numerical integration algorithm. The probability density function can be considered as either part of f(x) or as G(x). This thesis considers only the constant probability distribution and Gaussian probability distribution. The weights $w_i$ are particular to each quadrature algorithm order N.

For specific choices of G(x), Gaussian quadrature yields the exact solution when f(x) can be represented as a polynomial. Higher order polynominal representation requires the summation of a correspondingly higher number of terms. In our case, the trajectory algorithm is assumed to be represented by some polynomial. When there are no singularities within the effective limits of the integral, this is a good assumption. Higher order polynomial assumptions lead to higher accuracy.

Our case generally involves uncertainty in all six orbital elements. Therefore, the probabilistic integrals are six-dimensional. The Gaussian quadrature algorithm must be repeated six times within nested loops.

## B. Gauss-Legendre Quadrature For Constant Probability Density Functions

The case considered here is that of constant probability density functions for independent variables. The probabilistic integrals have finite limits and G(x) is just a constant. Therefore, the integral that is being computed is a six-dimensional integral of the trajectory function.

The quadrature scheme used is called Gauss-Legendre. Within the algorithm, the limits of the integral are scaled to (-1,1) automatically. The quadrature order is determined by user input. There is a trade-off between accuracy and algorithm speed. If the algorithm is part of a real-time guidance scheme, this can be a very important issue. The weights and abscissae can be found in many mathematical table handbooks [12]. A few of them are shown in the table below.

| $\pm x$ | N | w |
|---|---|---|
| .577 | 2 | 1.00 |
| .775 | 3 | .556 |
| .000 | 3 | .889 |
| .861 | 4 | .348 |
| .340 | 4 | .652 |

## C. Gauss-Hermitian Quadrature For Gaussian Probability Density Functions

The second case considered is that for independently distributed Gaussian variables with infinite limits. The weighting function G(z) is given below.

$$G(z) = e^{-z^2} \tag{252}$$

Recall that the Gaussian probability density function has the following form.

$$p(x) = \frac{1}{\sqrt{2\pi}\,\sigma} \exp\left(-\frac{(x-\mu)^2}{2\sigma^2}\right) \tag{253}$$

It can be transformed to the appropriate form with the following change of variables.

$$z = \frac{(x-\mu)}{\sqrt{2}\sigma} \tag{254}$$

Despite the infinite limits, the integrals can still be computed with a finite sum. The number of terms is again determined by the order of quadrature that the user selects. Several of the weights and abscissae are listed in the table below.

| $\pm x$ | N | w |
|---|---|---|
| .707 | 2 | .886 |
| .000 | 3 | 1.18 |
| 1.22 | 3 | .295 |
| .525 | 4 | .805 |
| 1.65 | 4 | .081 |

### D. Dependent Gaussian Distributed Variables

The above discussion assumed independently distributed variables. Typically in actual applications, the orbital elements are presented as dependent Gaussian variables. The probability density function is given as follows.

$$p(x) = \frac{1}{(2\pi)^3\sqrt{|S|}} \exp\left(-\frac{(x-\mu)^T S^{-1} (x-\mu)}{2}\right) \tag{255}$$

S is the 6x6 covariance matrix containing both diagonal and off-diagonal nonzero elements. A transformation matrix is constructed as follows.

$$y = A\,x \tag{256}$$

$$x = A^{-1}\,y \tag{257}$$

$A$ = transformation matrix

This transformation matrix is constructed from the eigenvectors of S so that the following holds true.

$$A\ S\ A^{-1} = \Lambda \tag{258}$$

$\Lambda$ = diagonal matrix

After substituting the transformation into the original probability density function expression, the following simplified expression results.

$$p(y) = \prod_{j=1}^{6} \frac{1}{\sqrt{2\pi}\ \sigma_j} \exp\left(-\frac{(y_j-\mu_j)^2}{2\sigma_j^2}\right) \tag{259}$$

From this point, the same change of variables as previously used is applied.

$$z = \frac{(y-\mu)}{\sqrt{2}\sigma} \tag{260}$$

The probability density function is now in the appropriate form for the application of the multi-dimensional Gauss-Hermitian algorithm.

## E. Comments on the Application of Romberg Integration Methods

The more traditional method of numerical integration is known as Romberg Integration where the area under the curve is estimated with a summation of trapezoids. This method can also be applied to Gaussian distributions with infinite limits through the following transformation.

$$\int_{-\infty}^{-2} e^{-x^2\backslash 2}\, dx = \int_{1/2}^{0} \frac{1}{t^2} e^{-1\backslash(2t^2)}\, dt \tag{261}$$

An algorithm was developed that implemented this technique. It was much too inefficient for convenient computation of the six-dimensional integrals. Therefore, it is a conclusion of this thesis that the Gaussian quadrature schemes are superior to the Romberg Integration methods for the uncertain space trajectory application.

# VI. Computer Demonstrations of Algorithms

This chapter contains actual results from computer programs utilizing the algorithms described in the previous chapters. The purpose is to demonstrate and compare the results of the various algorithms. These include the analytic algorithm, the Gaussian quadrature algorithm, the linear approximation algorithm, and the Romberg integration algorithm.

This chapter also includes examples that demonstrate the full effects of the nonlinearity on the mean and variance to emphasize the necessity of accounting for their presence. Cases where the effects are large will be compared to those where the effects are small.

The resulting graphs from these studies are shown in Appendix A. The final orbital element values are plotted versus varying deviations in the initial conditions of the trajectory. Recall that the deviation is the square root of the variance. The first three elements are the position vector elements and the second three elements are the velocity vector elements. The variation in the initial uncertainty is made by multiples of the following deviations in each position and velocity element.

Position Deviation = .5773503 km
Velocity Deviation = .0005773503 km/sec

These correspond to the deviations of constant probability distributions with limits of one unit. The mean initial trajectory state used for elliptic trajectory analysis is as follows.

$r_1 = 6700$ km
$r_2 = 100$ km
$r_3 = 50$ km
$v_1 = 0$ km/sec
$v_2 = 7.7$ km/sec
$v_3 = 1$ km/sec

It represents a typical low Earth orbit such as that used for the Space Shuttle. The mean initial trajectory state used for hyperbolic trajectory analysis is as follows.

$r_1 = 67000$ km
$r_2 = 1000$ km
$r_3 = 500$ km
$v_1 = 0$ km/sec
$v_2 = 7.7$ km/sec
$v_3 = 1$ km/sec

## A. Demonstration of the Analytic Solution Algorithm

The analytic solution algorithm is demonstrated on the elliptic trajectory above with the given uncertainties in the initial conditions. The method used here was to assume at each algorithm step that the input variables are independent and have constant probability density functions. The density function limits were set such that the variances were equal to that from the previous steps' calculations for those input variables.

Graphs 1 through 6 show the variation of the six final mean orbital elements with increasing initial deviations. Graphs 7 through 12 show the variation of the six final orbital element deviations with increasing initial deviations. Note how increasing initial deviation results in increasing variation from the nominal state.

The speed is the same as computing the nominal trajectory and does not vary with different cases. Accuracy also doesn't vary with different cases. A comparison with the complete numerical solution will be made below.

## B. Demonstration of the Romberg Integration Algorithm

The case considered here is the same as used above with the same uncertainty scheme. The results were very unsatisfactory even for higher order runs. Graph 13 shows the variation of the mean first orbital element with increasing uncertainty. Note the inaccuracy evident in the graph compared to the nominal trajectory value. Furthermore, the time required for integration is too excessive for any practical application.

## C. Demonstration of the Gauss-Legendre Quadrature Algorithm

The case considered here is the same as used above with the same uncertainty scheme. This algorithm gives good results in a reasonable time. Graph 14 shows the variation of

accuracy with quadrature order. The accuracy is very good and a third order quadrature is typically sufficient for most applications. Graph 15 shows the variation of computer time with quadrature order. The times are very reasonable for practical applications. Note that these times were from a personal computer with an "Intel 386" processor.

Graphs 16 through 21 show the variation of the six mean orbital elements with increasing uncertainty. Graphs 22 through 27 show the variation of the six orbital element deviations with increasing uncertainty.

### D. Demonstration of the Gauss-Hermitian Quadrature Algorithm

This case uses the same trajectory initial conditions as above. However, the probability density functions are Gaussian distributions. The variances are such that they are the same as those of the constant probability density functions used above. Graph 28 shows the variation of accuracy with quadrature order. The computer time variation with quadrature order is the same as Graph 15 of the Gauss-Legendre algorithm.

Graphs 29 through 34 show the variation of the six mean orbital elements with increasing uncertainty. Graphs 35 through 40 show the variation of the six orbital element deviations with increasing uncertainty.

### E. Demonstration of the Linear Approximation Algorithm

This case uses the same trajectory initial conditions and uncertainty scheme as that used in the Gauss-Hermitian algorithm demonstration above. The time of execution is very short and does not vary with different cases. Accuracy will be addressed below in comparison to the quadrature algorithm results.

Graphs 41 through 46 show the variation of the six orbital element deviations with increasing uncertainty. Recall that the mean final orbital state remains constant.

### F. Comparison of the Analytic Algorithm With the Quadrature Algorithm

The assumptions made for application of the analytic algorithm were quite bold. Yet, there seems to be a favorable comparison between the results of final mean orbital state and those from the quadrature algorithm. The trends are identical. Since the analytic algorithm is computationally faster, it may be of practical value. Its results seem to be consistently greater

than those of the quadrature algorithm's, which suggests a way to conservatively account for nonlinear effects.

Similar to the mean results, the covariance results of the partial analytic algorithm are far excessive of those from the quadrature algorithm. However, this may again have the benefit of conservative design impact while providing efficient computational effort.

### G. Comparison of the Gaussian Distributions With the Constant Distributions

A comparison can be made between cases which differ only in which probability density shape they use. In the above examples, the constant distribution was replaced with a Gaussian distribution with the same variance. Both the mean and variance results were very similar, especially when compared to the linear approximation algorithm. This suggests that the distribution shape details are less important than the general picture. The variance gives the user an idea of how the distribution is spread. Similar variances suggests similar spreads which give virtually identical results.

### H. Comparison of the Linear Approximation Algorithm With the Quadrature Algorithm

The neglect of nonlinear effects in the linear approximation algorithm are significant in the above examples. Errors increase with increasing initial uncertainty. Both the mean and the variance results show differences due to nonlinearity. This suggests that the linearization method used today may not be adequate and that engineers should at least consider nonlinear effects which are being neglected.

### I. Example Analysis of a Hyperbolic Trajectory

A hyperbolic trajectory with uncertain Gaussian distributed initial conditions was analyzed with both the quadrature algorithm and the linear approximation algorithm. Graphs 47 through 52 show the variation of the six mean orbital elements with increasing initial uncertainty as computed with the quadrature algorithm. Graphs 53 through 58 show the variation of the six orbital element deviations with increasing initial uncertainty as computed with the quadrature algorithm. The six mean orbital elements don't vary with increasing initial uncertainty as computed with the linear approximation algorithm. Graphs 59 through 64 show the variation of the six orbital element deviations with increasing uncertainty as

computed with the linear approximation algorithm.

There are small differences once again in all of the computations due to nonlinear effects. Those engineers using the linear algorithm must possibly consider these errors even with hyperbolic trajectories.

## J. Comparison Between Elliptic and Hyperbolic Trajectory Analyses

In the above examples, both elliptic and hyperbolic trajectories have been analyzed with the quadrature and linear approximation algorithms. A noticable difference between the two cases is that the nonlinear effects are much less in the hyperbolic case than in the elliptic case. This result is expected from previous discussion of regions with strongest nonlinearity. It suggests that the linear approximation algorithm may be considered acceptable for some trajectories where nonlinear effects are minimal.

## K. Example Analysis With Dependent Variables

In a previous chapter, theory was developed to accommodate dependent Gaussian distributed variables. This capability is now demonstrated with an example. The case used is from the Galileo Mission launched in 1989 on a trajectory to Jupiter by a Boeing-made upper stage called the IUS. The covariance information was obtained from a Boeing document [13]. The covariance matrix and orbital state were obtained at the end of the propulsive burn. This trajectory information was then propagated with both the quadrature algorithm and the linear approximation algorithm. The results are shown below.

Time of Flight = 3929.73 sec

| Mean Initial Orbital State | Approx. Method Resultant Orbital State | Quadrature Method Resultant Orbital State |
|---|---|---|
| -6653.15 km | 4650.95 km | 4648.24 km |
| 482.81 km | -27007.33 km | -27004.90 km |
| 1995.01 km | 13341.78 km | 13340.04 km |
| -1.0615 km/sec | 3.3597 km/sec | 3.3582 km/sec |
| -9.8316 km/sec | -5.3348 km/sec | -5.3339 km/sec |
| 5.7933 km/sec | 1.8056 km/sec | 1.8049 km/sec |

Initial Covariance Matrix

| | | | | | |
|---|---|---|---|---|---|
| 1.7 | 39.94 | -22.62 | -.0483 | .00589 | .00841 |
| 39.94 | 2079.19 | -1243.37 | -2.48 | .42 | .59 |
| -22.62 | -1243.37 | 750.14 | 1.48 | -.26 | -.36 |
| -.0483 | -2.48 | 1.48 | .00297 | -.000494 | -.000695 |
| .00589 | .42 | -.26 | -.000494 | .0000947 | .000137 |
| .00841 | .59 | -.36 | -.000695 | .000137 | .000203 |

Approx. Method Resultant Covariance Matrix

| | | | | | |
|---|---|---|---|---|---|
| 8882.43 | -1345.55 | -2161.29 | 1.4365 | .7224 | -.9180 |
| -1345.55 | 493.45 | 456.67 | -.1995 | -.05432 | .1771 |
| -2161.29 | 456.67 | 885.67 | -.3461 | -.1633 | .3057 |
| 1.4365 | -.1995 | -.3461 | .0002334 | .000121 | -.000147 |
| .7224 | -.05432 | -.1633 | .000121 | .00007 | -.00007 |
| -.9180 | .1771 | .3057 | -.000147 | -.00007 | .000113 |

Quadrature Method Resultant Covariance Matrix

| | | | | | |
|---|---|---|---|---|---|
| 8951.57 | -1202.49 | -2192.98 | 1.4615 | .7777 | -.9434 |
| -1202.49 | 2011.63 | -70.59 | -.1908 | .3757 | .005327 |
| -2192.98 | -70.59 | 1082.54 | -.3396 | -.3061 | .3624 |
| 1.4615 | -.1908 | -.3396 | .0002441 | .000130 | -.000152 |
| .7777 | .3757 | -.3061 | .000130 | .000196 | -.000121 |
| -.9434 | .005327 | .3624 | -.000152 | -.000121 | .000135 |

An interesting comparison between the quadrature algorithm and the linear approximation algorithm shows that differences exist. The actual mission used the linear method results. Since the differences are relatively small, the impact of including the nonlinear effects would have been minimal. However, the existence of the errors raises concern over the accuracy of current practices.

# VII. Conclusions

The work in this thesis demonstrates the effects of nonlinearity on uncertainty propagation in space trajectories that have not been accounted for previously. Until this work, a linear approximation algorithm was the only way to propagate the covariance matrix. A quadrature algorithm was developed that considers the full nonlinearity of the problem. It shows that errors exist in both the mean and the variance calculations of the linear method. These errors are most severe when the trajectory is close to the gravitational center. This occurs more in elliptic trajectories than in hyperbolic trajectories farther from the planet.

Contributions were also made regarding analytic solutions. The mean and variance expressions were computed for each step in the conic trajectory algorithm. These can be used to study the probabilistic relationships between orbital elements analytically.

One nonlinear effect is that the mean final orbital state is a function of the initial uncertainties' magnitudes. The linear approximation algorithm separates the variance and mean state problems because the initial variance magnitudes have no impact on the final means. However, when all nonlinear effects are considered, the variances affect the means. This puts much greater importance on the accuracy of the initial variances than before. Previous variance estimates could be conservative. However, now they must be more accurately estimated. This is also true of the probability density function shape. The problem with this is that engineers may not have the techniques to achieve this accuracy. Regardless, the nonlinearity of the problem has been shown to be significant and is now computationally tractable.

# References

[1] Halsell, C.A., "Maneuver Analysis for the Mars Observer Mission," *Advances in the Astronautical Sciences*, Vol. 71, Part II, American Astronautical Society, San Diego, CA, 1990.

[2] Pfeiffer, P.E., *Concepts of Probability Theory*, Dover, N.Y., 1978.

[3] Bate, Mueller, White, *Fundamentals of Astrodynamics*, Dover, N.Y., 1971.

[4] Battin, R.H., *An Introduction to the Mathematics and Methods of Astrodynamics*, American Institute of Aeronautics and Astronautics, N.Y., 1987.

[5] Chapra, Canale, *Numerical Methods for Engineers*, McGraw-Hill, N.Y., 1988.

[6] Franklin, Powell, Workman, *Digital Control of Dynamic Systems*, Addison-Wesley, N.Y., 1990.

[7] Battin, R.H., "Statistical Optimizing Navigation Procedure for Space Flight," *ARS Journal*, September 1962.

[8] Kalman, R.E., "A New Approach to Linear Filtering and Prediction Problems," *J. Basic Eng.*, Trans. ASME, March 1960.

[9] McLean, Schmidt, McGee, "Optimal Filtering and Linear Prediction Applied to a Space Navigation System for the Circumlunar Mission," NASA TN D-1208, March 1962.

[10] Lesh, Moyer, Solloway, "Statistics of Orbit Determination," JPL EPD-386, Pasadena, June 1966.

[11] Press, Flannery, Teukolsky, Vetterling, *Numerical Recipes*, Cambridge University Press, Cambridge, 1989.

[12] Beyer, W.H., *CRC Standard Mathematical Tables*, CRC Press, Boca Raton, Florida, 1981.

[13] Hansen, Tursa, Tillotson, Knoben, "Galileo Injection Accuracy Report," 2-3934-PJS-083/89, Boeing Aerospace, Seattle, WA, August 1989.

# Appendix A - Graphs

GRAPH 1

Mean 1st Element vs. Multiple of Initial Deviations

(Analytic Solution Algorithm)

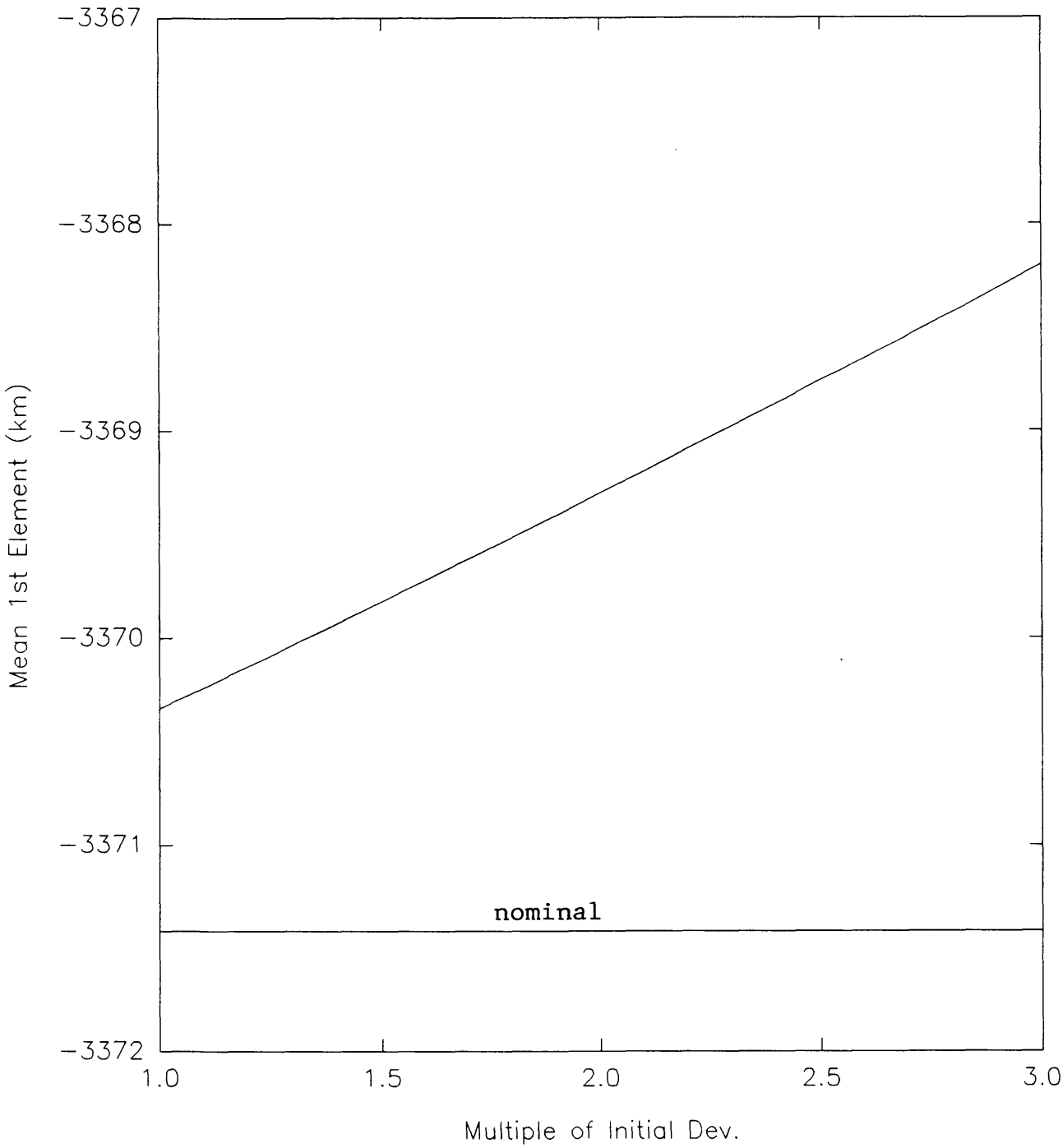

GRAPH 2

Mean 2nd Element vs. Multiple of Initial Deviations
(Analytic Solution Algorithm)

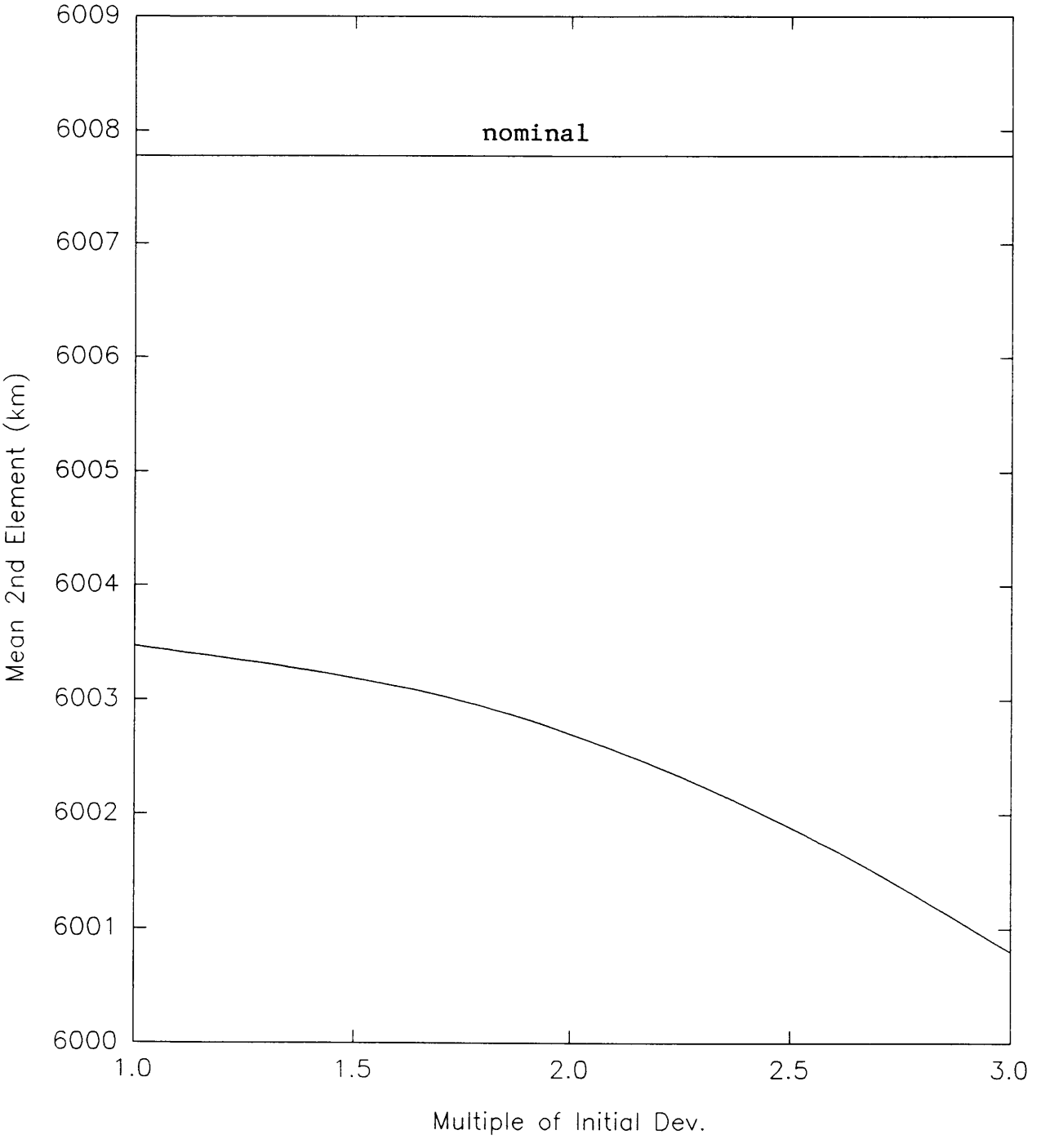

GRAPH 3

Mean 3rd Element vs. Multiple of Initial Deviations
(Analytic Solution Algorithm)

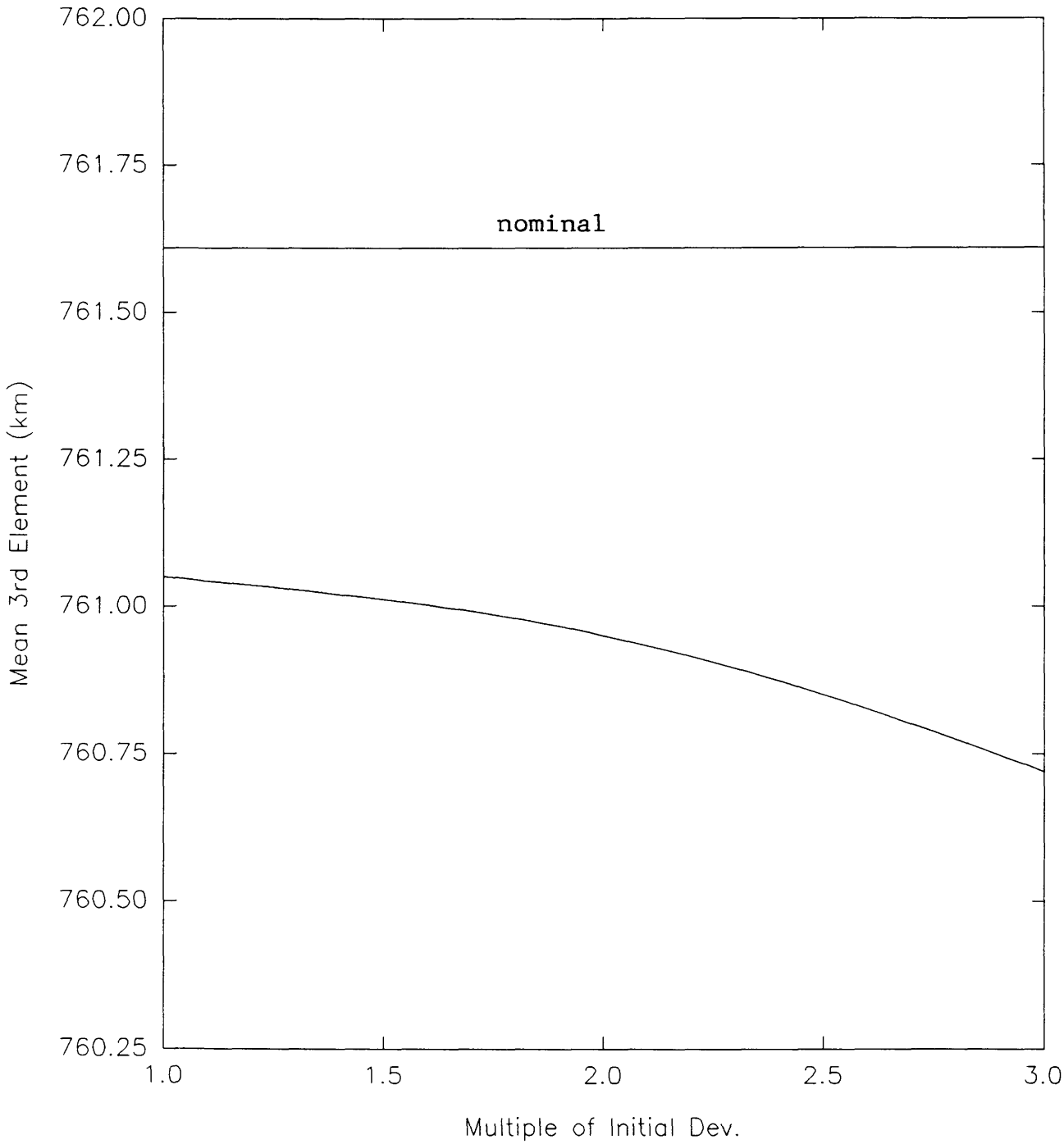

GRAPH 4

Mean 4th Element vs. Multiple of Initial Deviations
(Analytic Solution Algorithm)

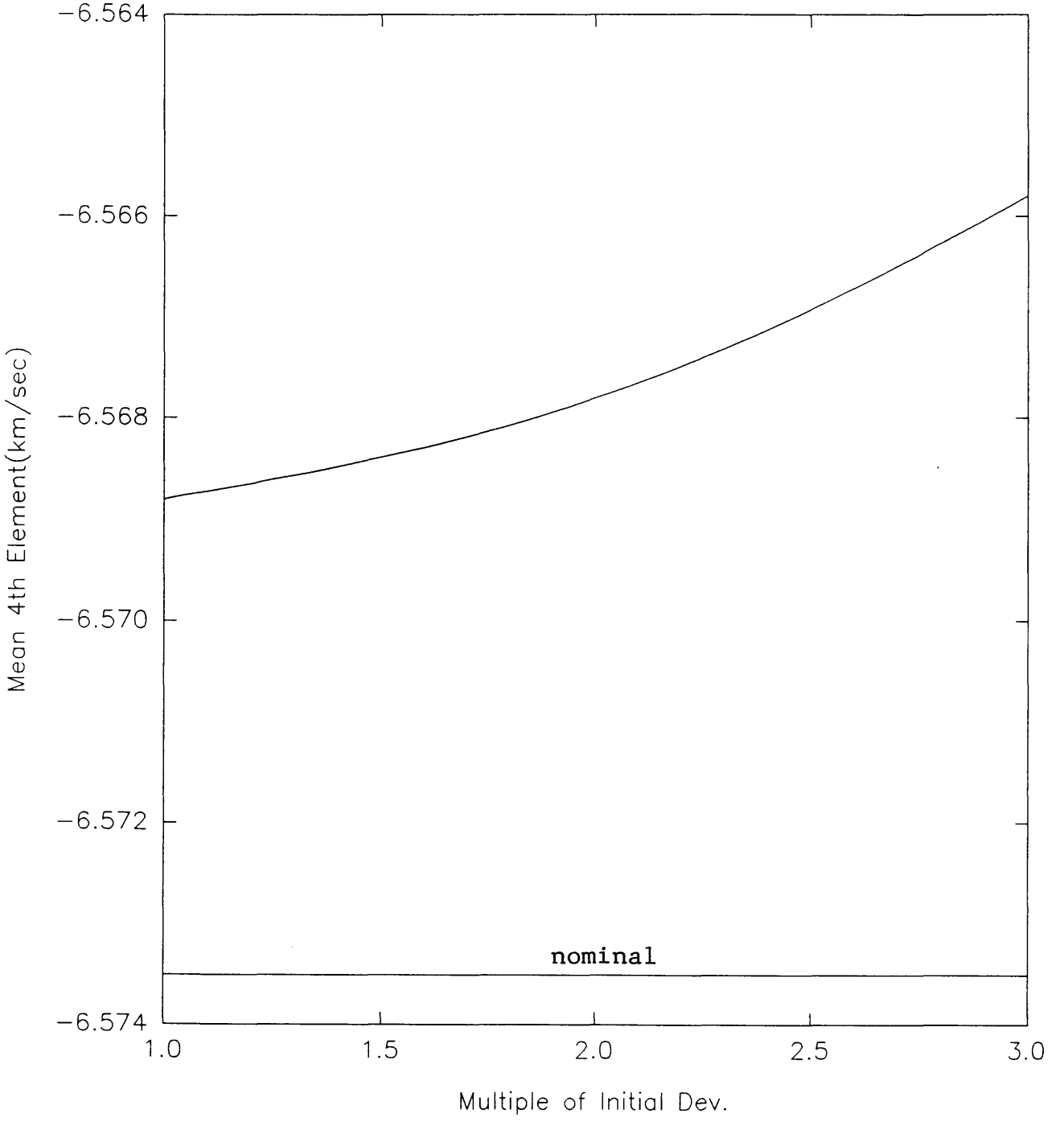

GRAPH 5

Mean 5th Element vs. Multiple of Initial Deviations
(Analytic Solution Algorithm)

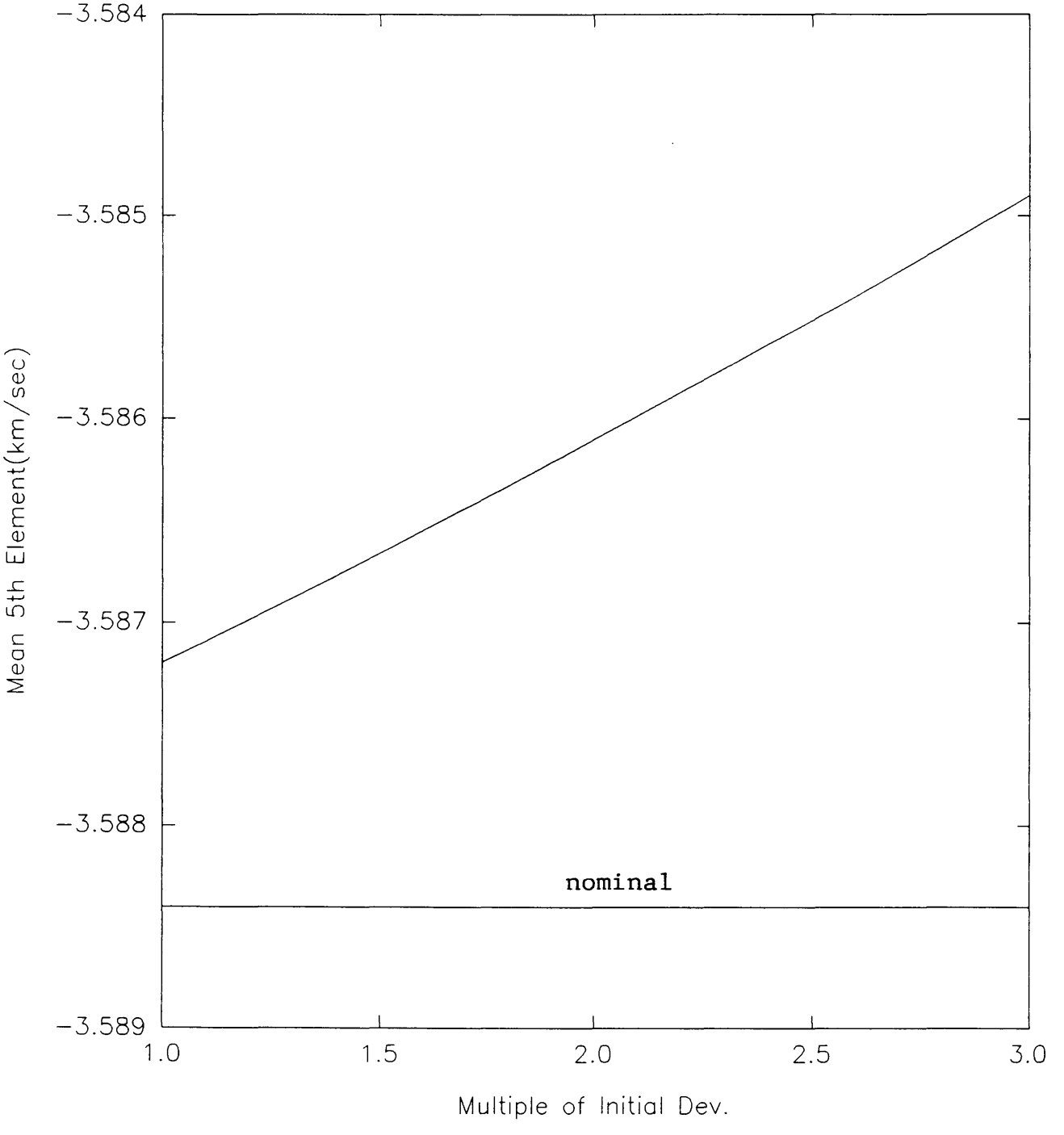

GRAPH 6

Mean 6th Element vs. Multiple of Initial Deviations

(Analytic Solution Algorithm)

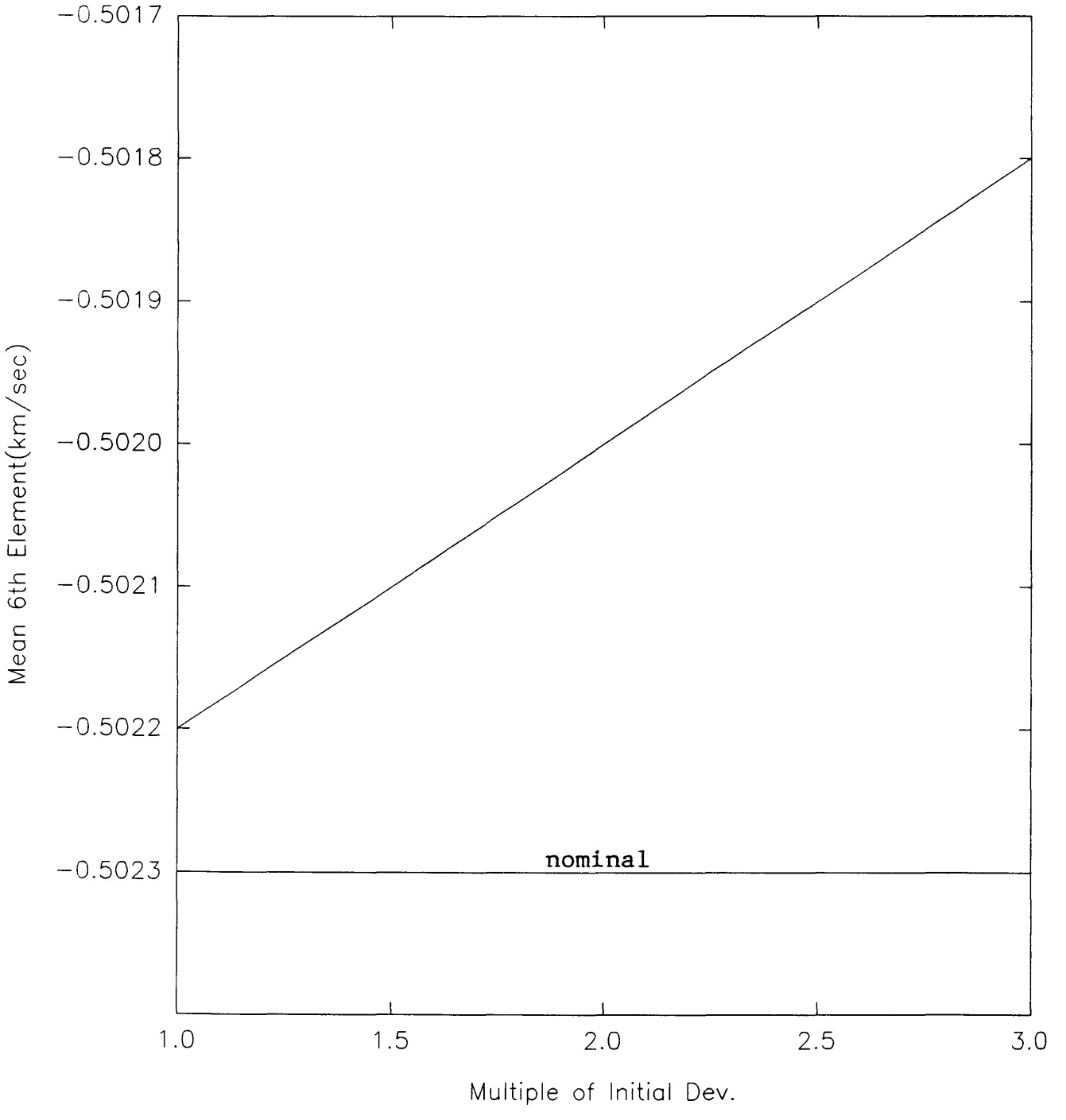

GRAPH 7

1st Element Deviation vs. Multiple of Initial Deviations
(Analytic Solution Algorithm)

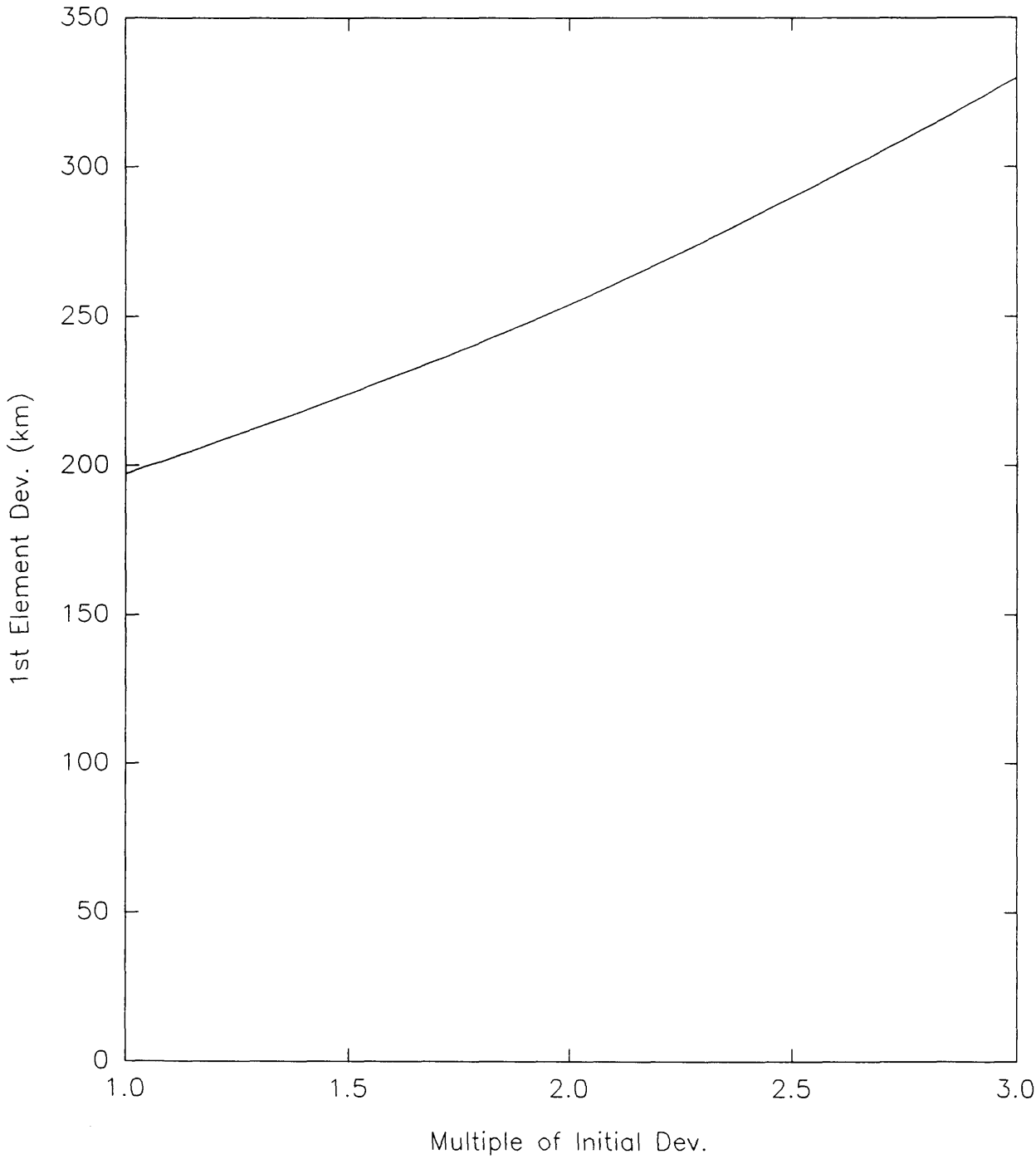

GRAPH 8

2nd Element Deviation vs. Multiple of Initial Deviations
(Analytic Solution Algorithm)

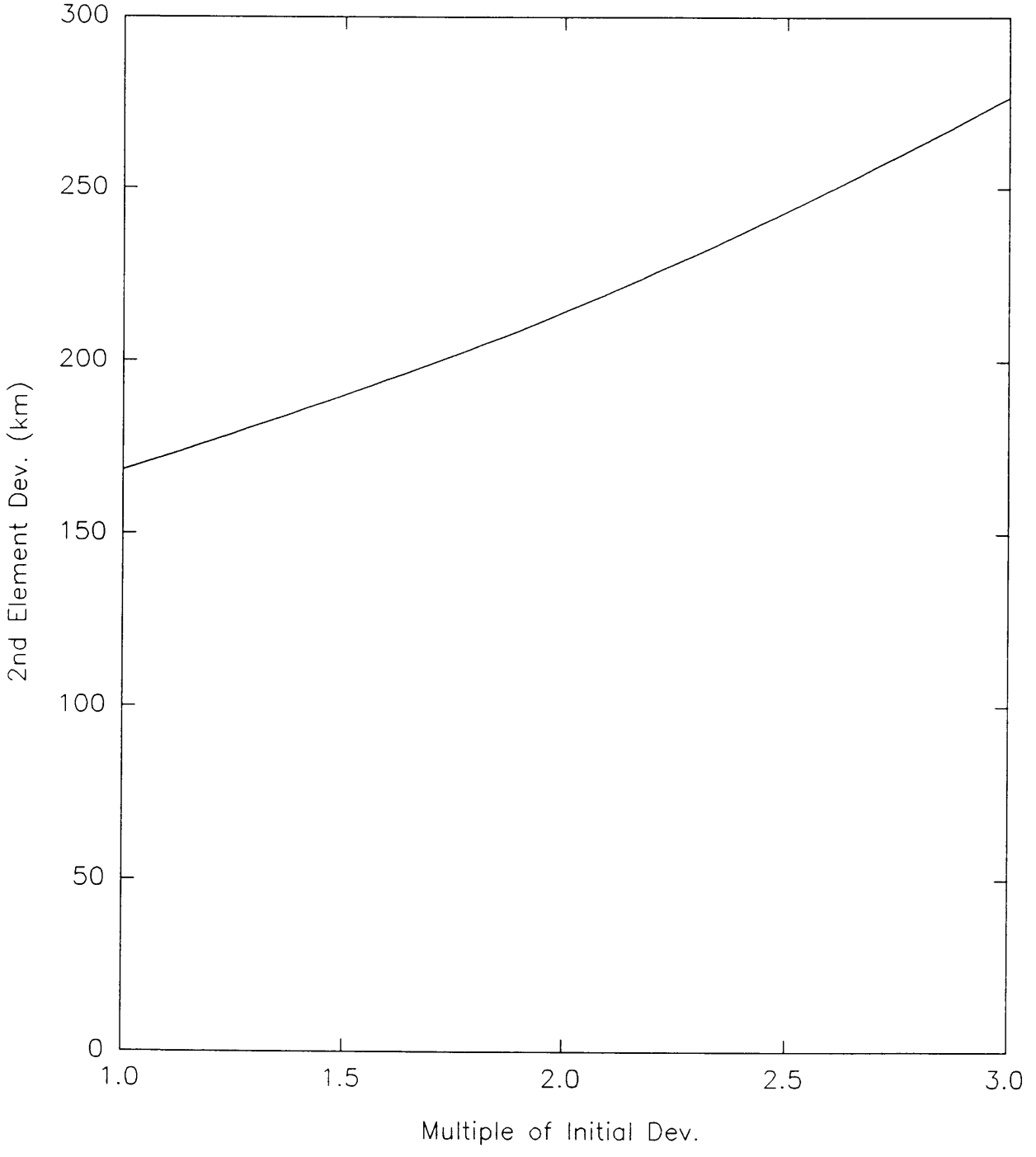

GRAPH 9

3rd Element Deviation vs. Multiple of Initial Deviations
(Analytic Solution Algorithm)

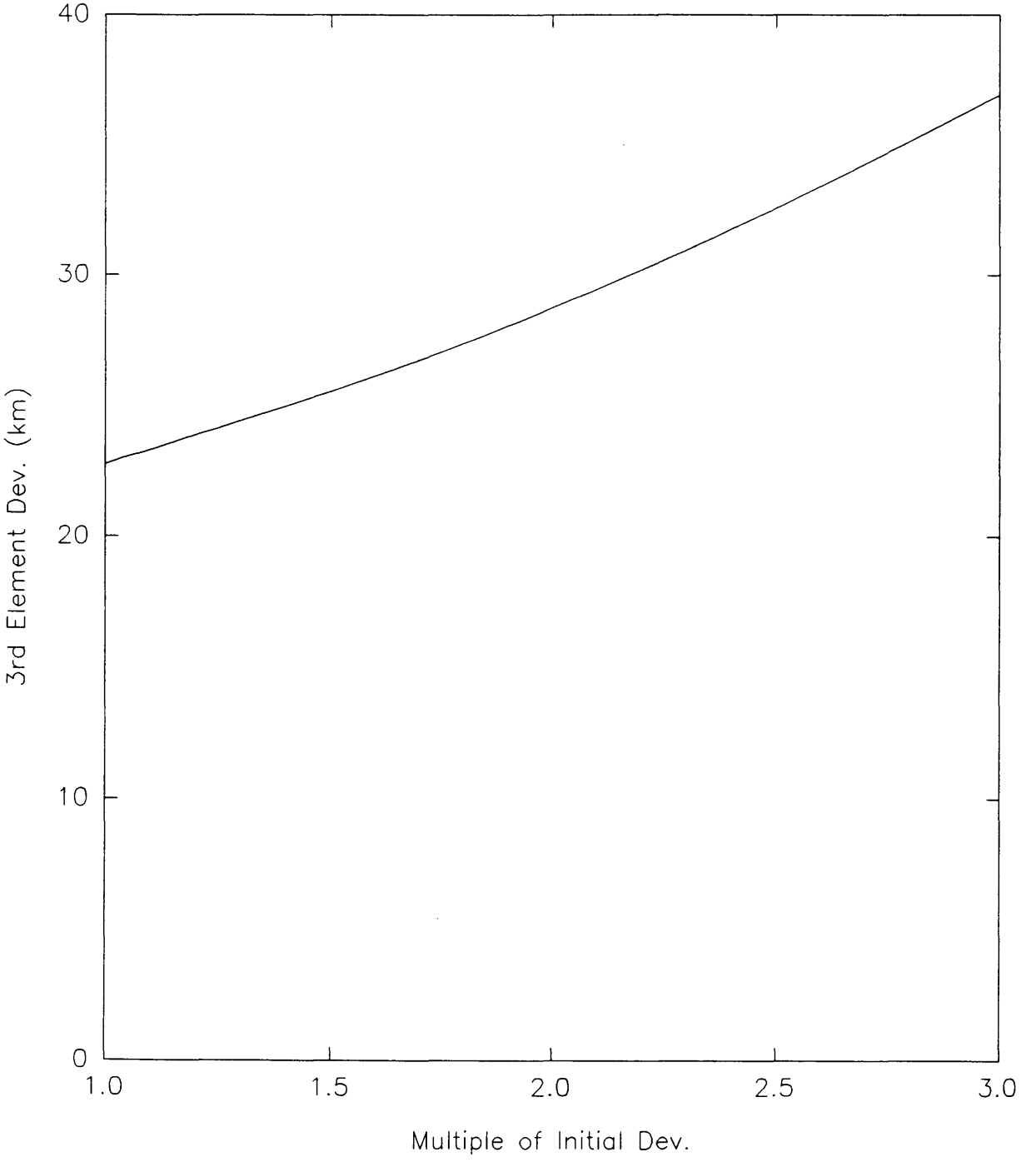

GRAPH 10

4th Element Deviation vs. Multiple of Initial Deviations
(Analytic Solution Algorithm)

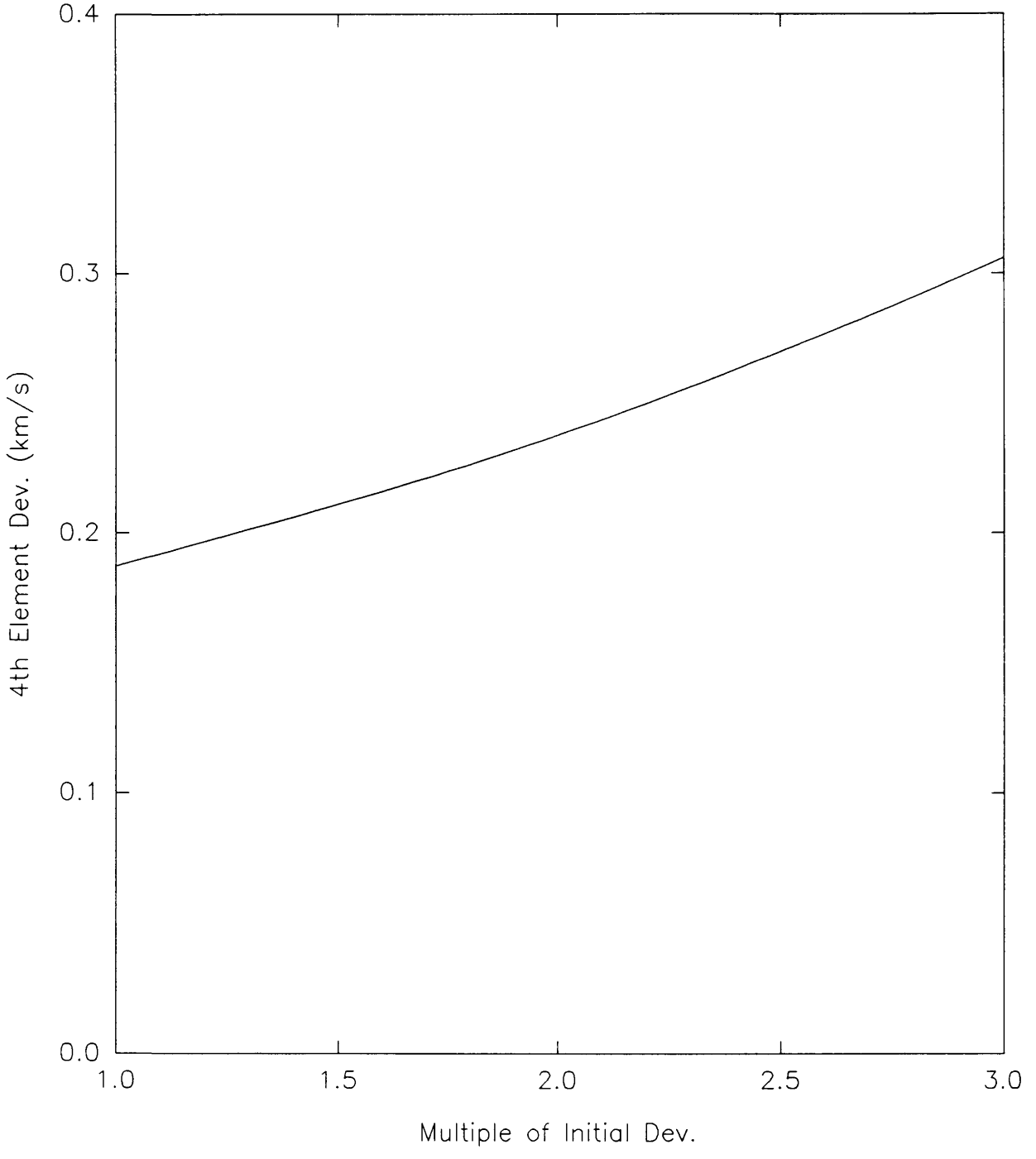

GRAPH 11

5th Element Deviation vs. Multiple of Initial Deviations
(Analytic Solution Algorithm)

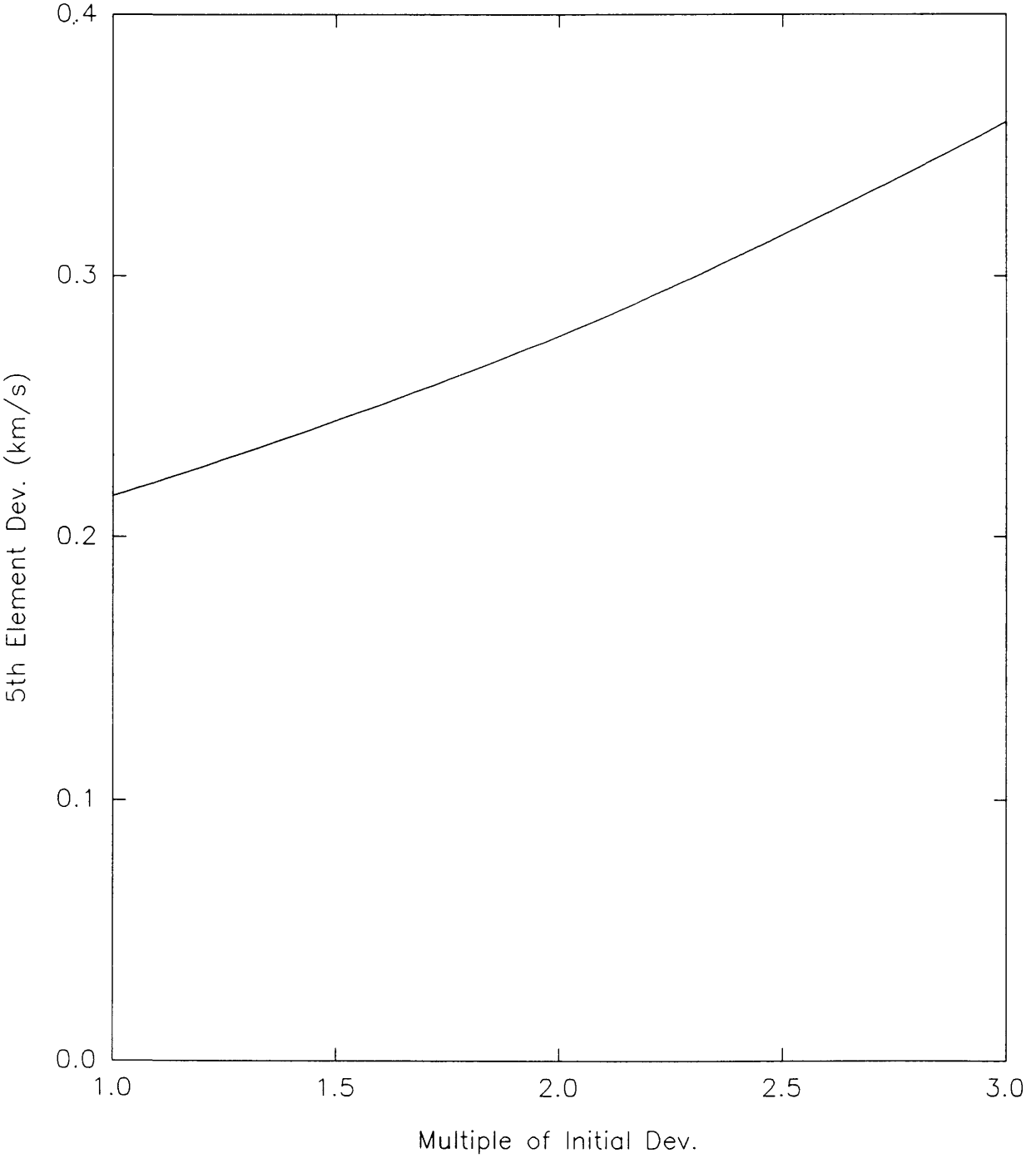

GRAPH 12

6th Element Deviation vs. Multiple of Initial Deviations
(Analytic Solution Algorithm)

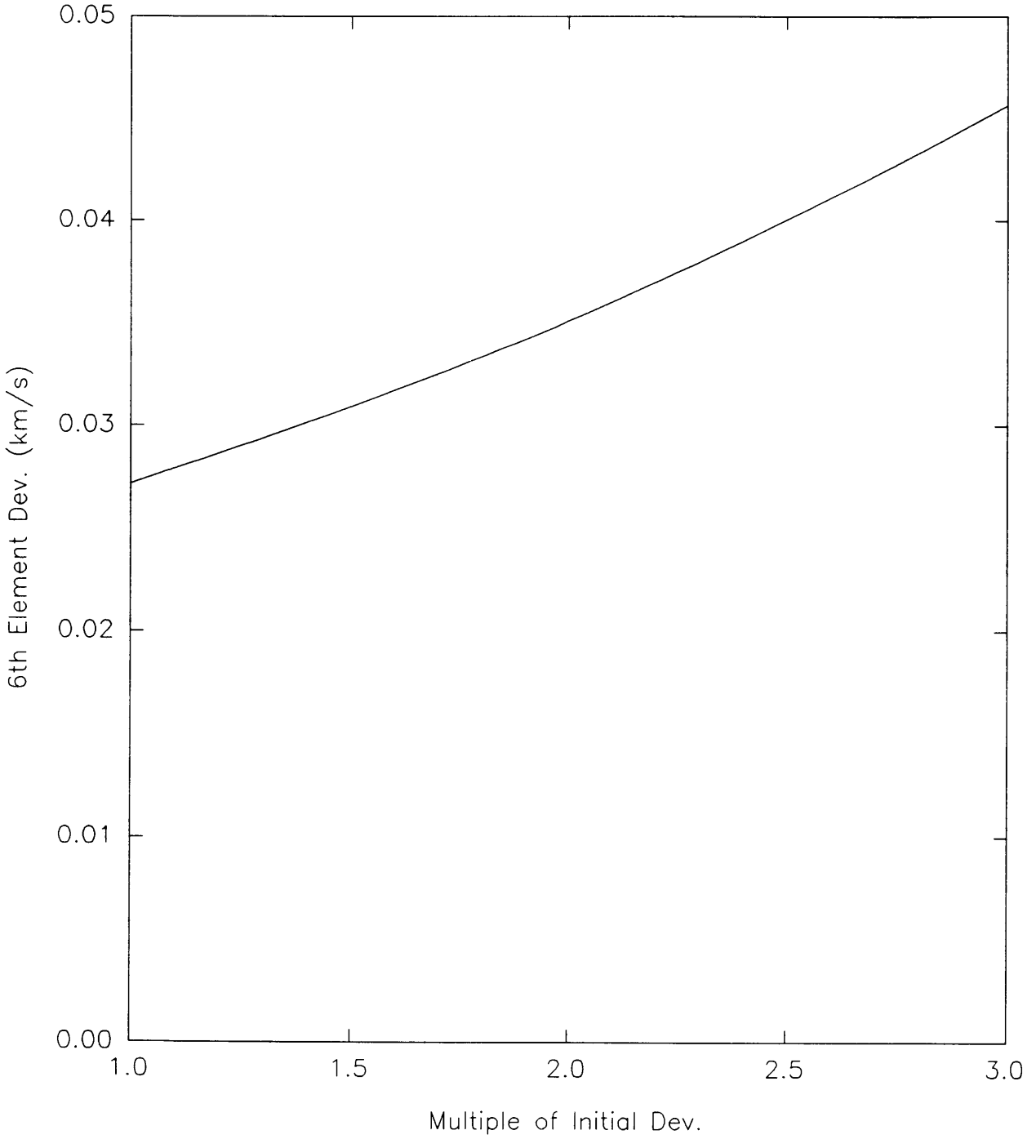

GRAPH 13

Mean 1st Element vs. Multiple of Initial Deviations

(Romberg Integration Algorithm)

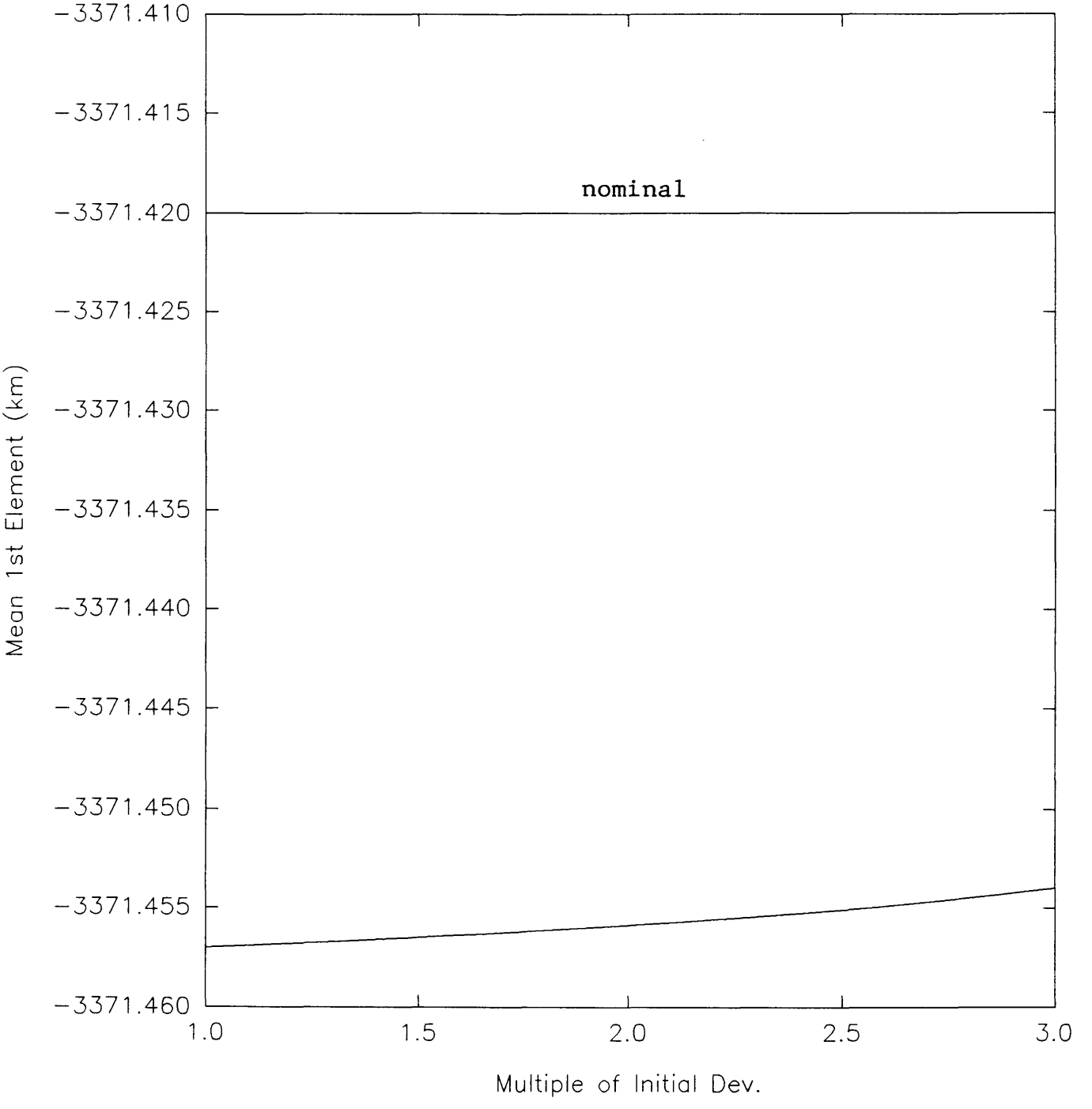

GRAPH 14
Accuracy vs. Quadrature Order
(Gauss-Hermitian Quadrature Algorithm)

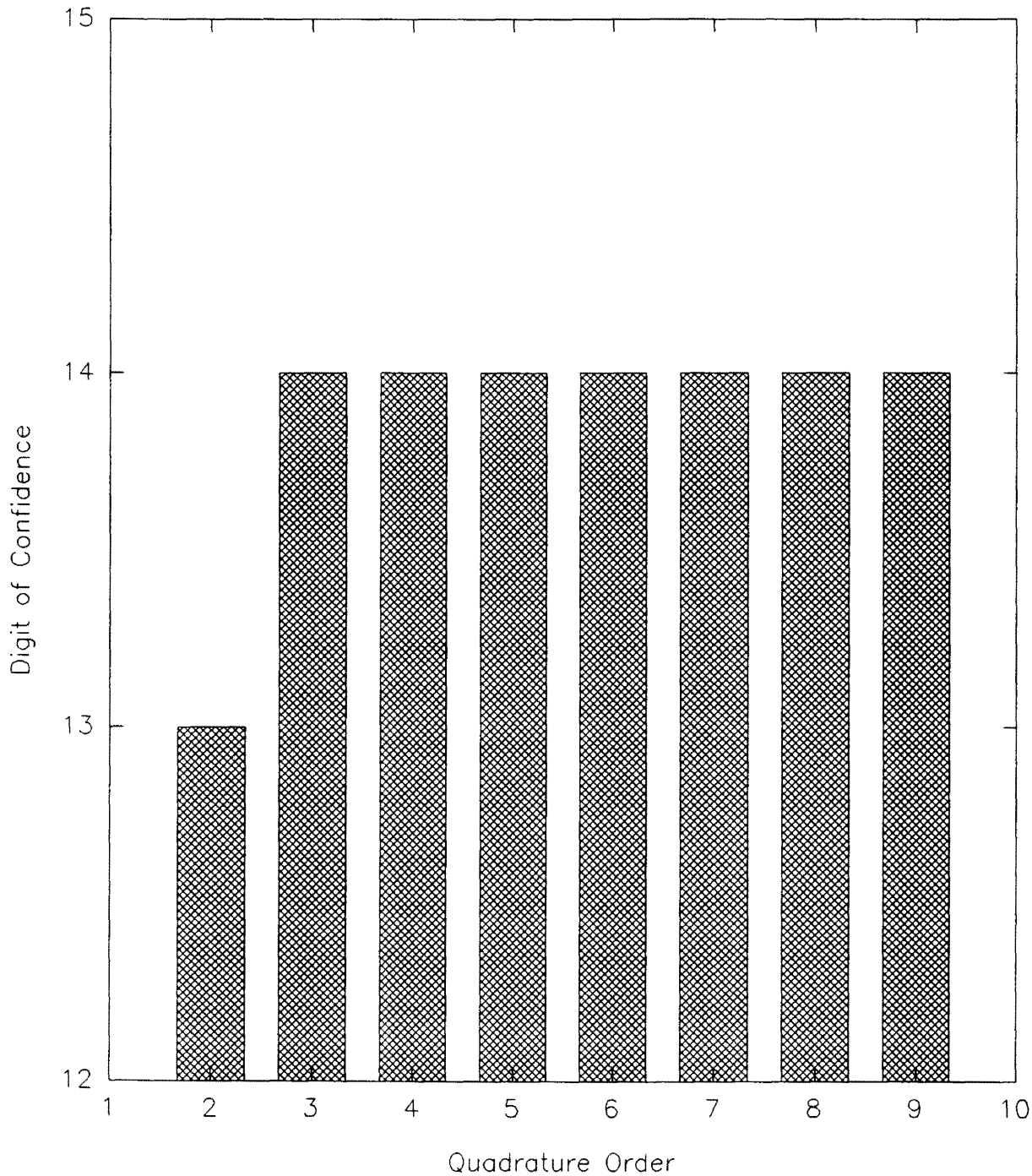

GRAPH 15
Computational Time vs. Quadrature Order
(Gauss-Legendre Quadrature Algorithm)

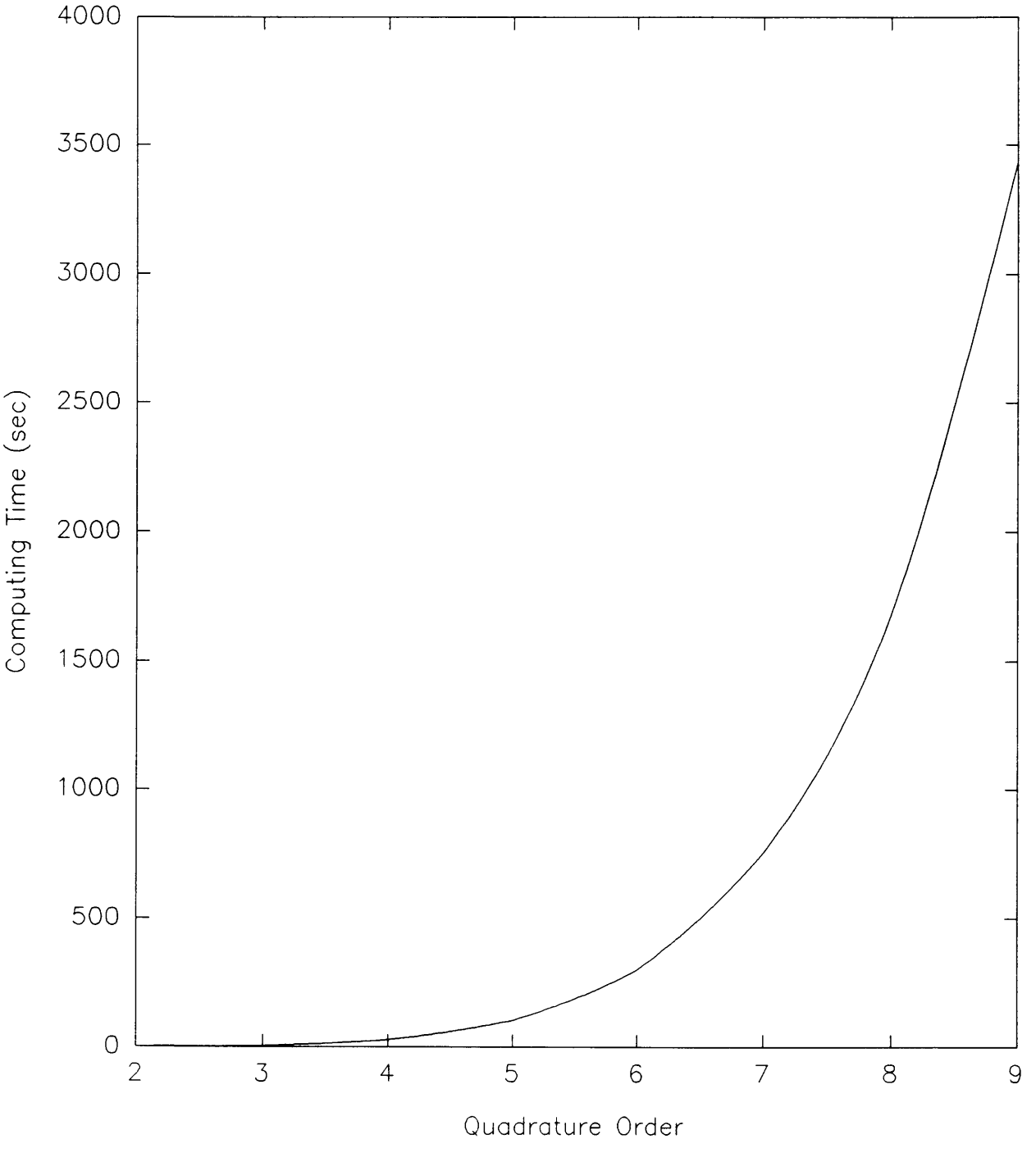

GRAPH 16

Mean 1st Element vs. Multiple of Initial Deviations

(Gauss-Legendre Quadrature Algorithm)

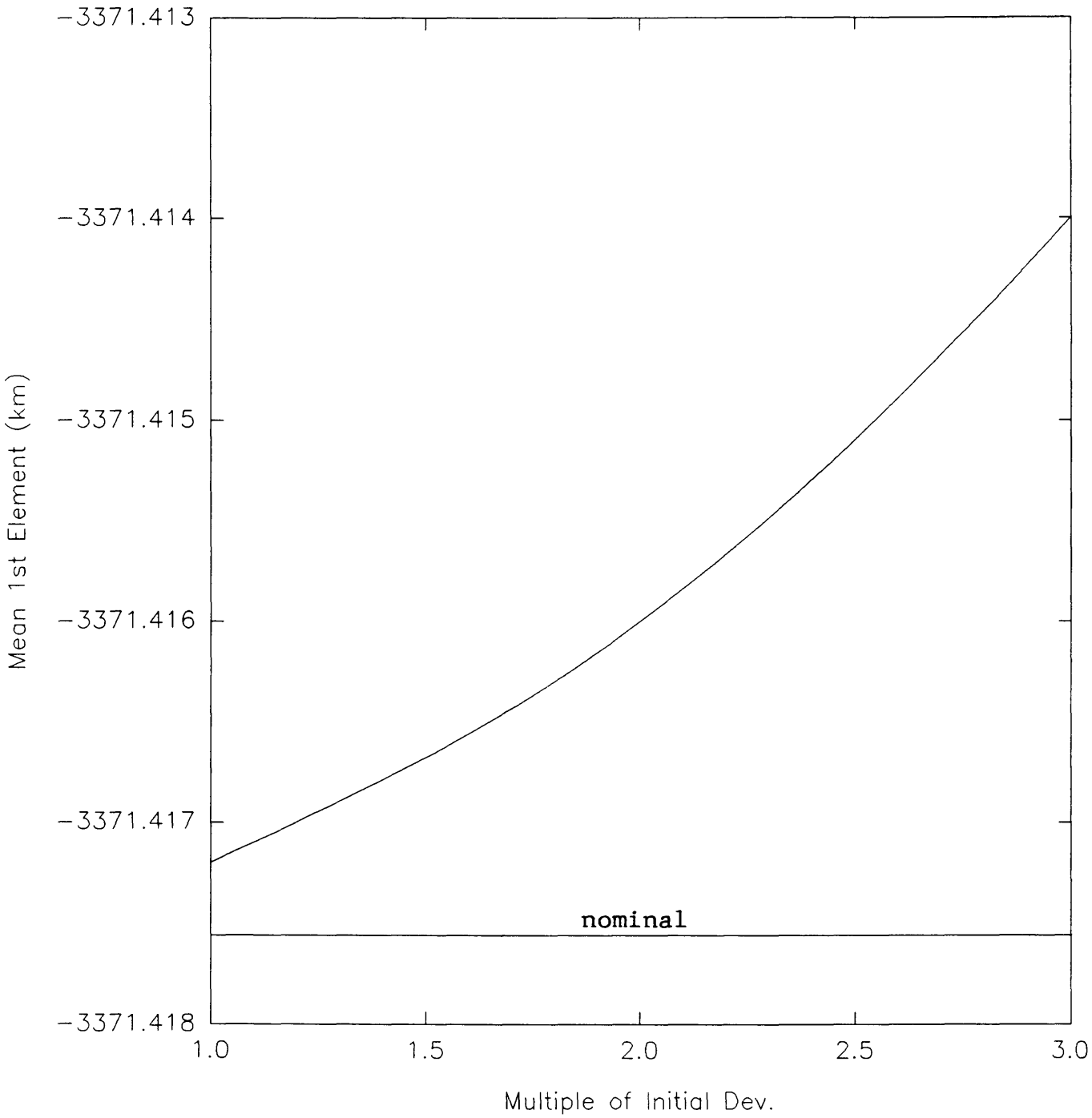

GRAPH 17

Mean 2nd Element vs. Multiple of Initial Deviations

(Gauss-Legendre Quadrature Algorithm)

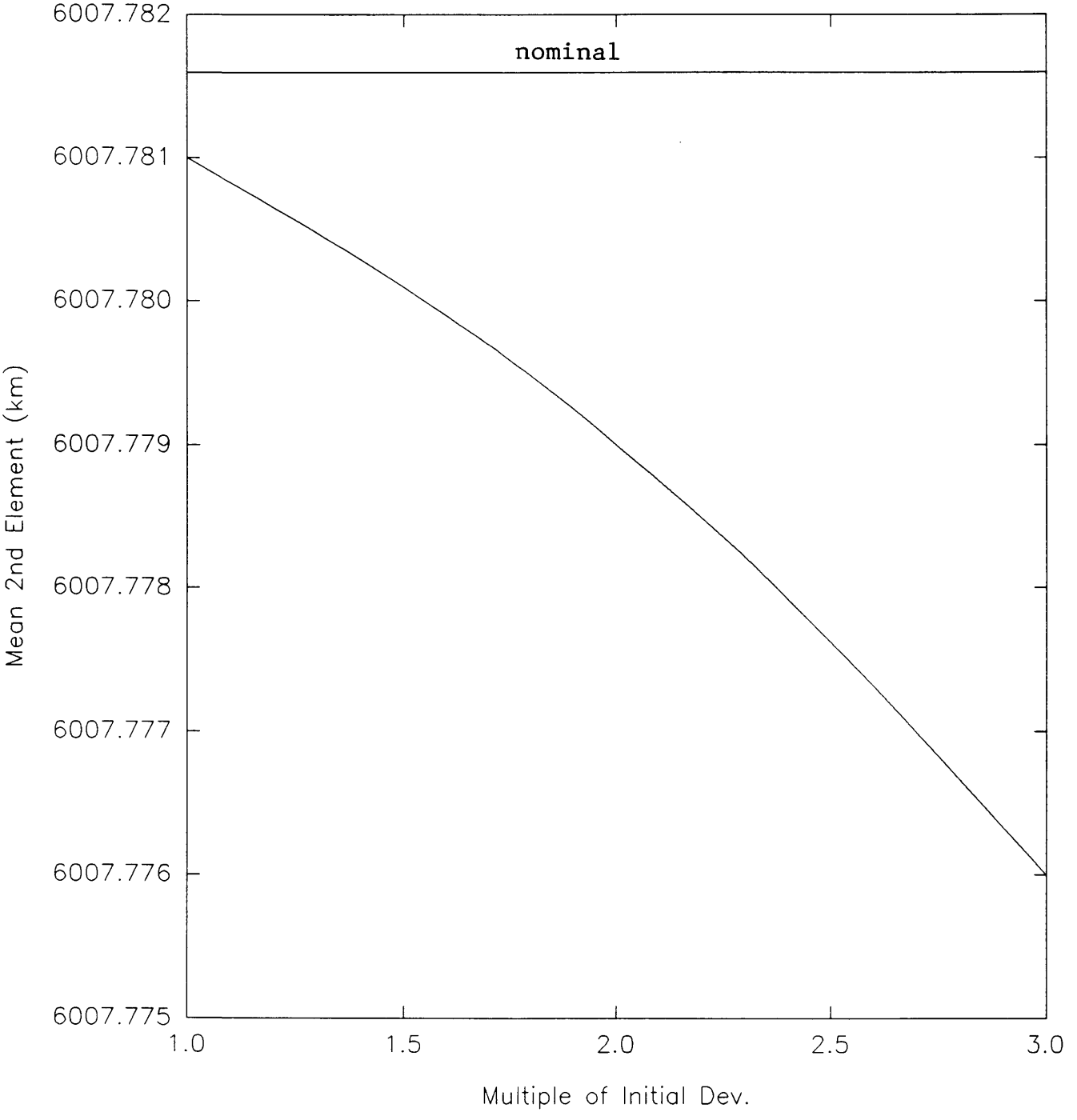

GRAPH 18

Mean 3rd Element vs. Multiple of Initial Deviations

(Gauss-Legendre Quadrature Algorithm)

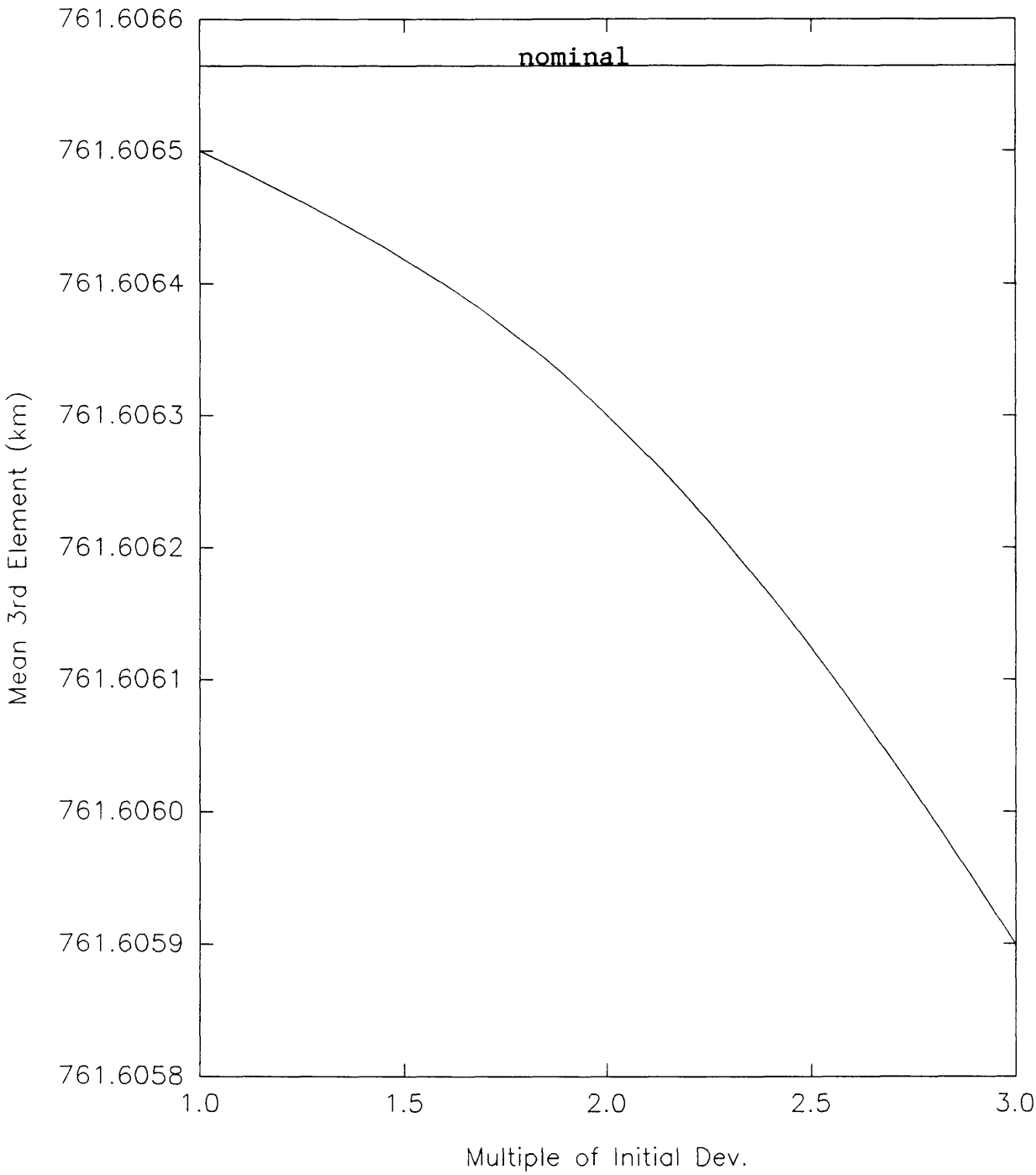

GRAPH 19

Mean 4th Element vs. Multiple of Initial Deviations
(Gauss-Legendre Quadrature Algorithm)

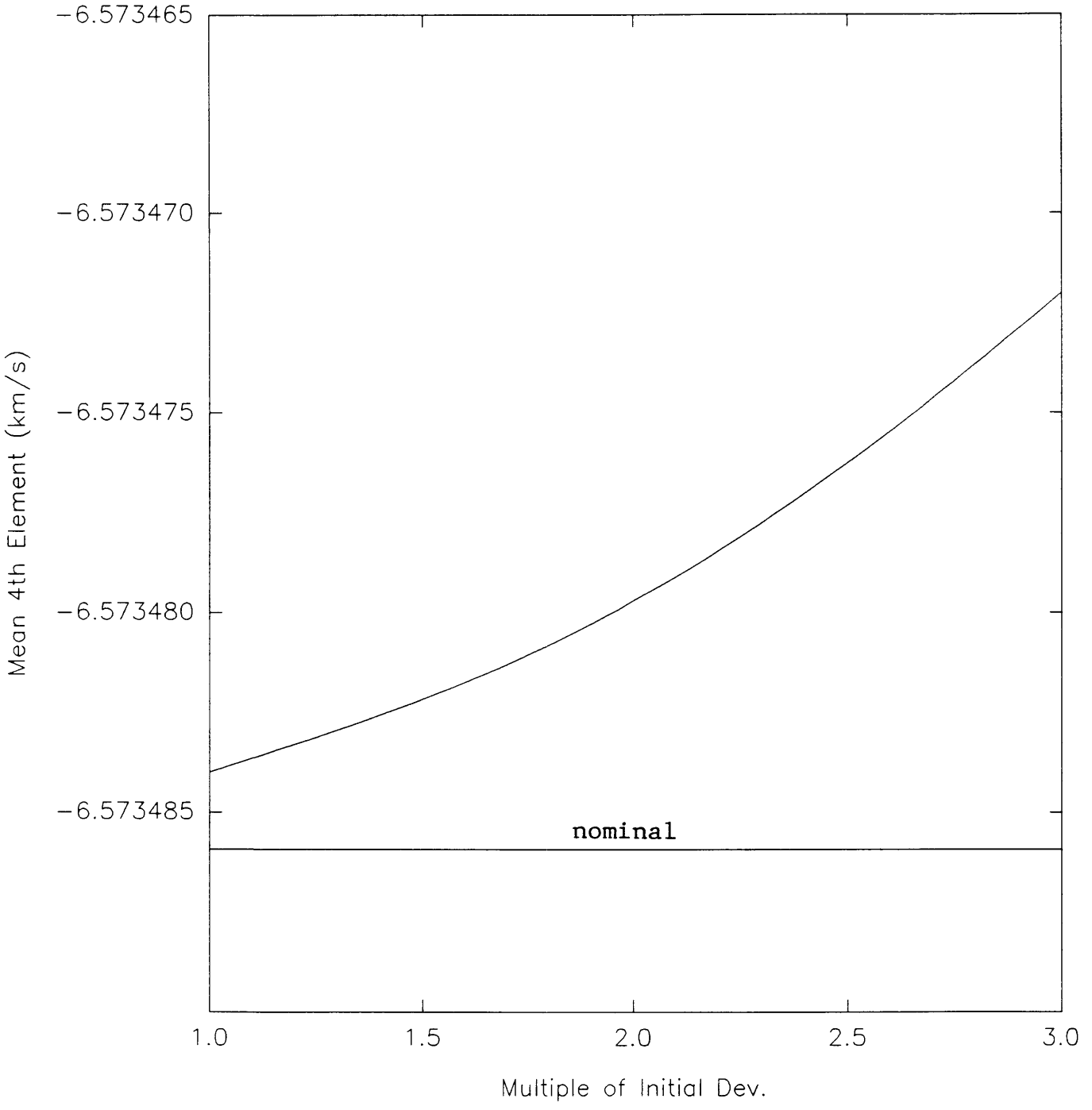

GRAPH 20

Mean 5th Element vs. Multiple of Initial Deviations

(Gauss-Legendre Quadrature Algorithm)

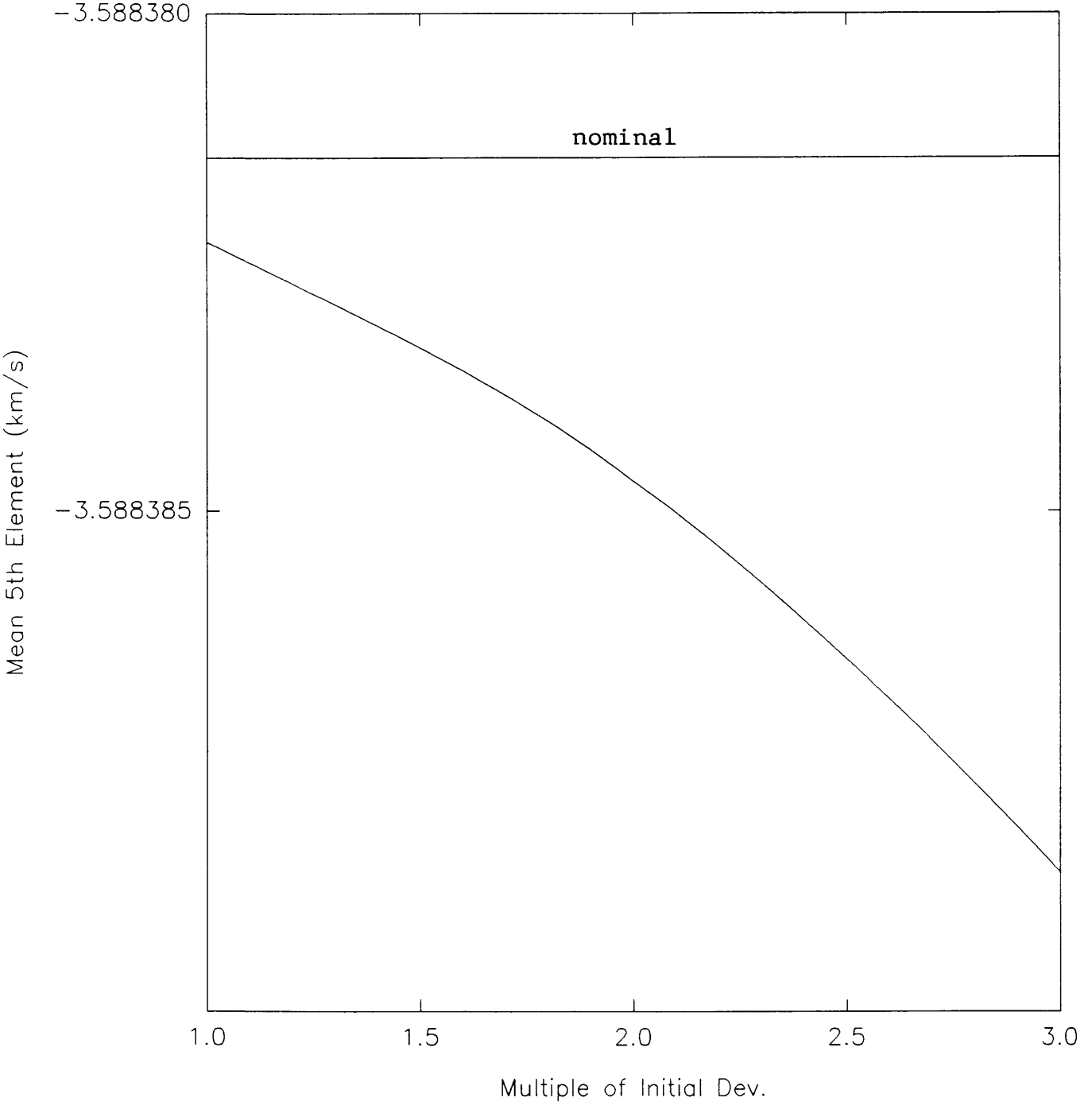

GRAPH 21

Mean 6th Element vs. Multiple of Initial Deviations

(Gauss-Legendre Quadrature Algorithm)

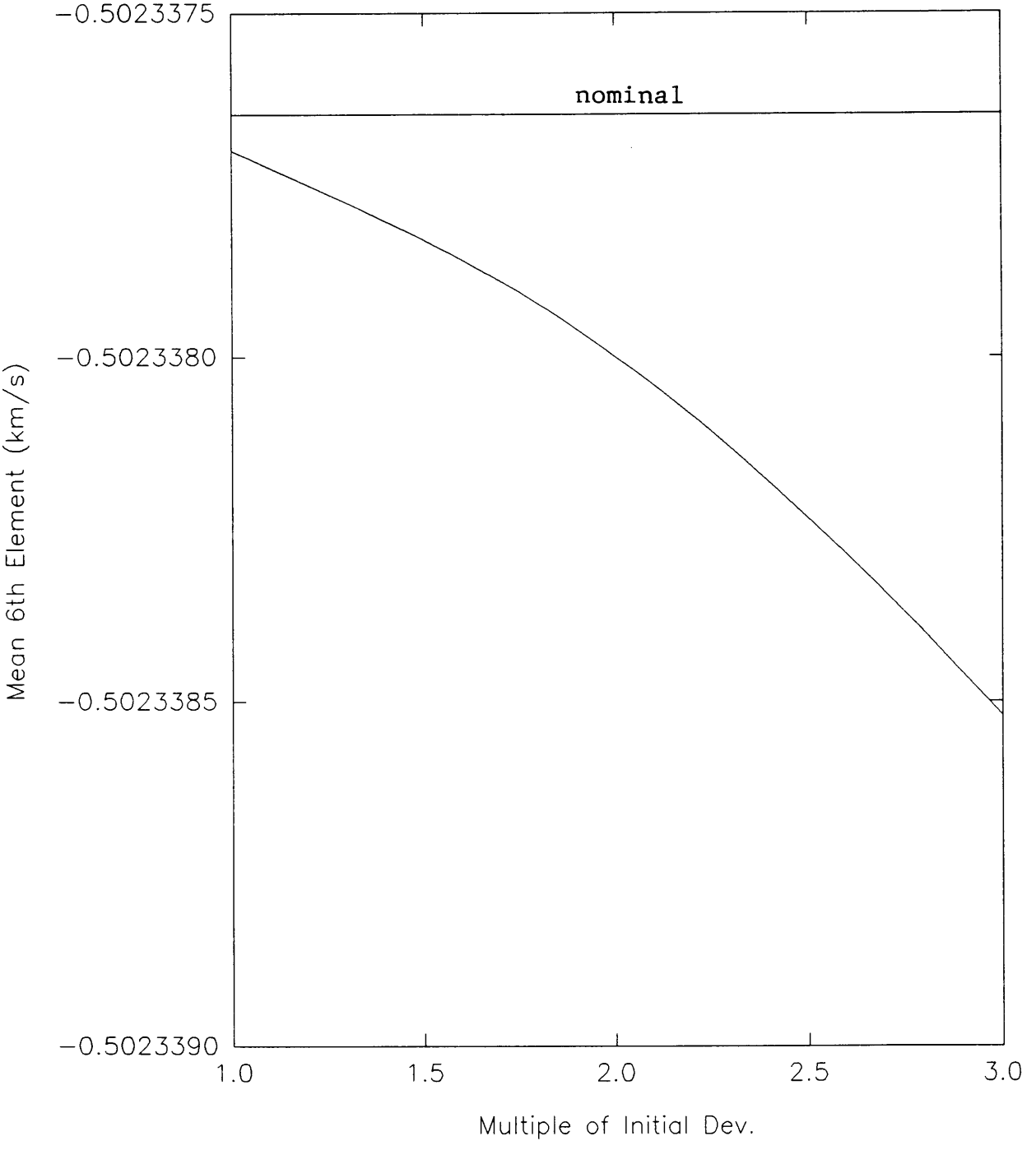

GRAPH 22

1st Element Deviation vs. Multiple of Initial Deviations
(Gauss-Legendre Quadrature Algorithm)

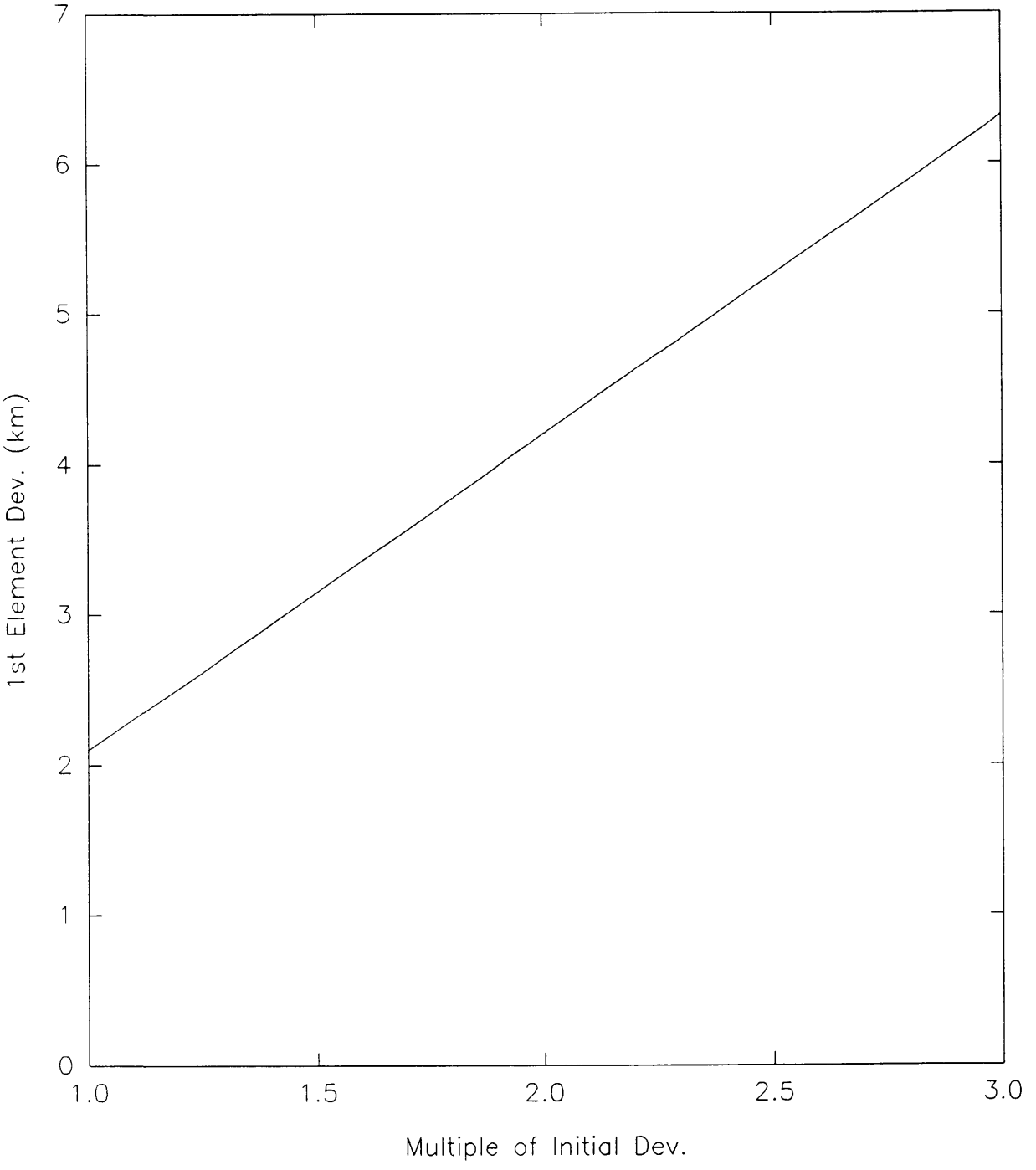

GRAPH 23

2nd Element Deviation vs. Multiple of Initial Deviations
(Gauss-Legendre Quadrature Algorithm)

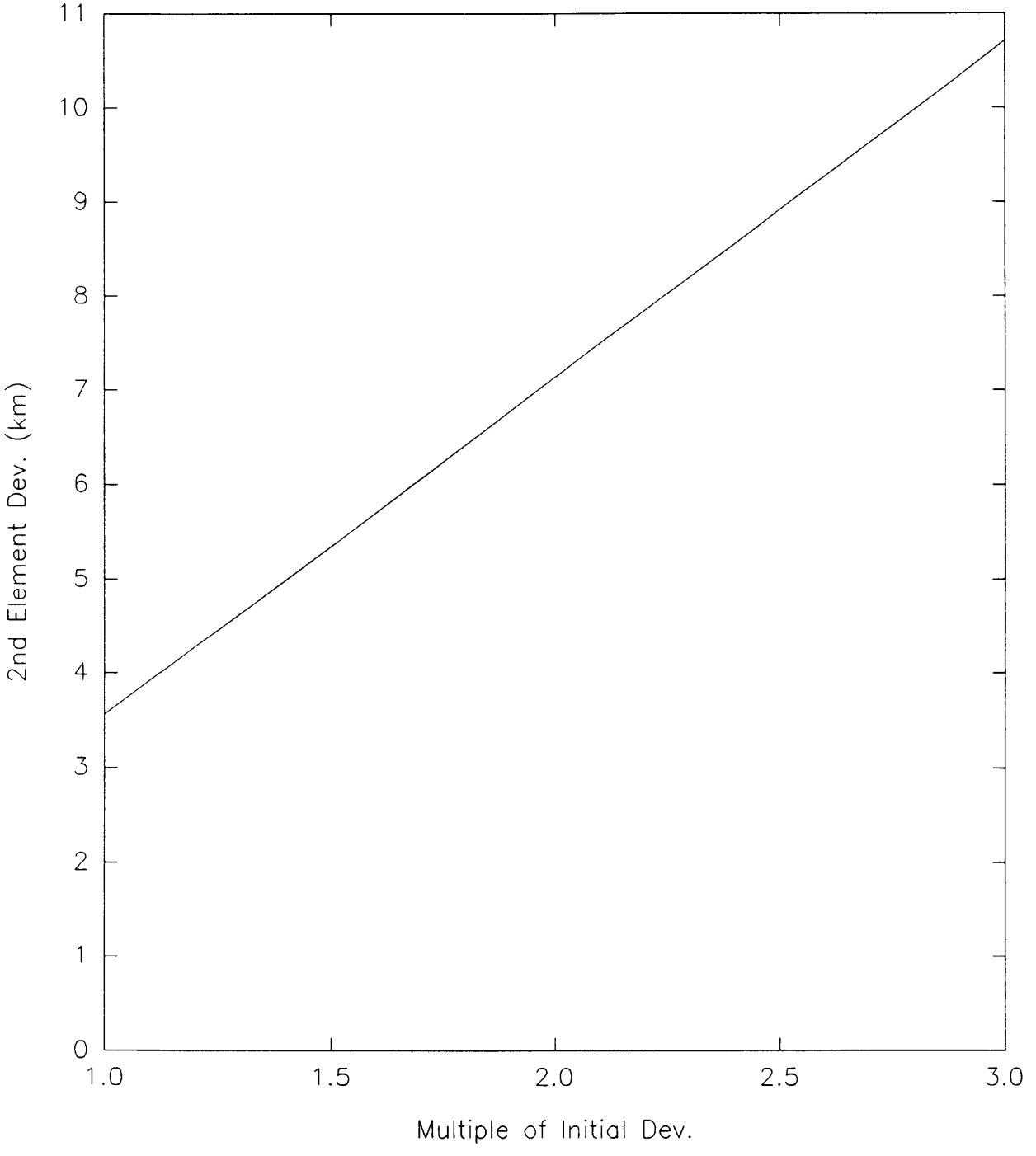

GRAPH 24

3rd Element Deviation vs. Multiple of Initial Deviations
(Gauss-Legendre Quadrature Algorithm)

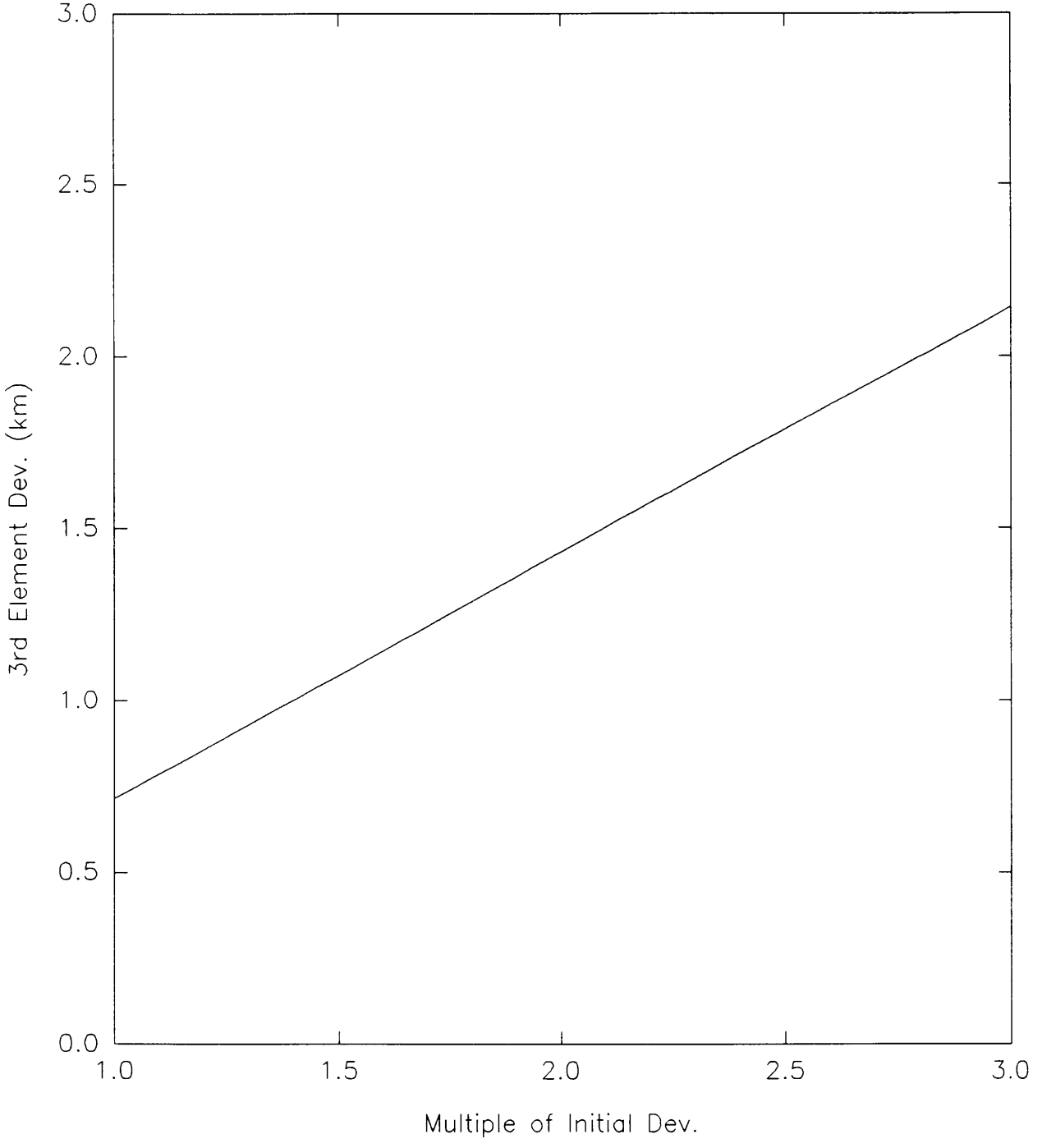

GRAPH 25

4th Element Deviation vs. Multiple of Initial Deviations
(Gauss-Legendre Quadrature Algorithm)

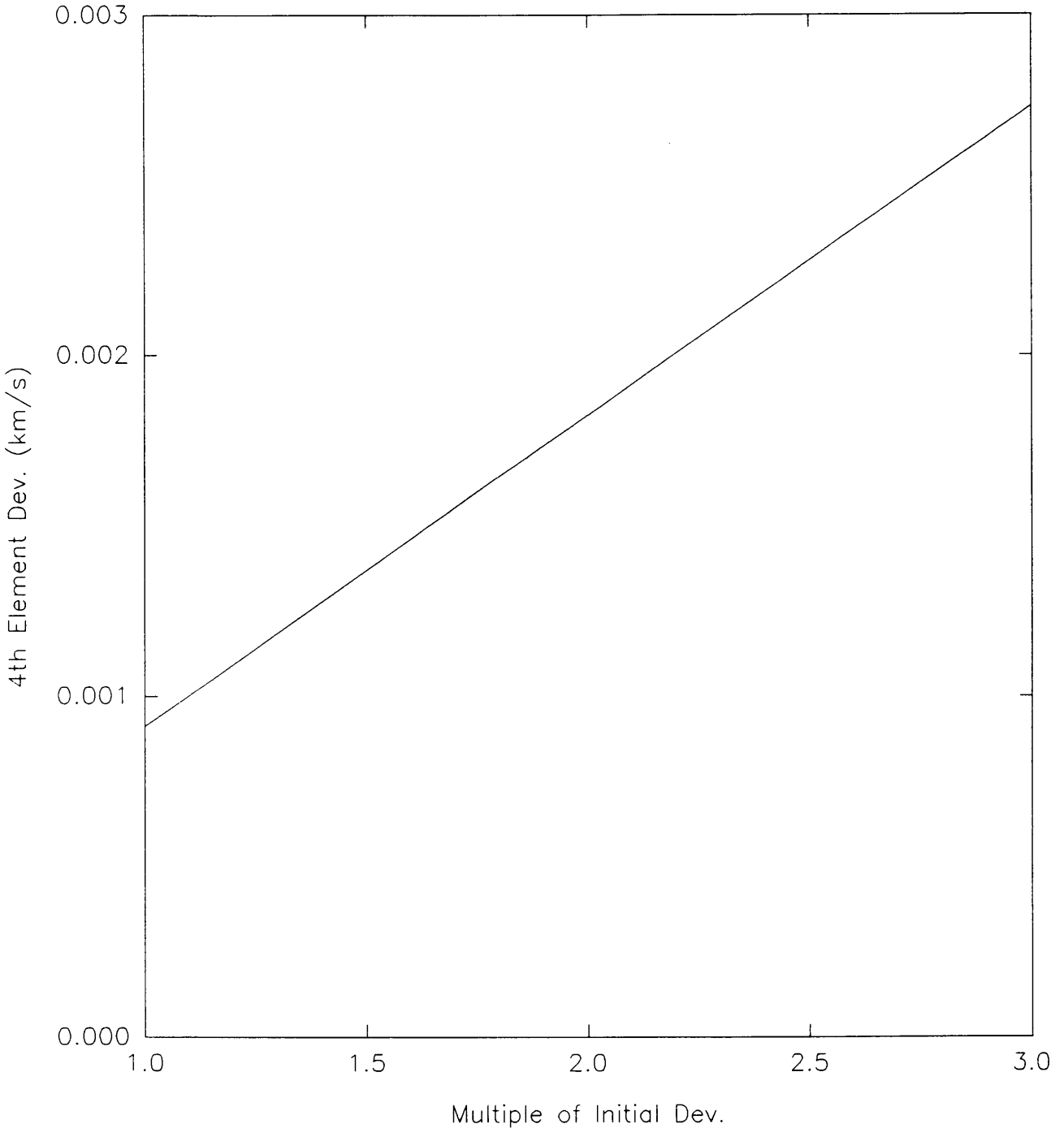

GRAPH 26

5th Element Deviation vs. Multiple of Initial Deviations
(Gauss-Legendre Quadrature Algorithm)

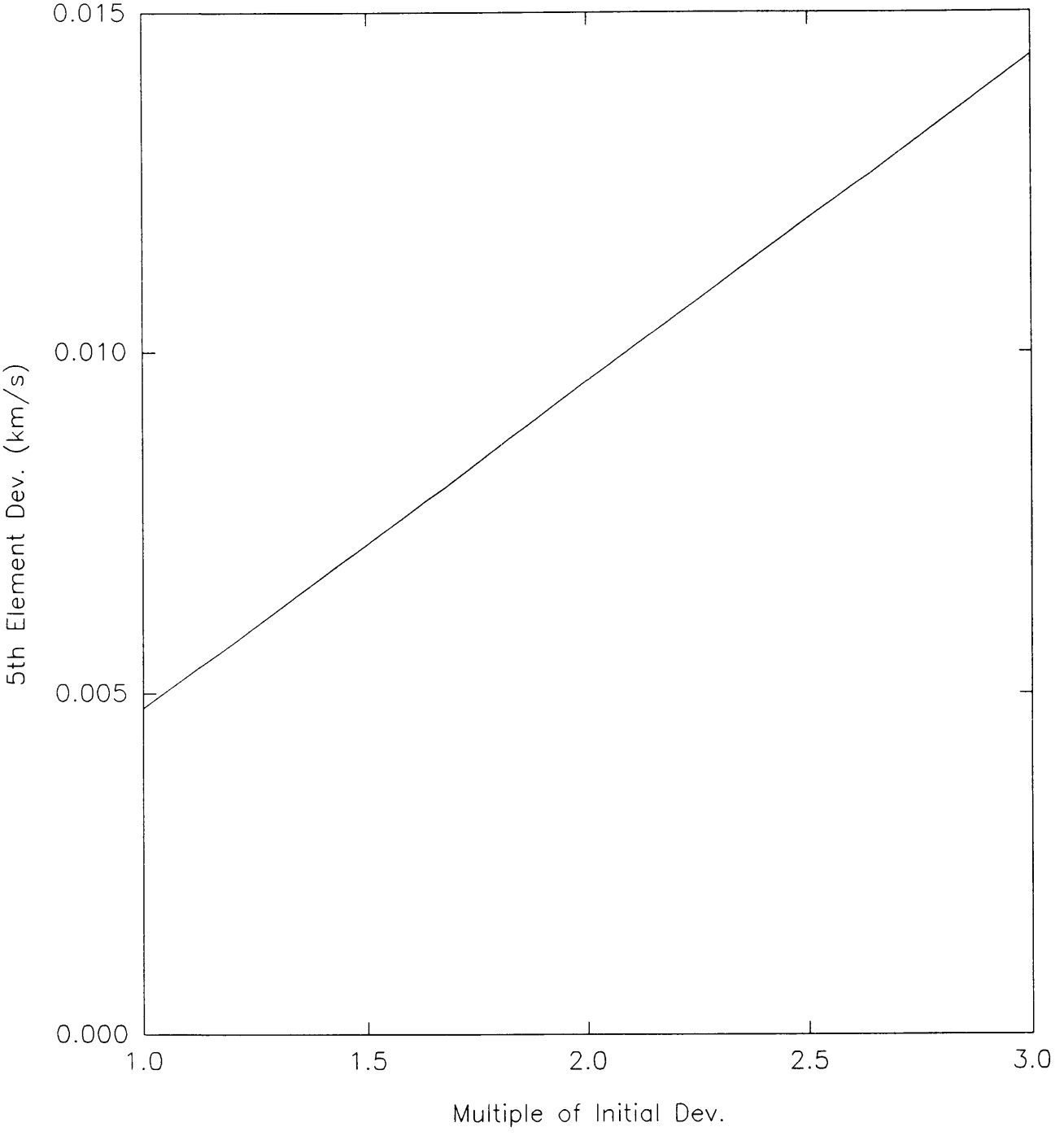

GRAPH 27

6th Element Deviation vs. Multiple of Initial Deviations
(Gauss-Legendre Quadrature Algorithm)

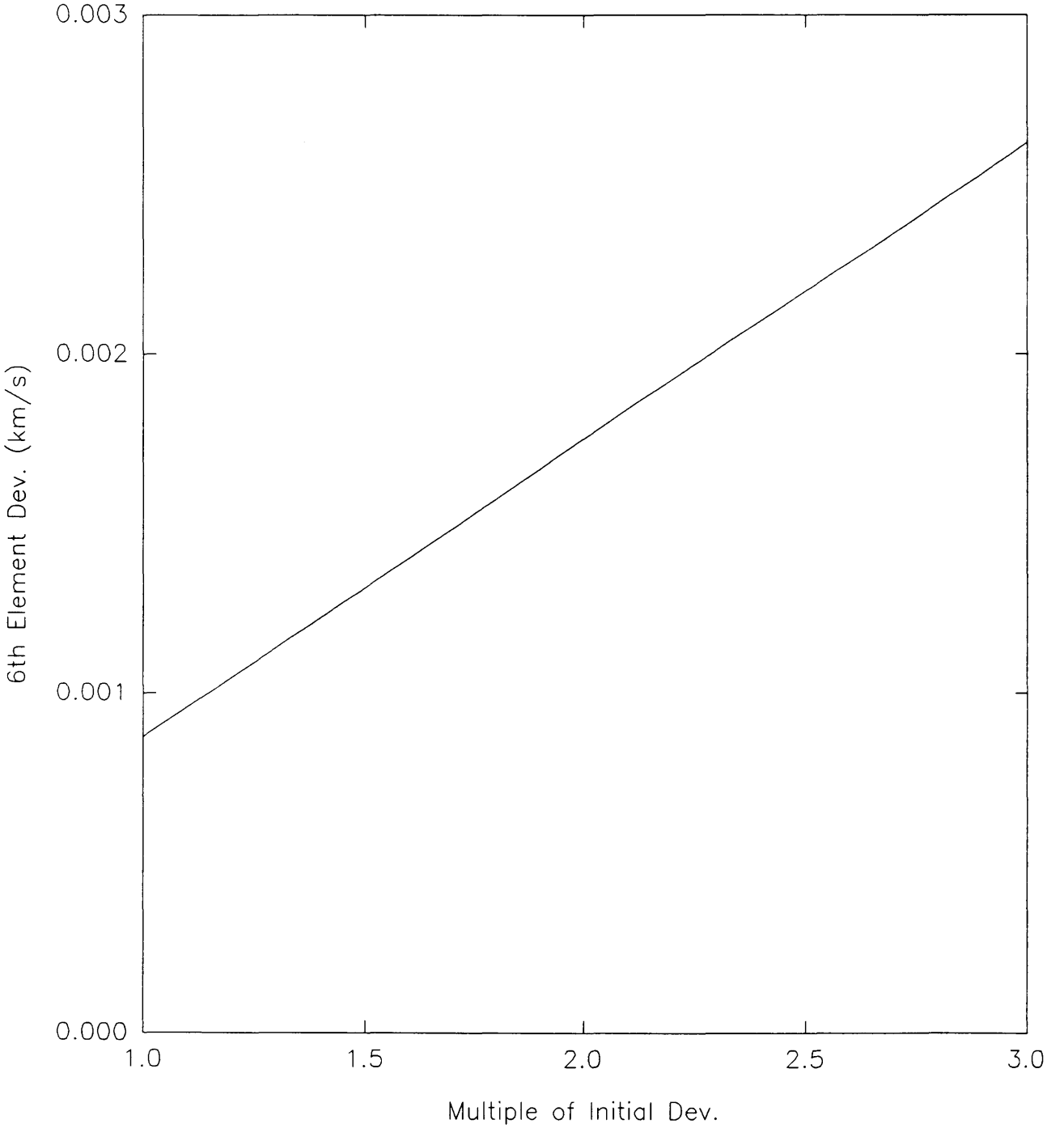

GRAPH 28

Accuracy vs. Quadrature Order

(Gauss-Hermitian Quadrature Algorithm)

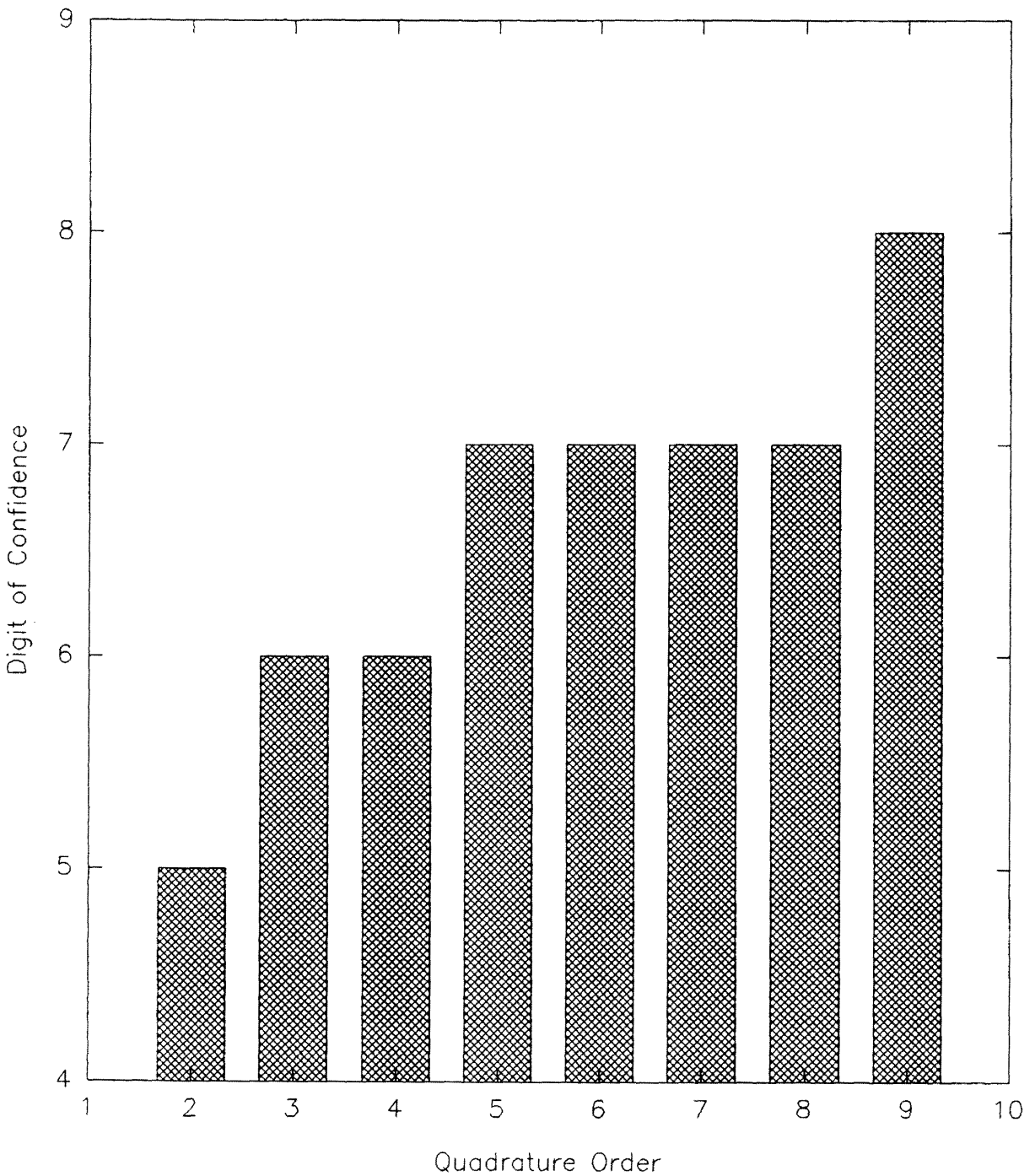

GRAPH 29

Mean 1st Element vs. Multiple of Initial Deviations

(Gauss-Hermitian Quadrature Algorithm)

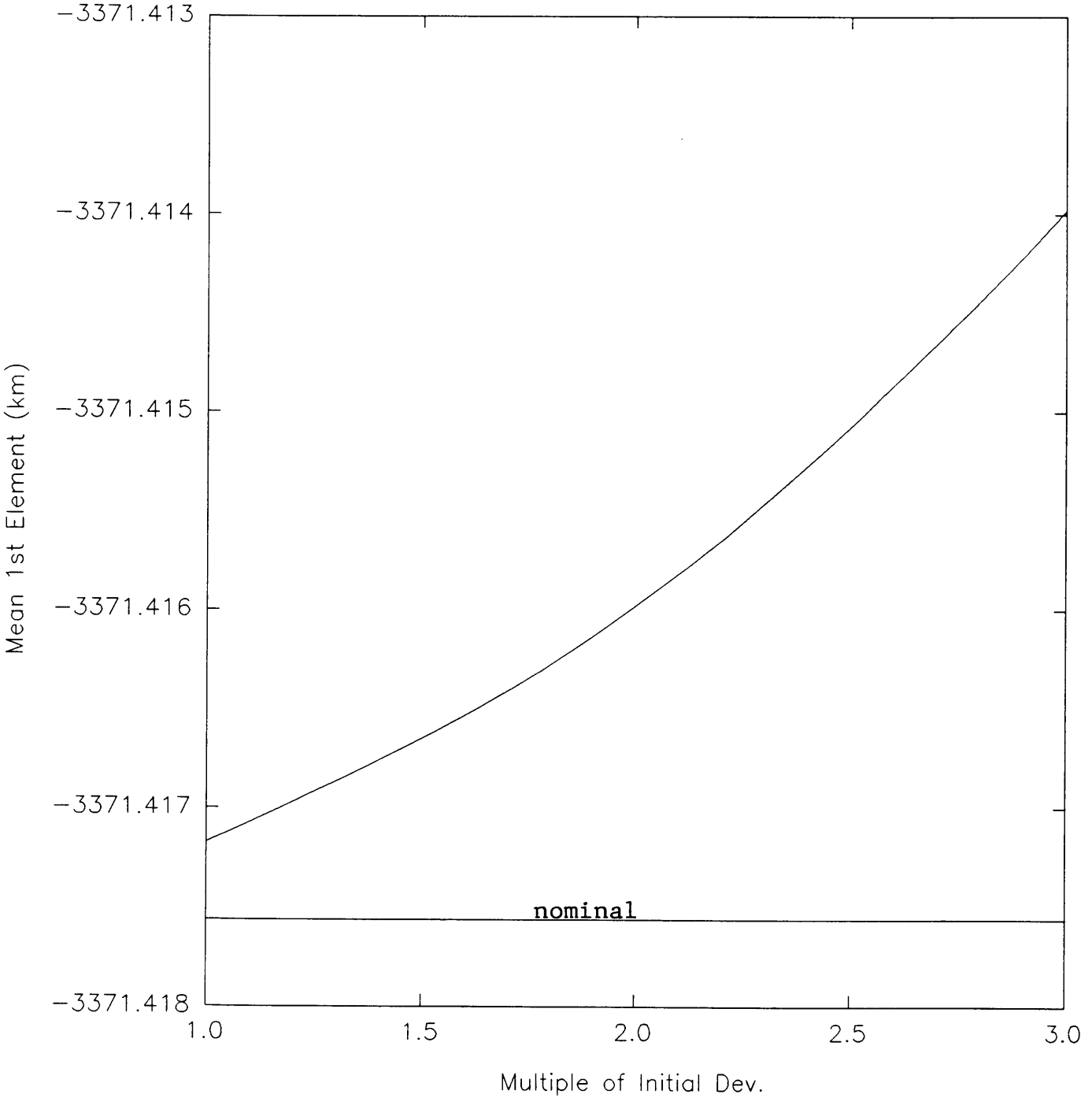

GRAPH 30

Mean 2nd Element vs. Multiple of Initial Deviations

(Gauss-Hermitian Quadrature Algorithm)

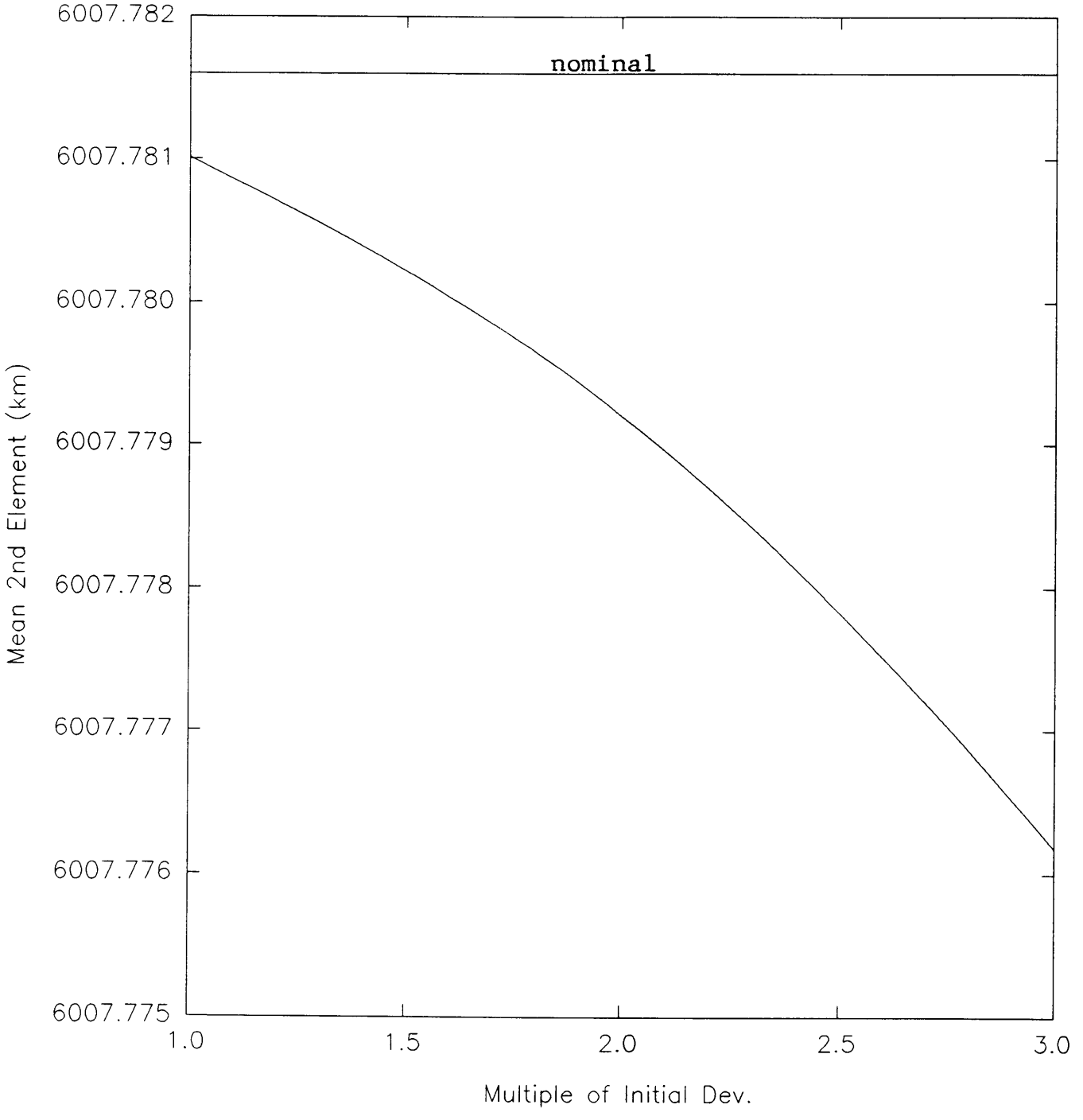

GRAPH 31

Mean 3rd Element vs. Multiple of Initial Deviations
(Gauss-Hermitian Quadrature Algorithm)

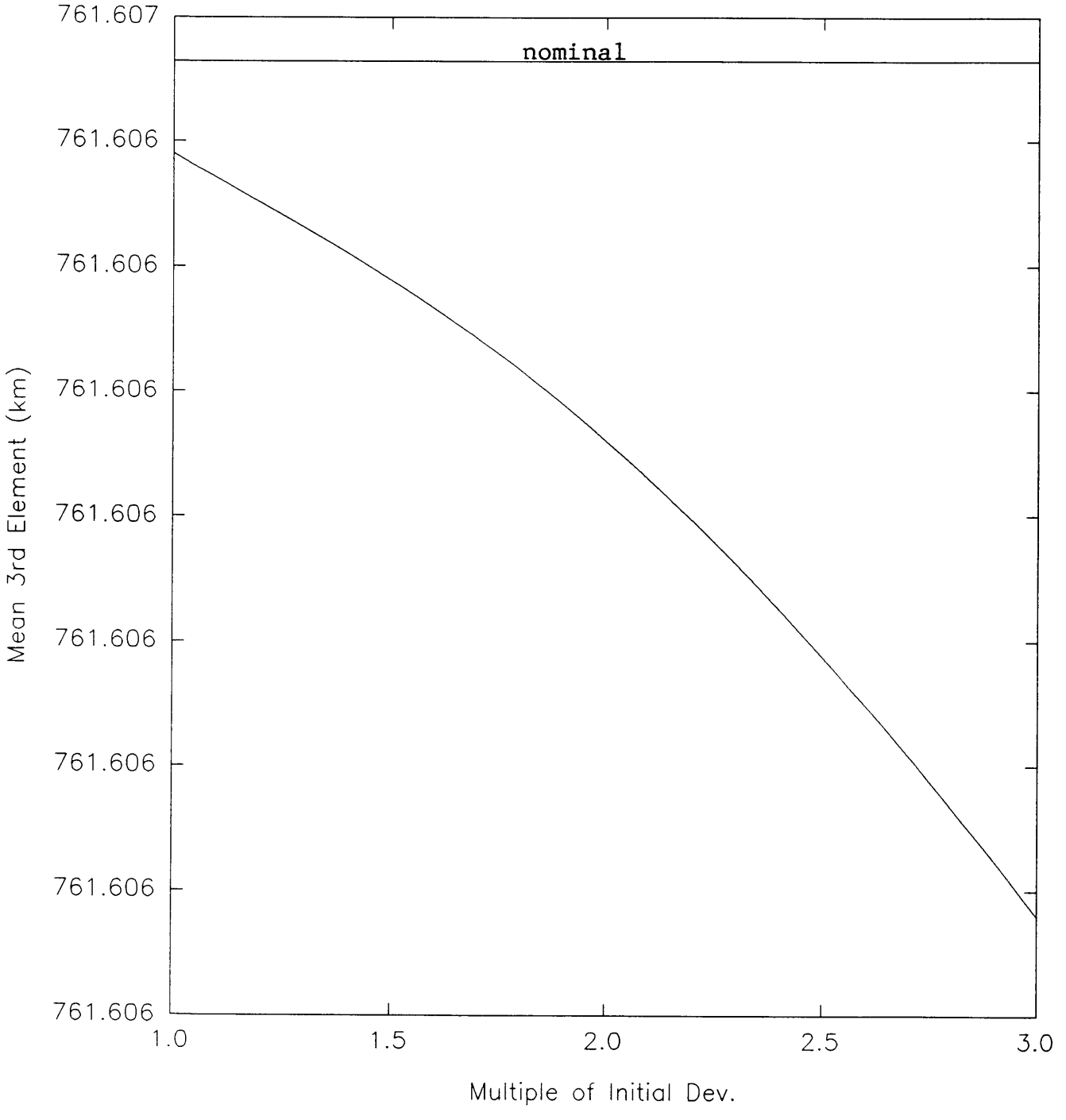

GRAPH 32

Mean 4th Element vs. Multiple of Initial Deviations
(Gauss-Hermitian Quadrature Algorithm)

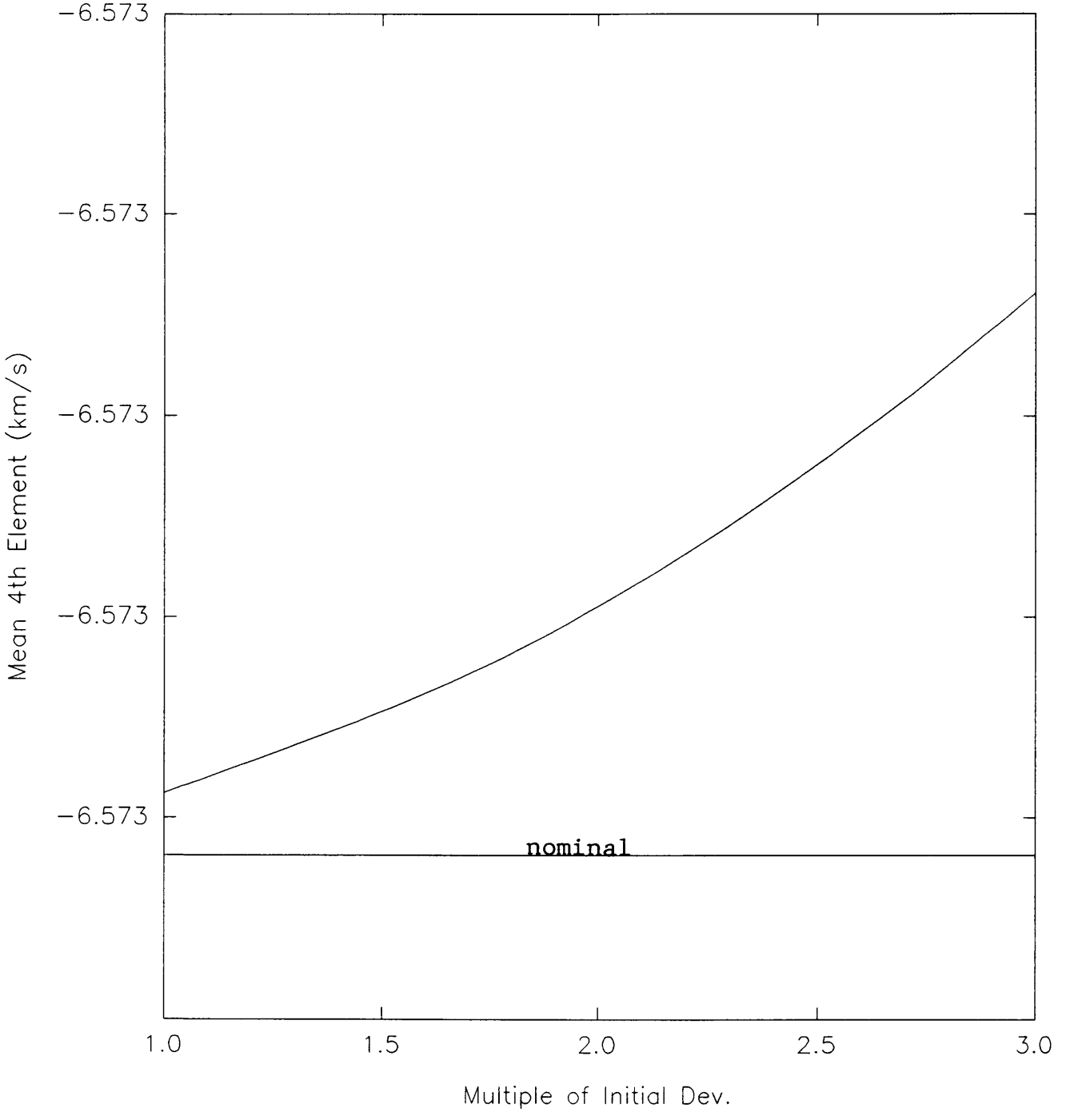

GRAPH 33

Mean 5th Element vs. Multiple of Initial Deviations
(Gauss-Hermitian Quadrature Algorithm)

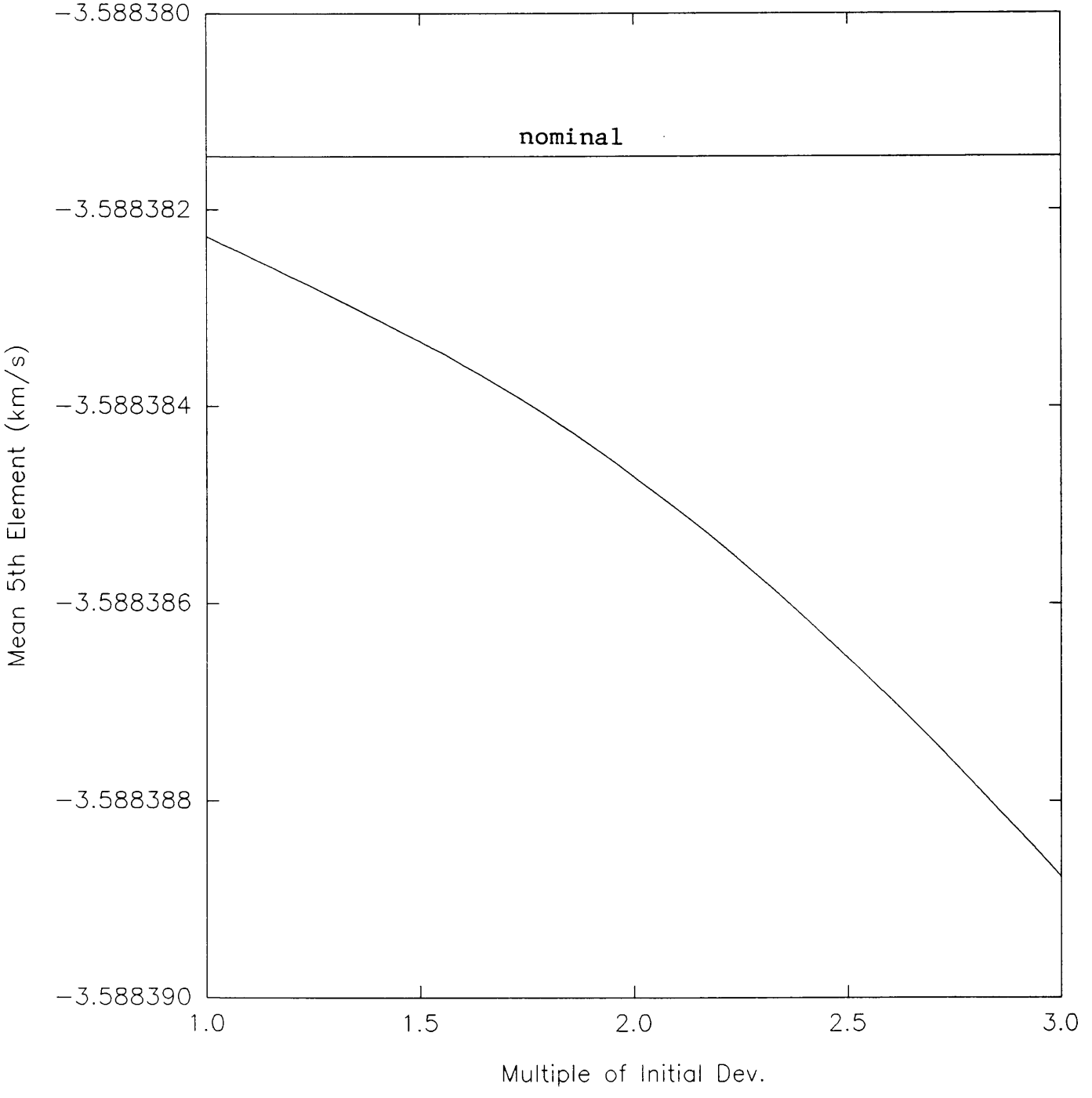

GRAPH 34

Mean 6th Element vs. Multiple of Initial Deviations
(Gauss-Hermitian Quadrature Algorithm)

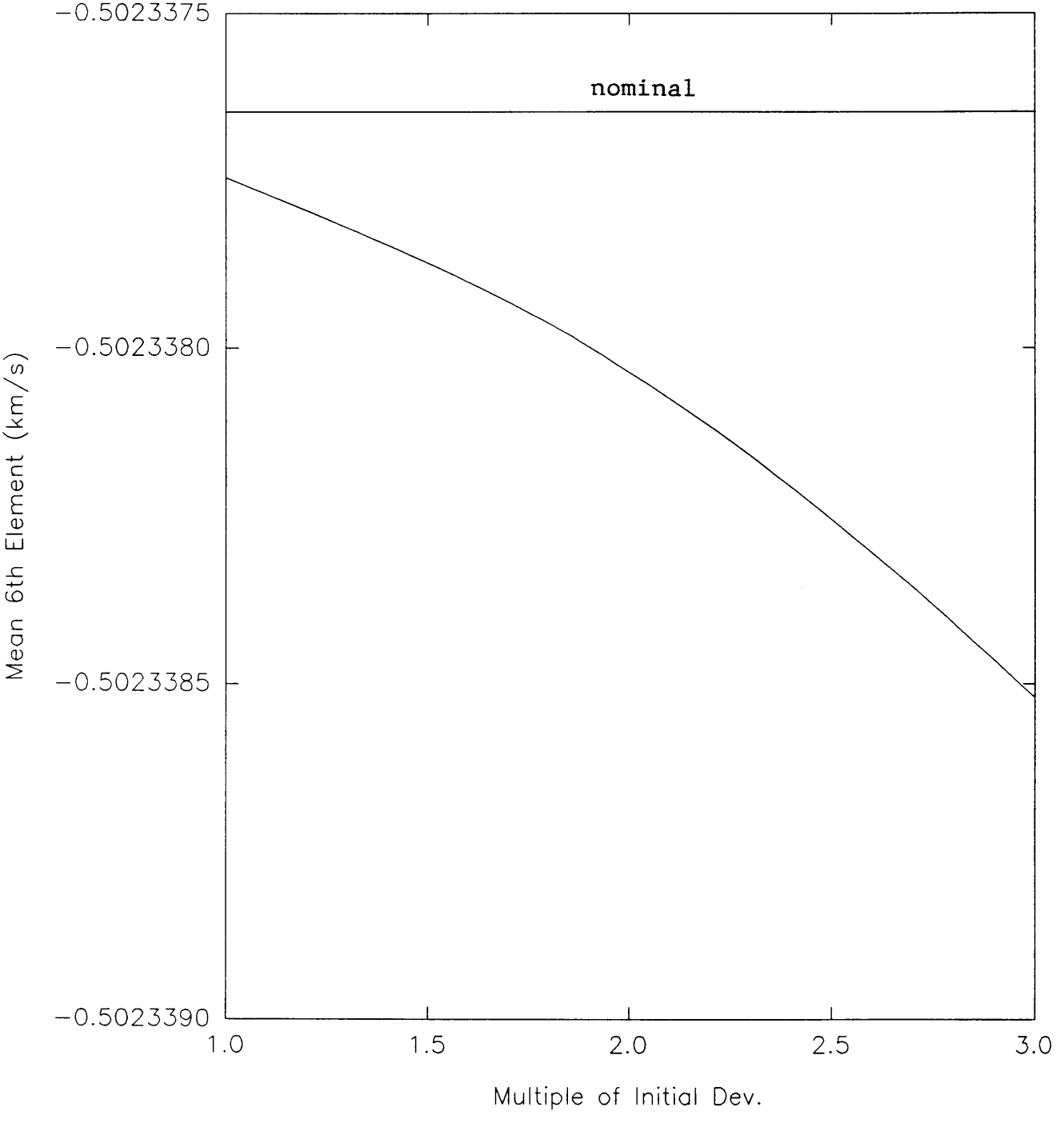

GRAPH 35

1st Element Deviation vs. Multiple of Initial Deviations
(Gauss-Hermitian Quadrature Algorithm)

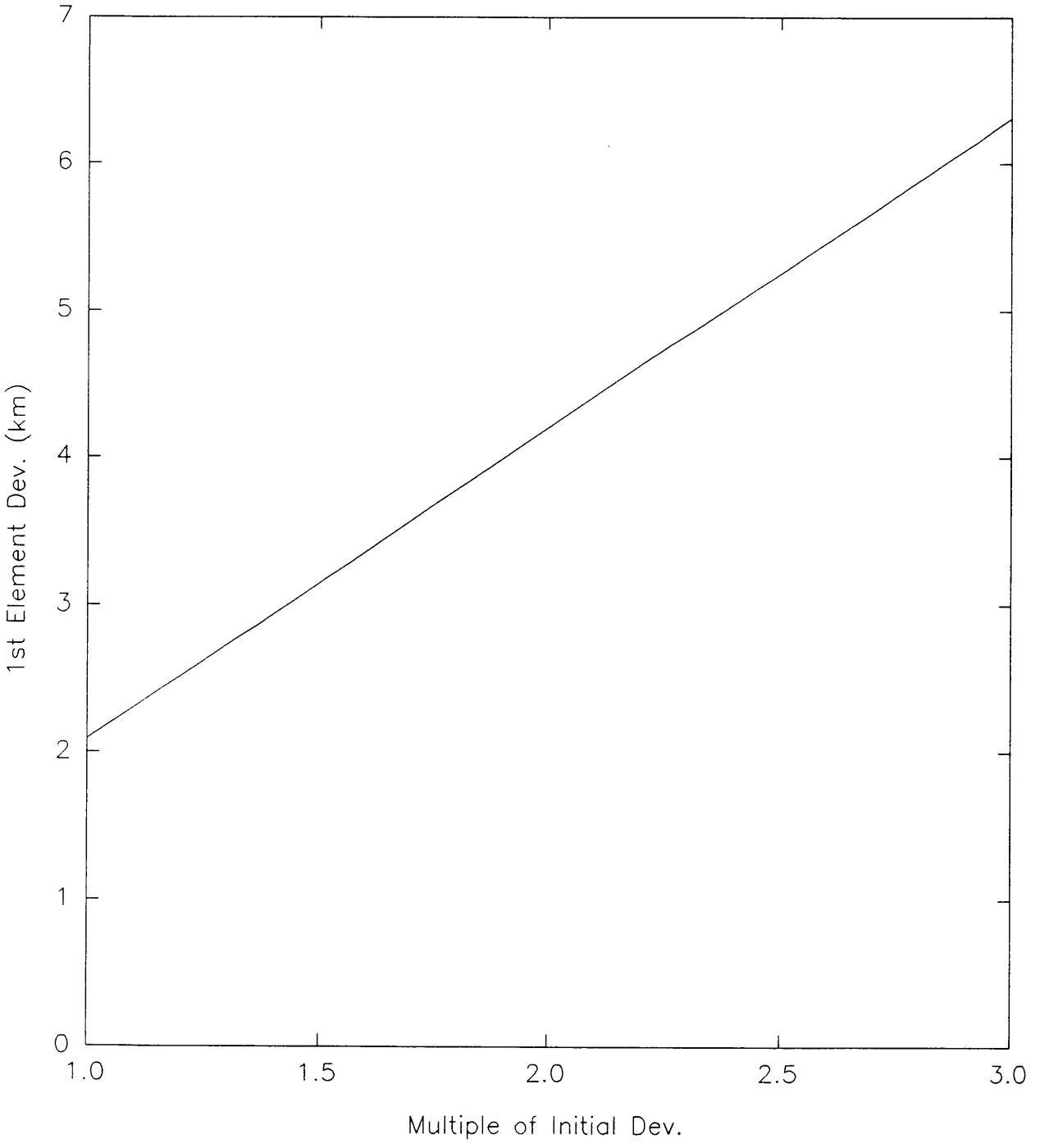

GRAPH 36

2nd Element Deviation vs. Multiple of Initial Deviations
(Gauss-Hermitian Quadrature Algorithm)

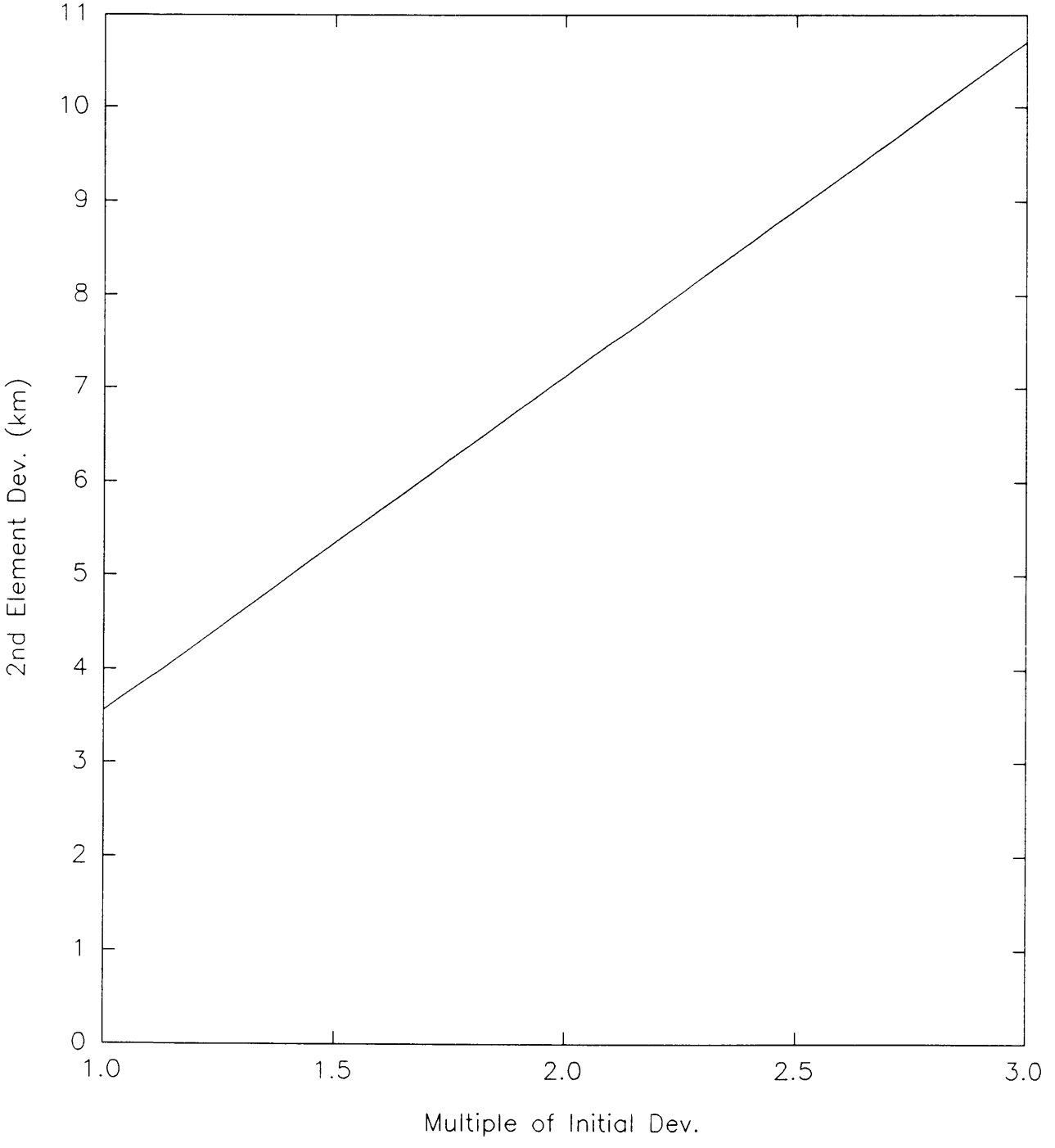

GRAPH 37

3rd Element Deviation vs. Multiple of Initial Deviations
(Gauss-Hermitian Quadrature Algorithm)

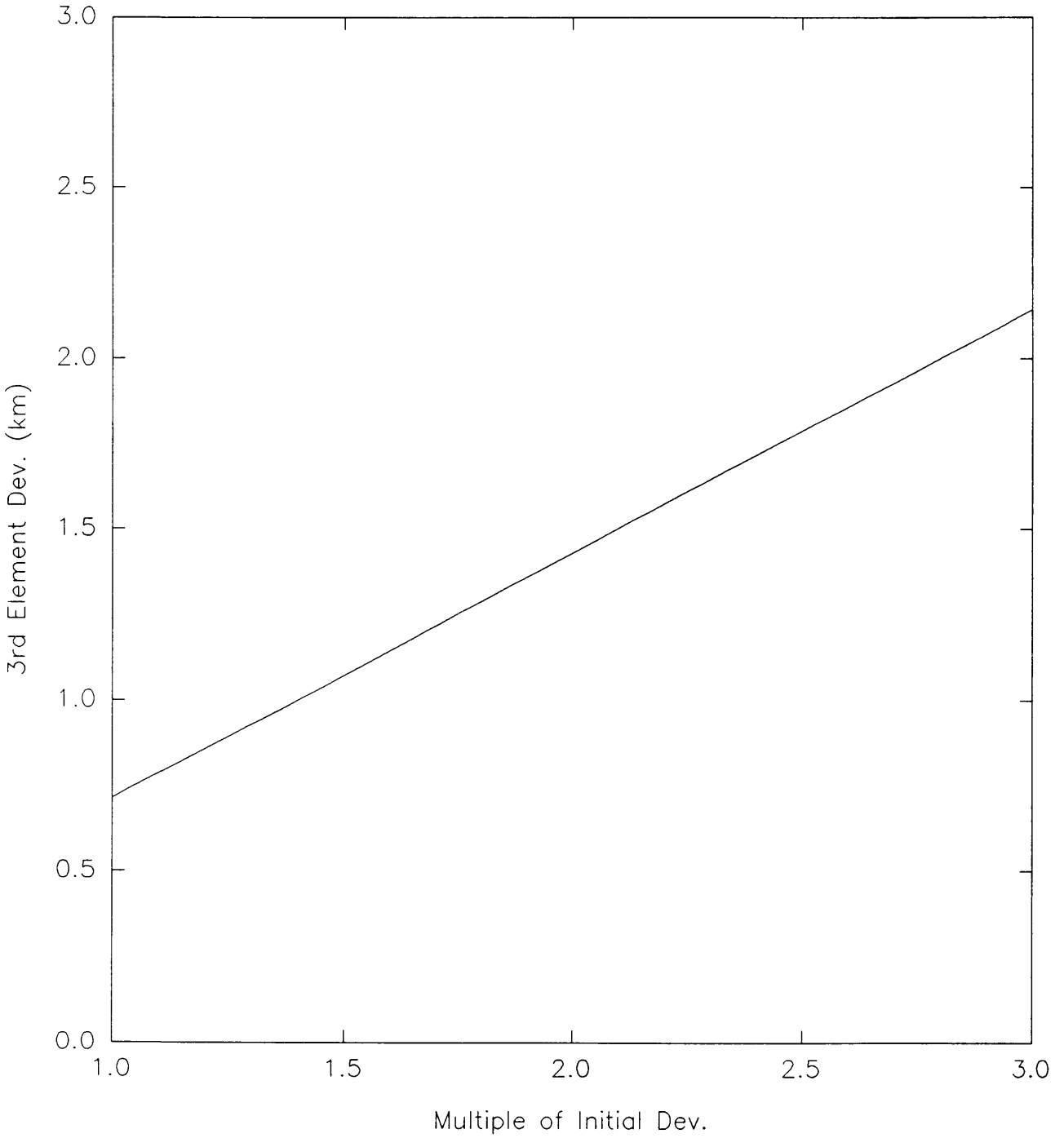

GRAPH 38

4th Element Deviation vs. Multiple of Initial Deviations
(Gauss-Hermitian Quadrature Algorithm)

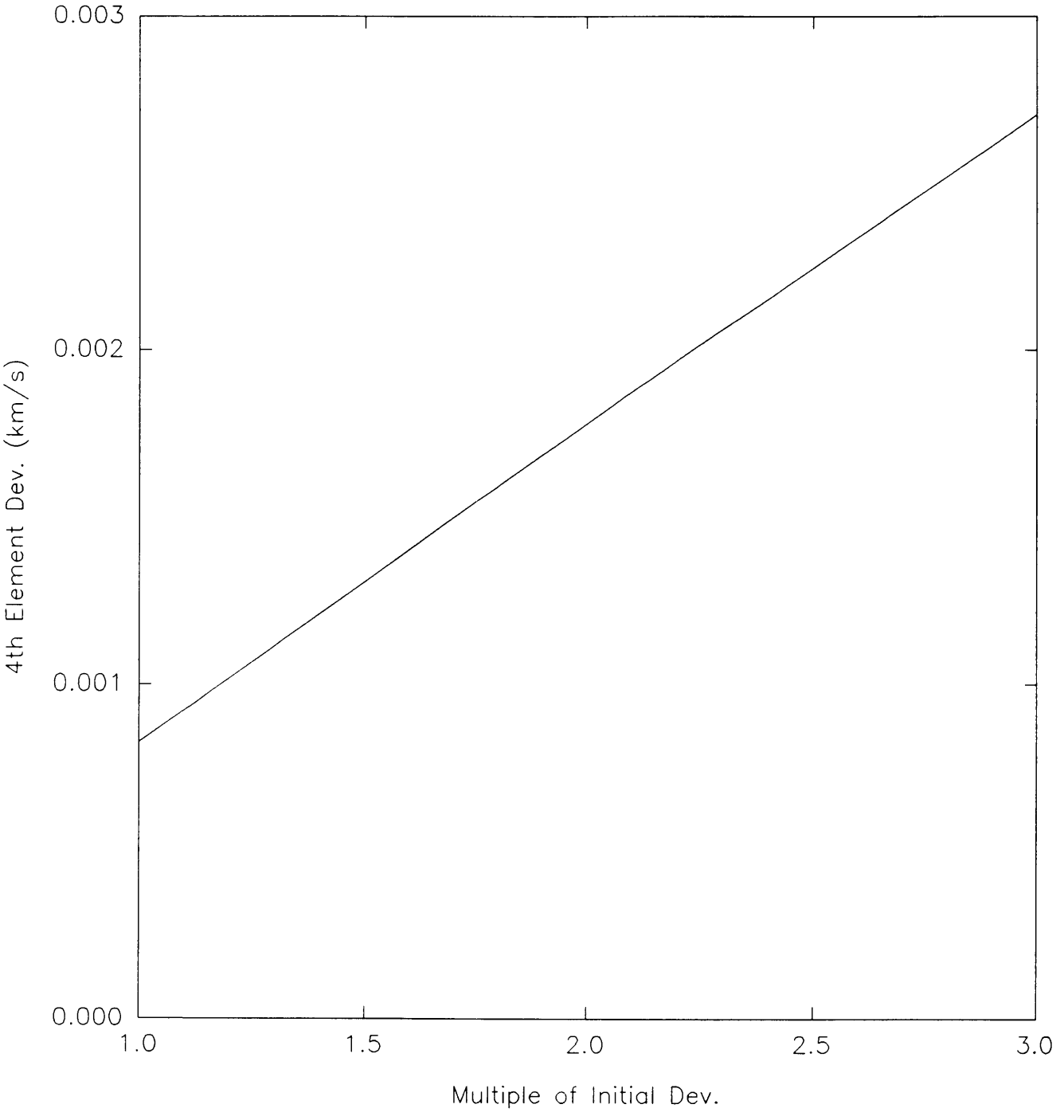

GRAPH 39

5th Element Deviation vs. Multiple of Initial Deviations
(Gauss-Hermitian Quadrature Algorithm)

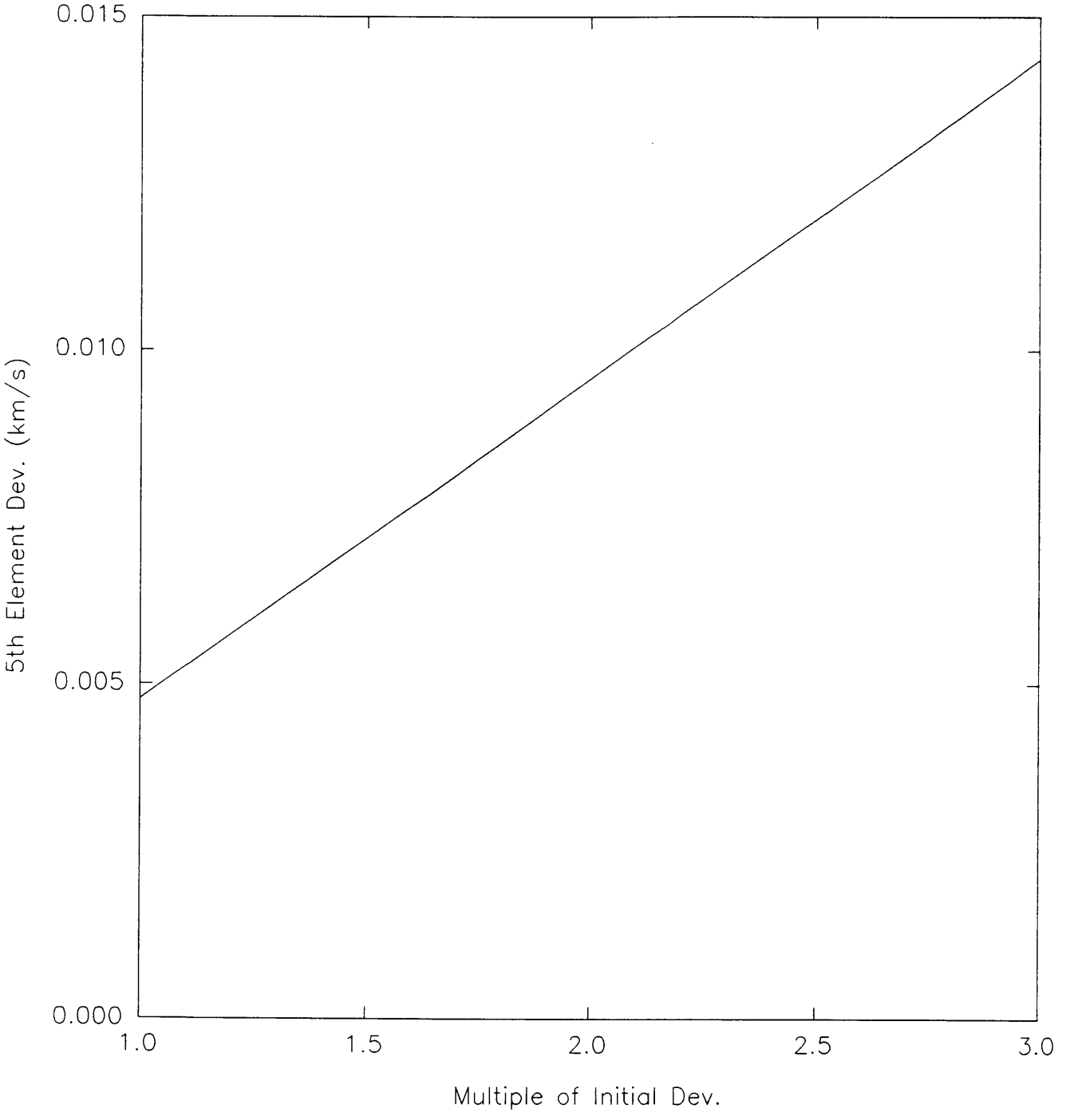

GRAPH 40

6th Element Deviation vs. Multiple of Initial Deviations
(Gauss-Hermitian Quadrature Algorithm)

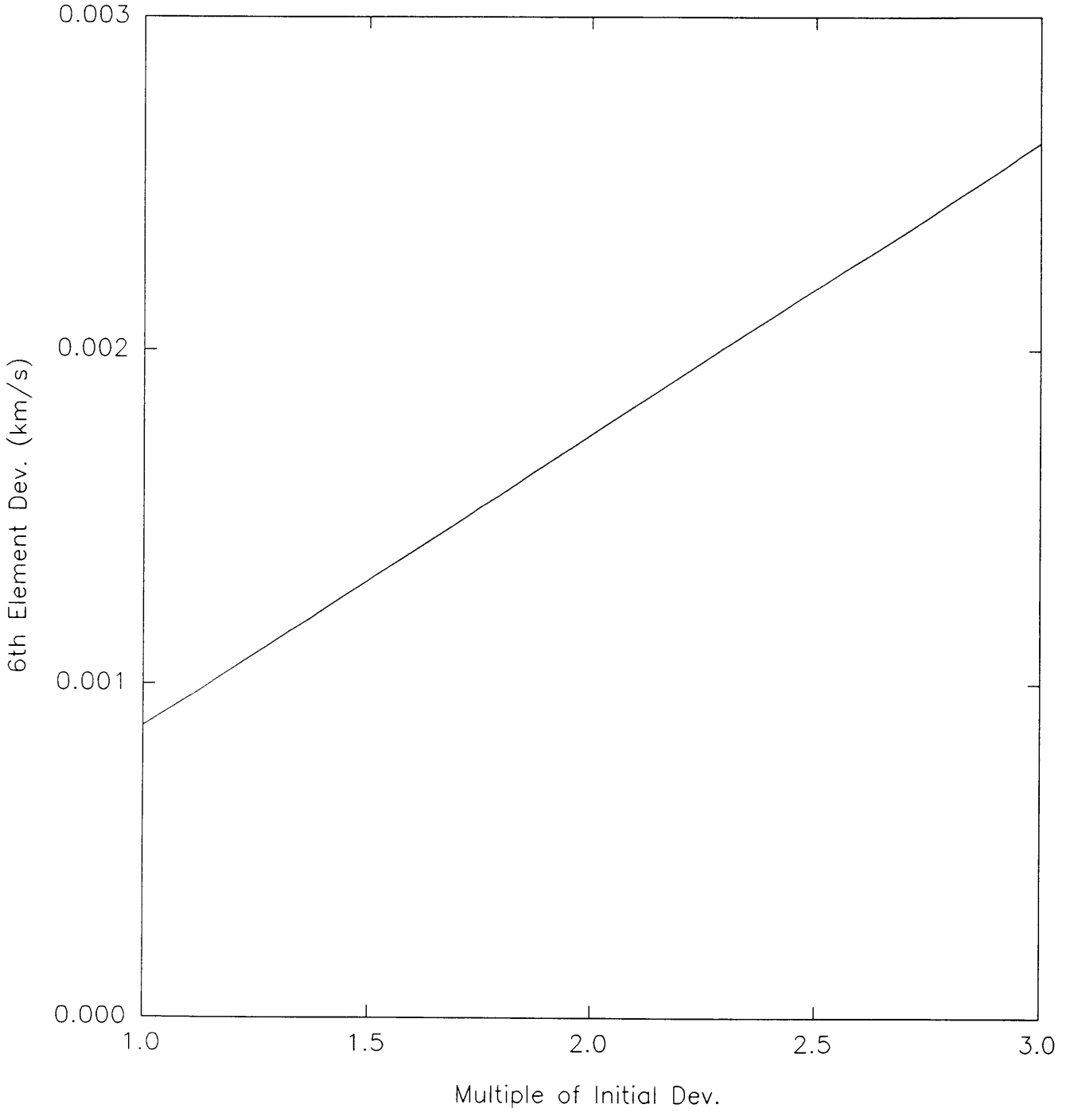

GRAPH 41

1st Element Deviation vs. Multiple of Initial Deviations
(Linear Approximation Algorithm)

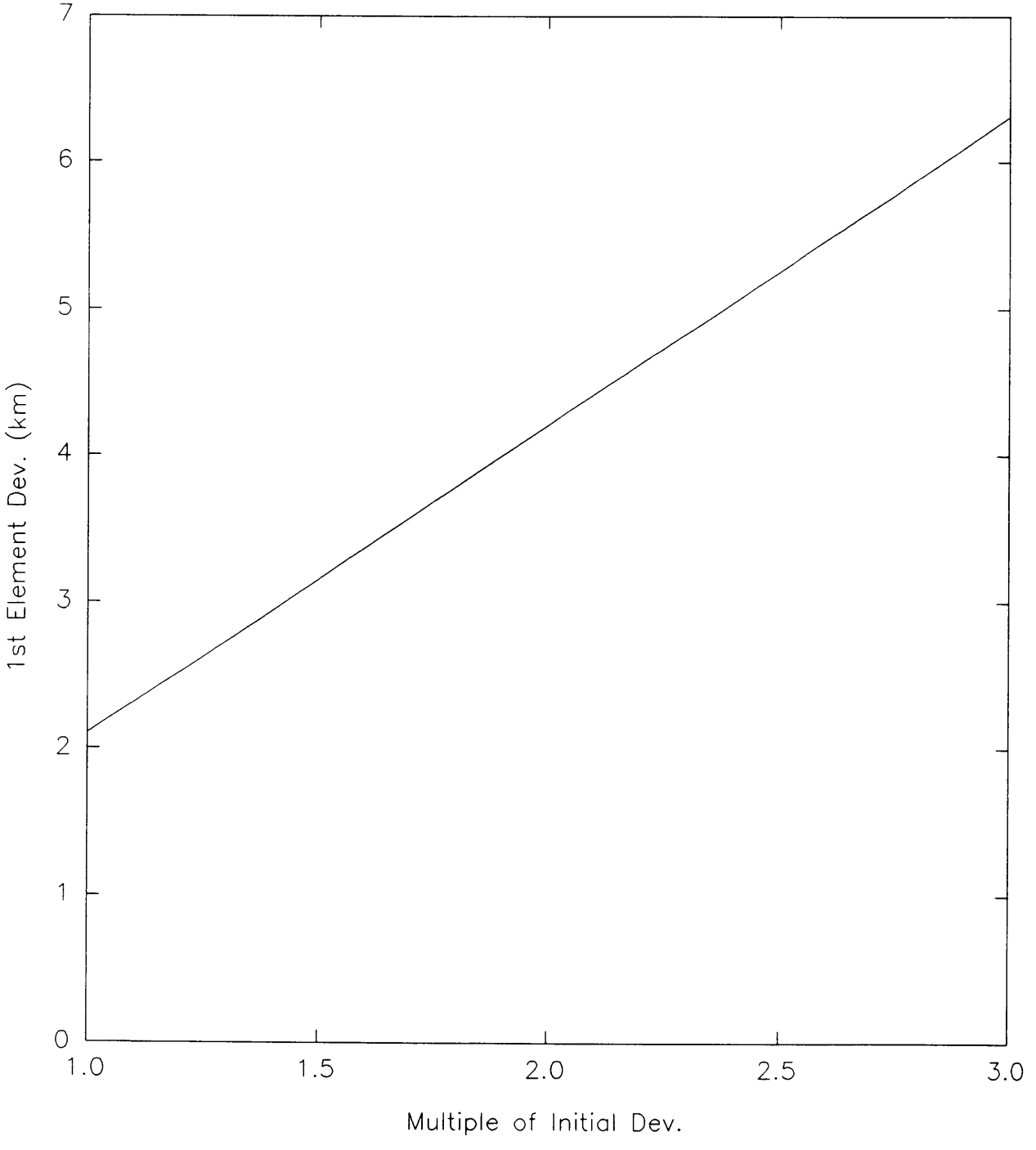

GRAPH 42

2nd Element Deviation vs. Multiple of Initial Deviations
(Linear Approximation Algorithm)

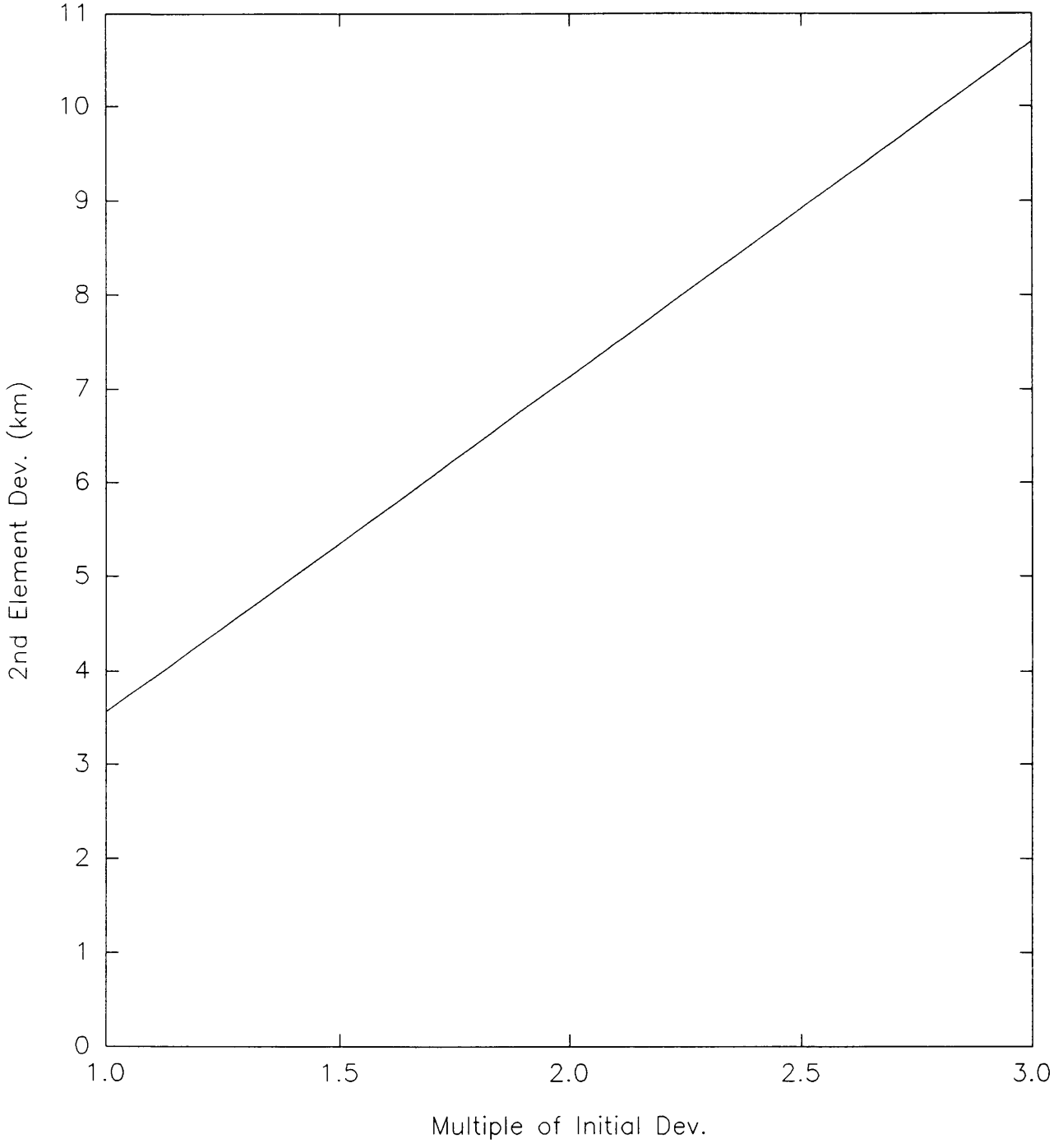

GRAPH 43

3rd Element Deviation vs. Multiple of Initial Deviations
(Linear Approximation Algorithm)

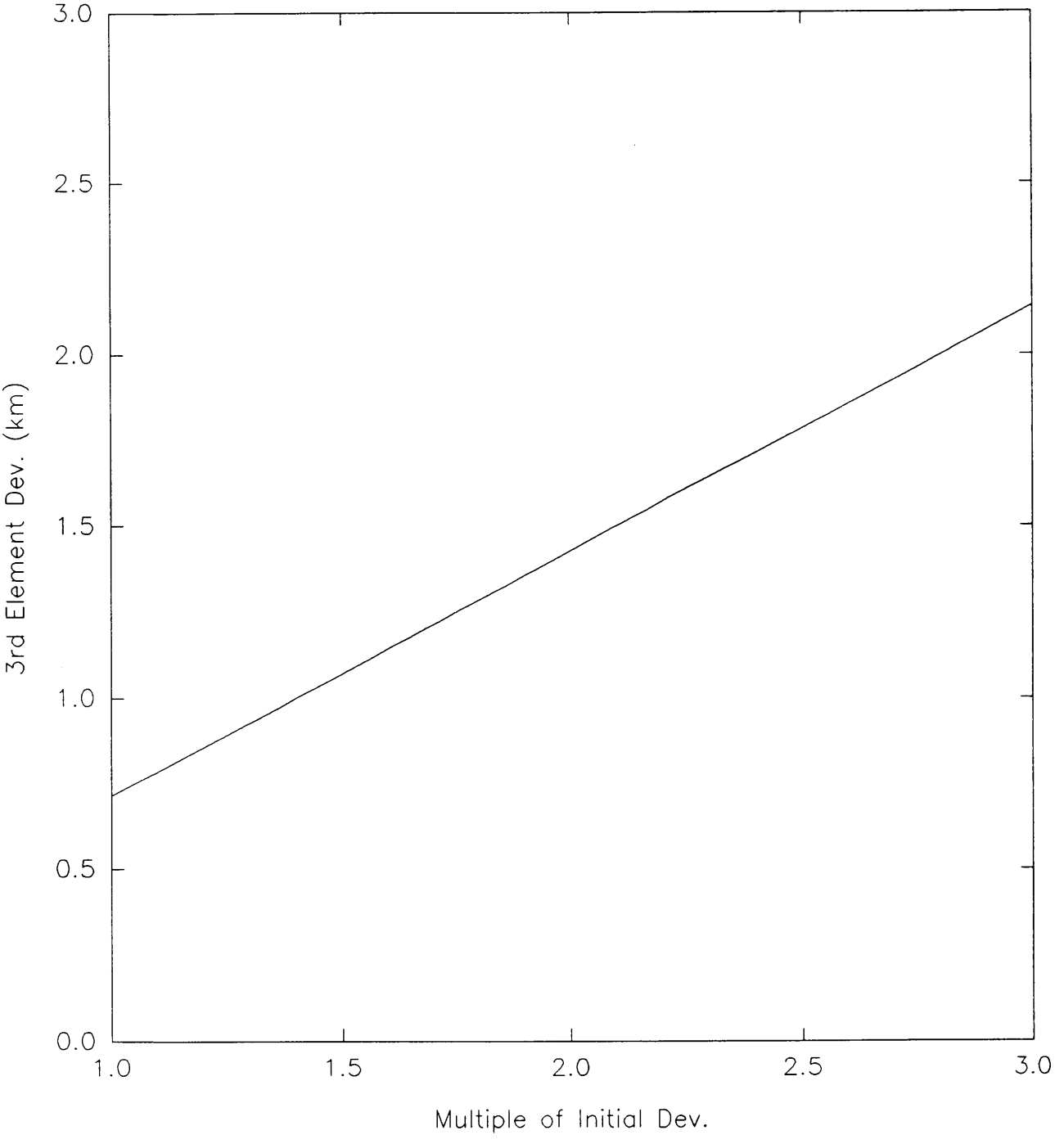

GRAPH 44

4th Element Deviation vs. Multiple of Initial Deviations
(Linear Approximation Algorithm)

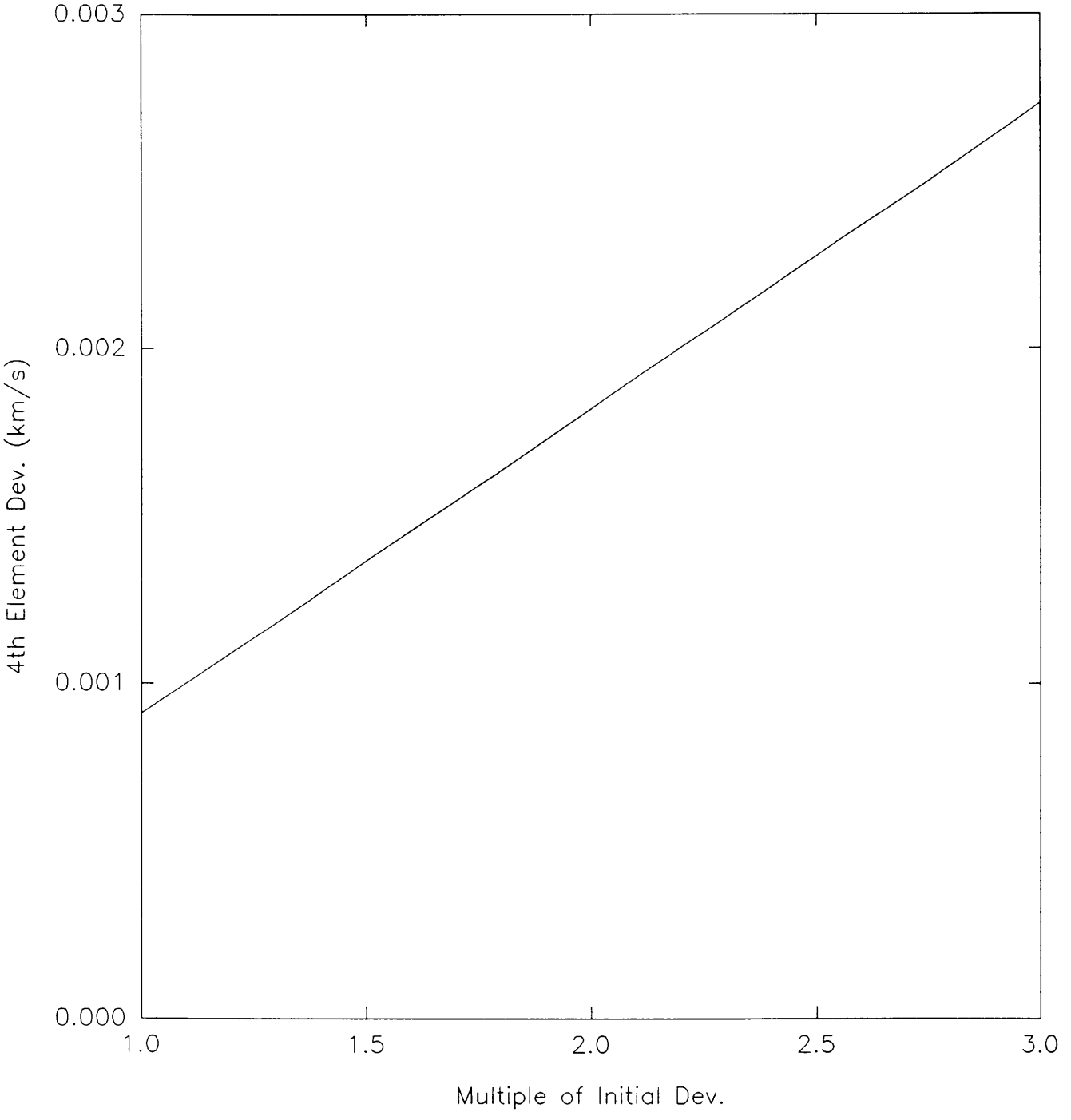

GRAPH 45

5th Element Deviation vs. Multiple of Initial Deviations
(Linear Approximation Algorithm)

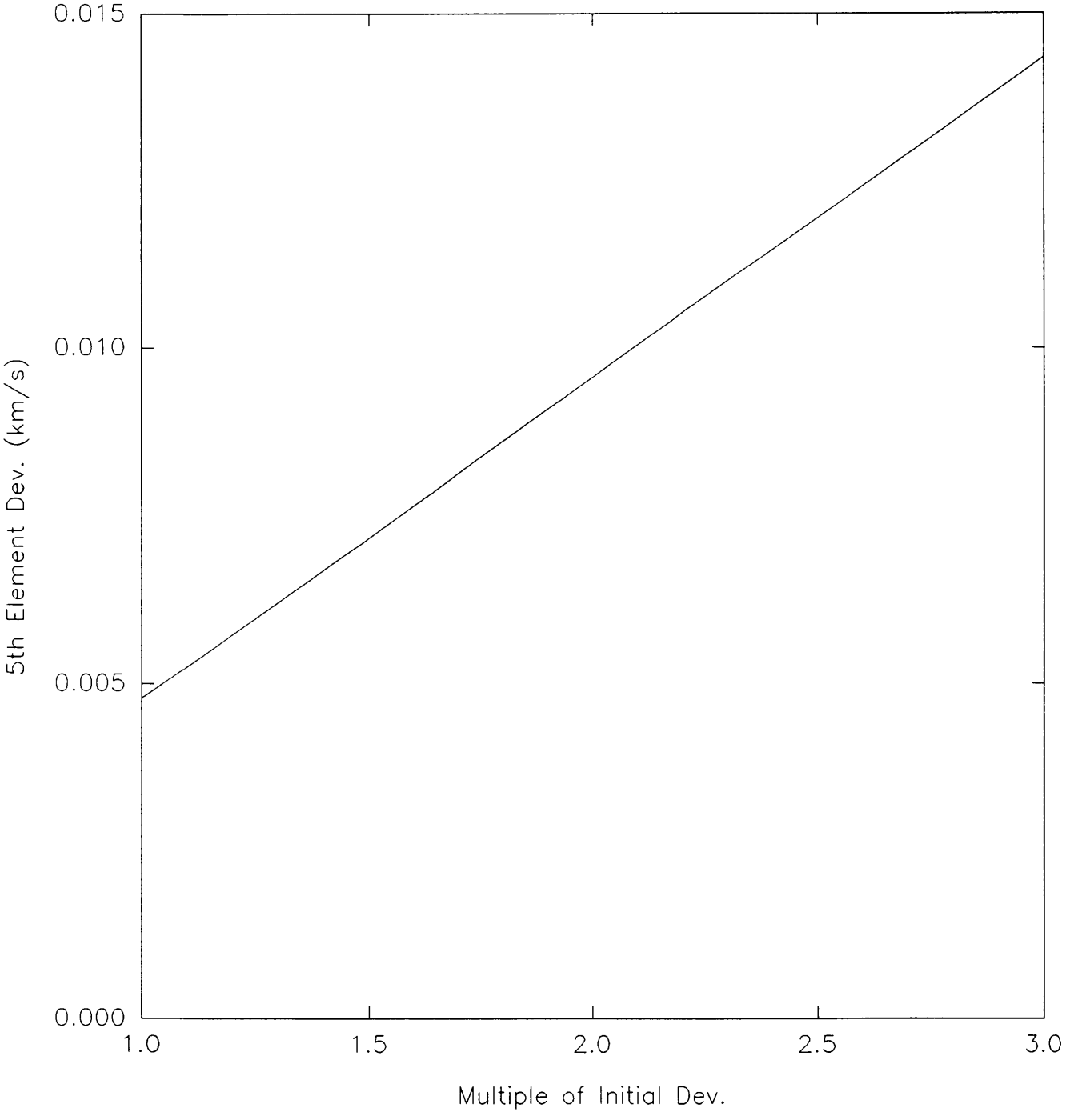

GRAPH 46

6th Element Deviation vs. Multiple of Initial Deviations
(Linear Approximation Algorithm)

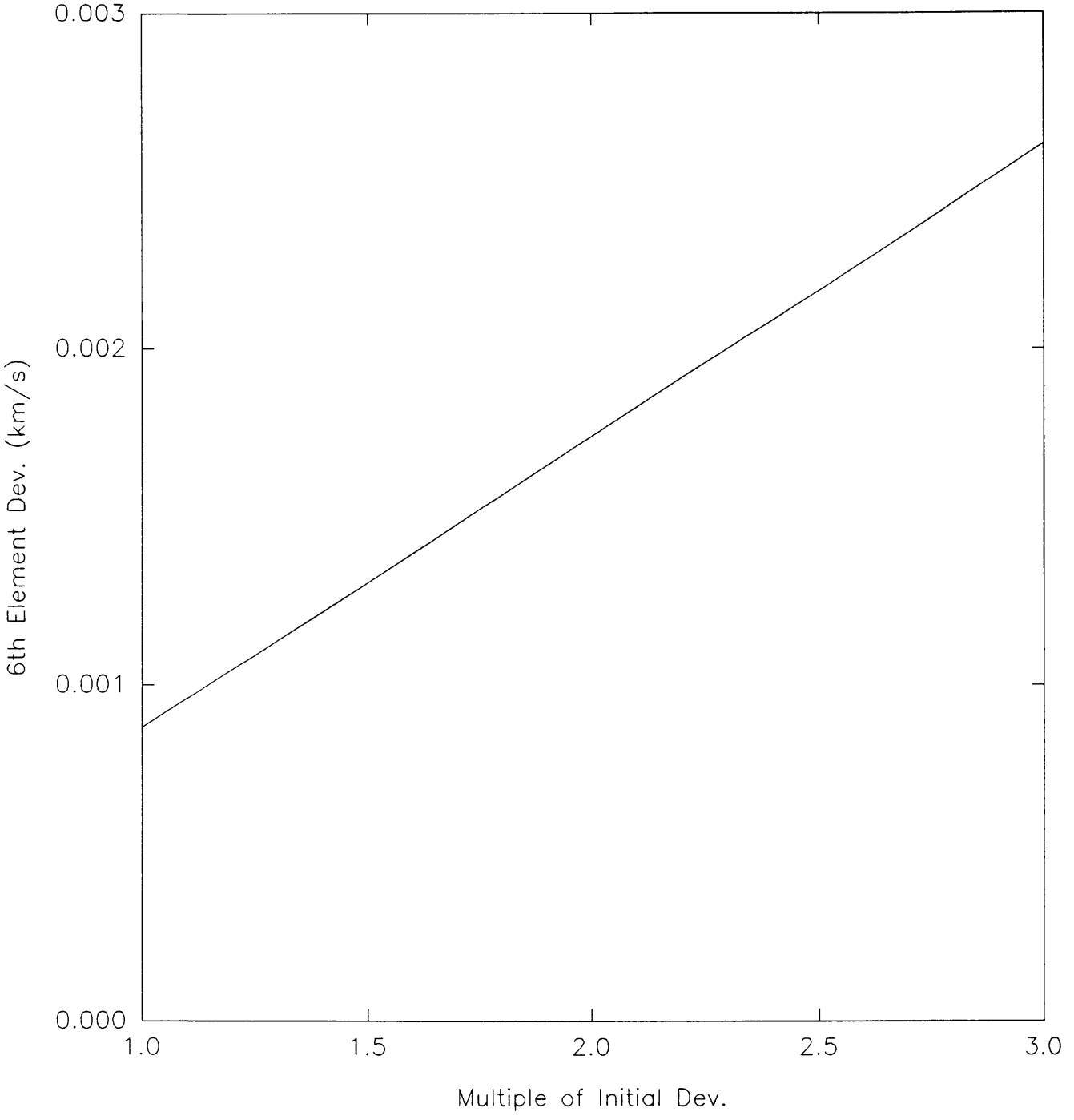

GRAPH 47

Mean 1st Element vs. Multiple of Initial Deviations

(Gauss-Hermitian Quadrature Algorithm)

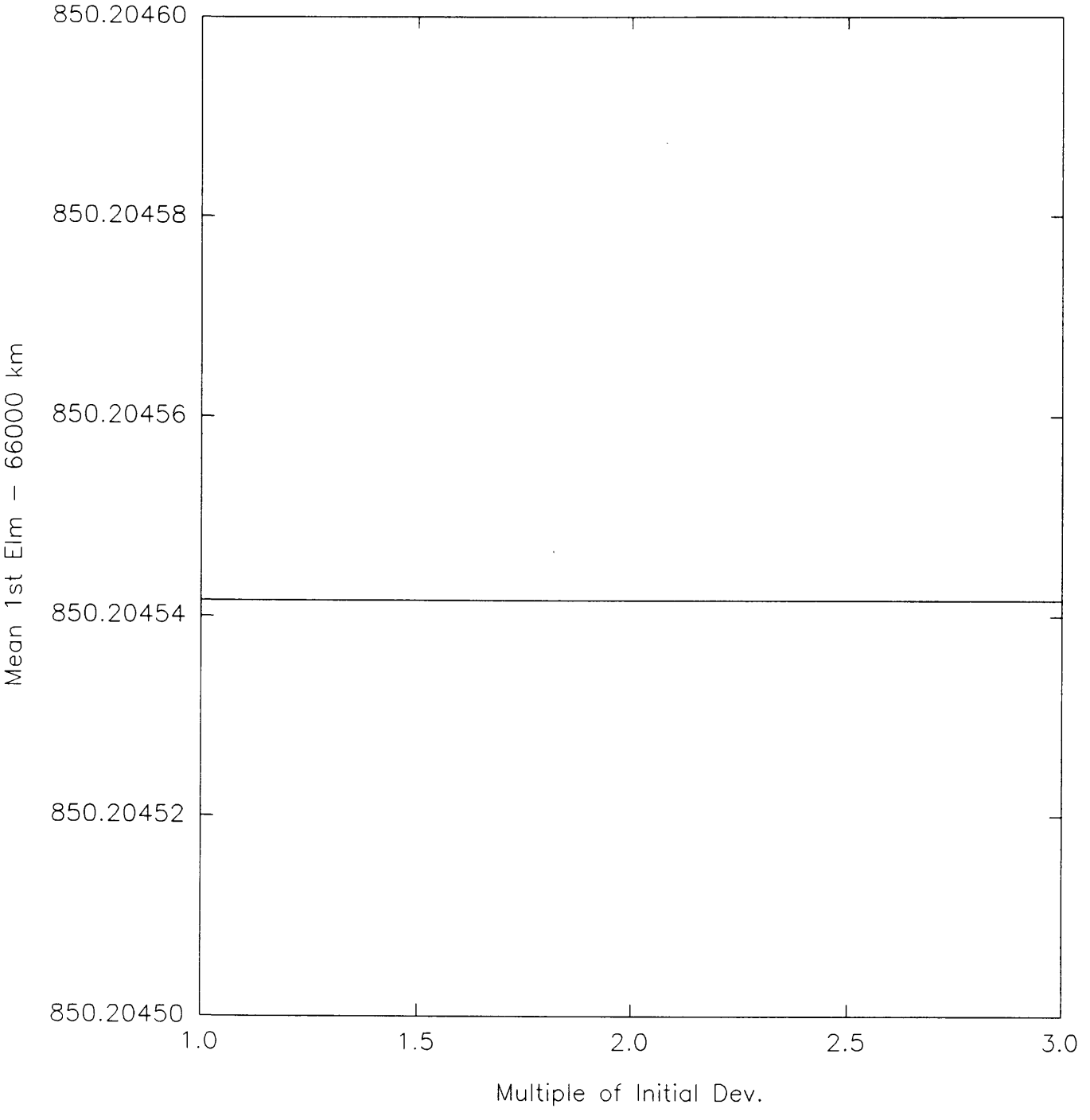

GRAPH 48

Mean 2nd Element vs. Multiple of Initial Deviations
(Gauss-Hermitian Quadrature Algorithm)

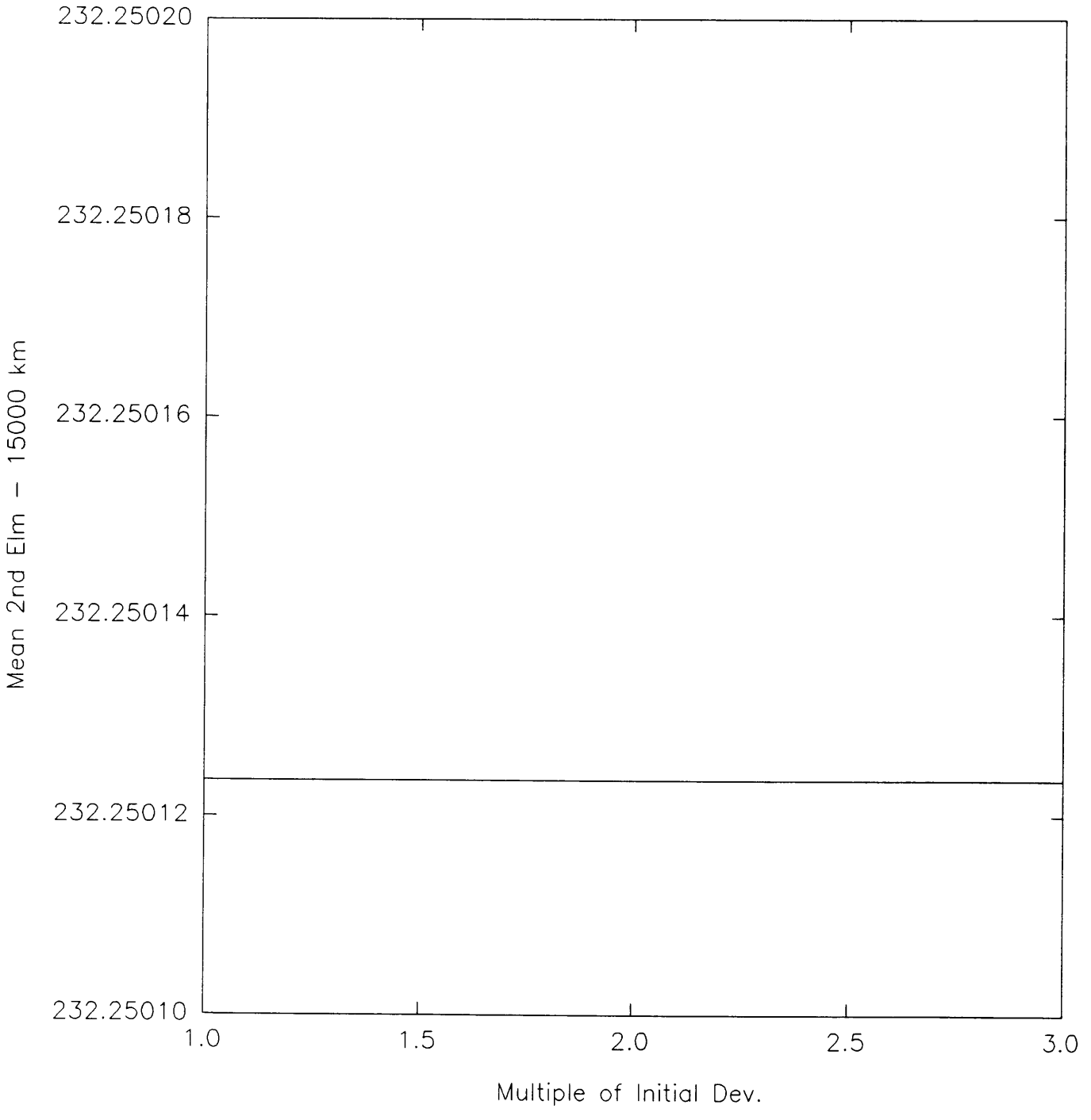

GRAPH 49

Mean 3rd Element vs. Multiple of Initial Deviations

(Gauss-Hermitian Quadrature Algorithm)

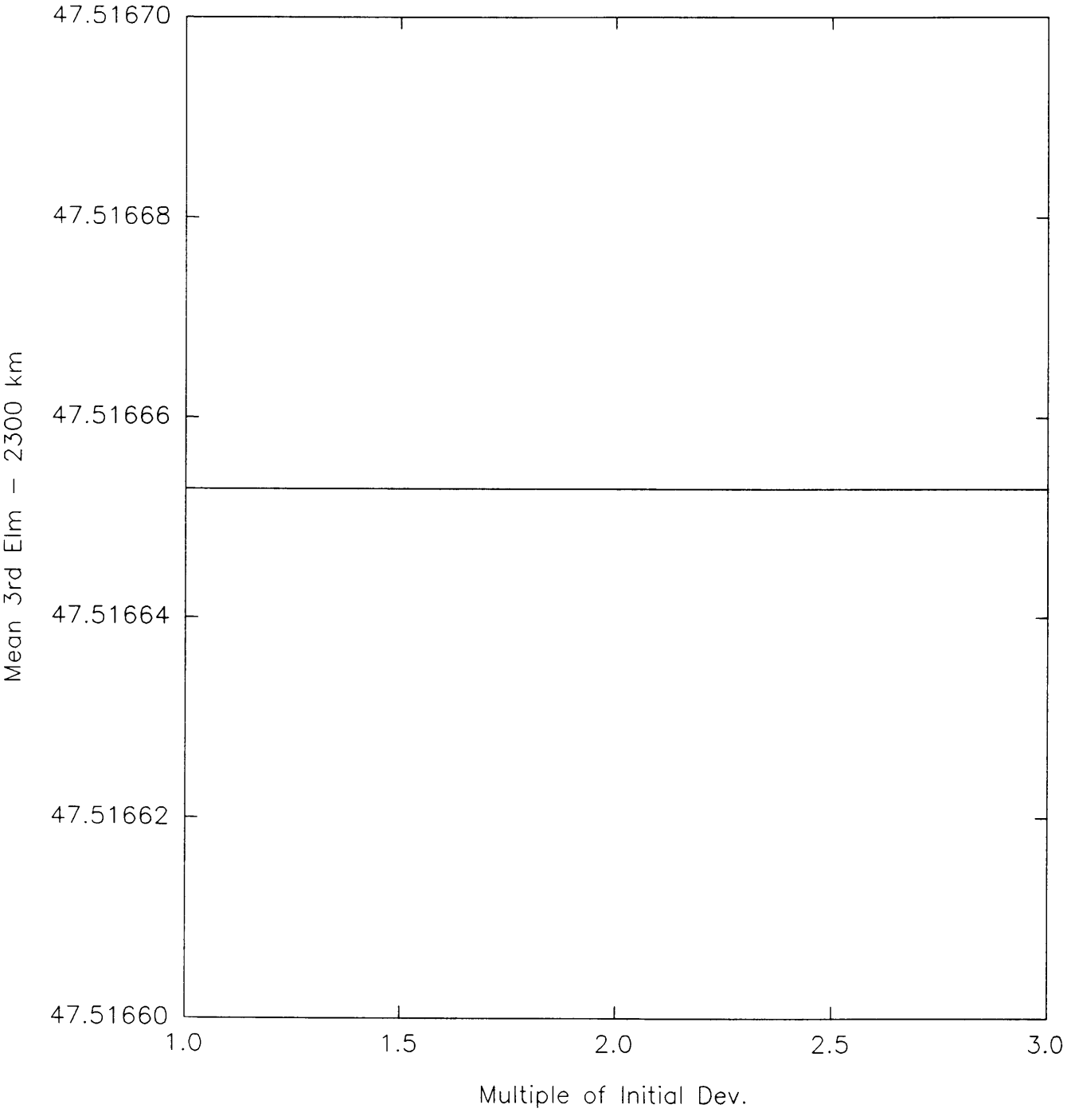

GRAPH 50

Mean 4th Element vs. Multiple of Initial Deviations

(Gauss-Hermitian Quadrature Algorithm)

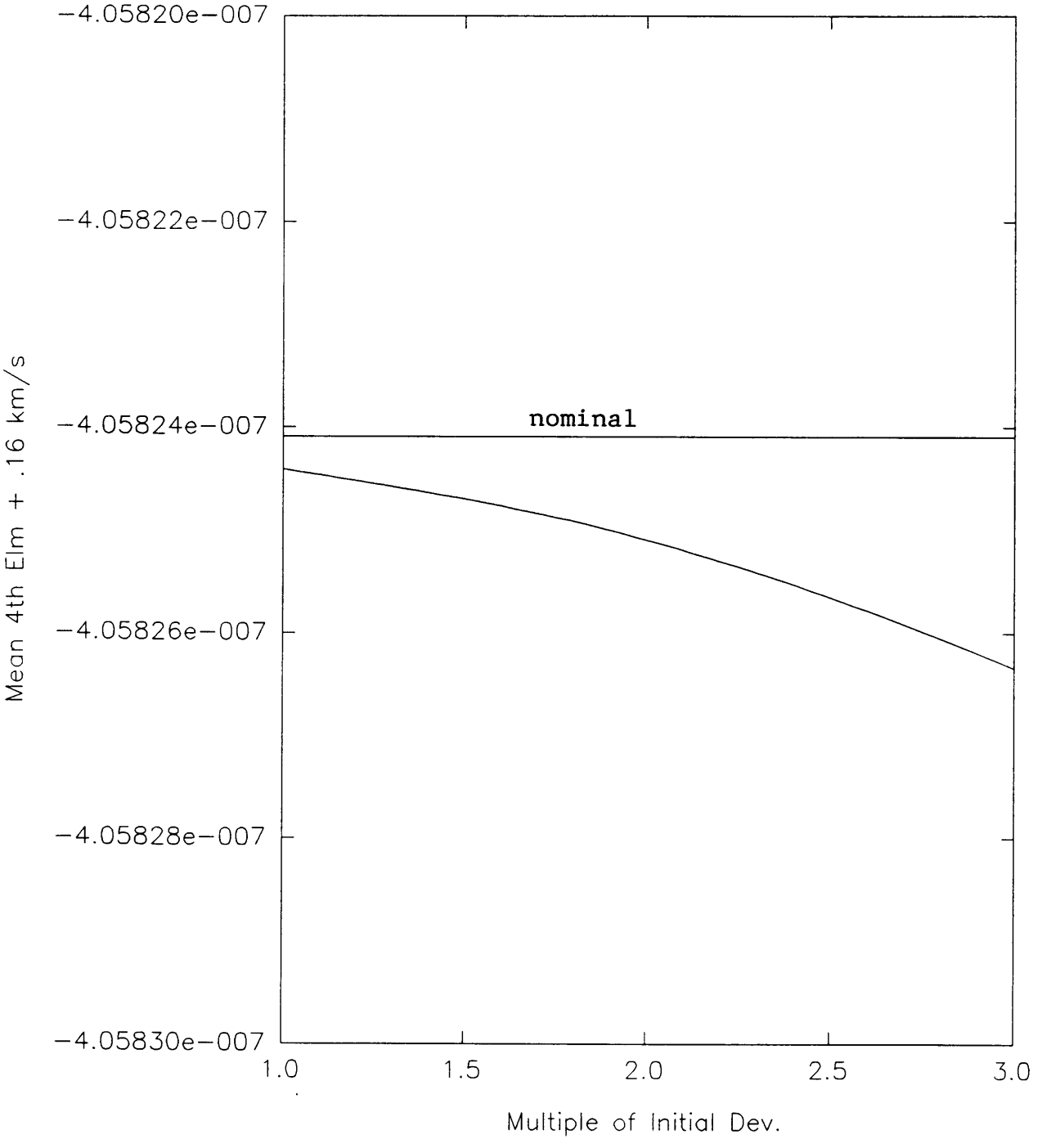

GRAPH 51

Mean 5th Element vs. Multiple of Initial Deviations

(Gauss-Hermitian Quadrature Algorithm)

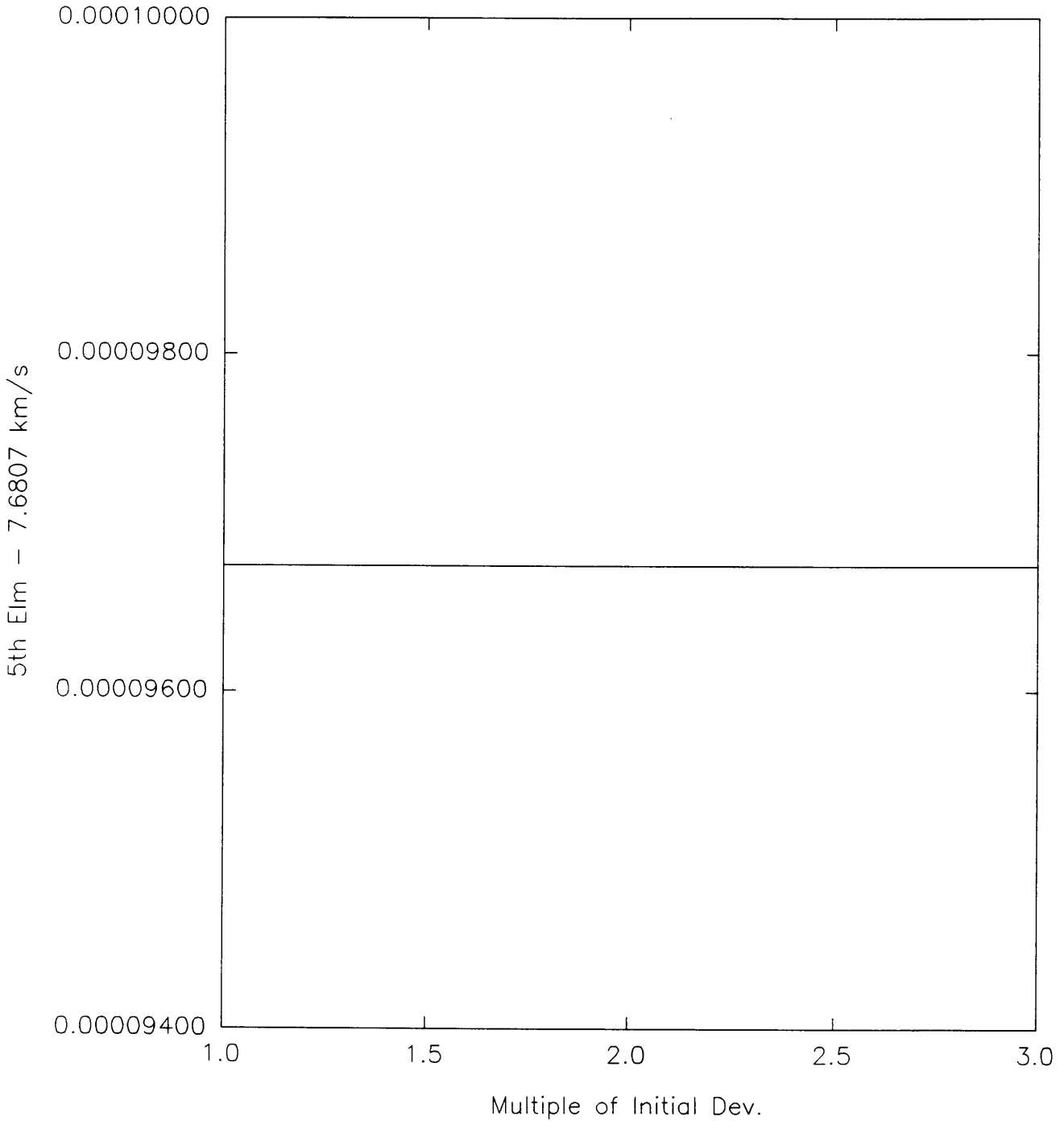

GRAPH 52

Mean 6th Element vs. Multiple of Initial Deviations
(Gauss-Hermitian Quadrature Algorithm)

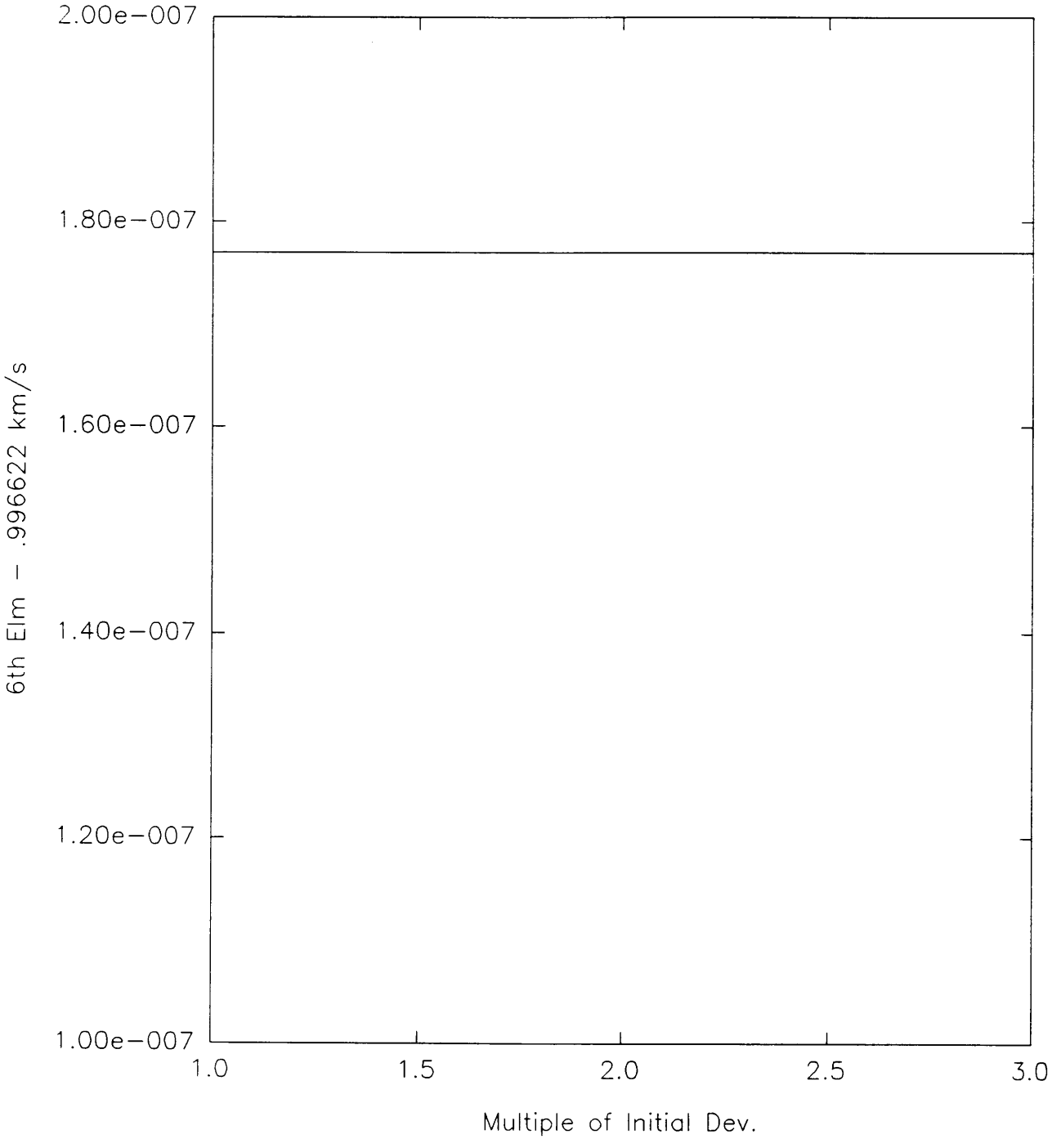

GRAPH 53

1st Element Deviation vs. Multiple of Initial Deviations
(Gauss-Hermitian Quadrature Algorithm)

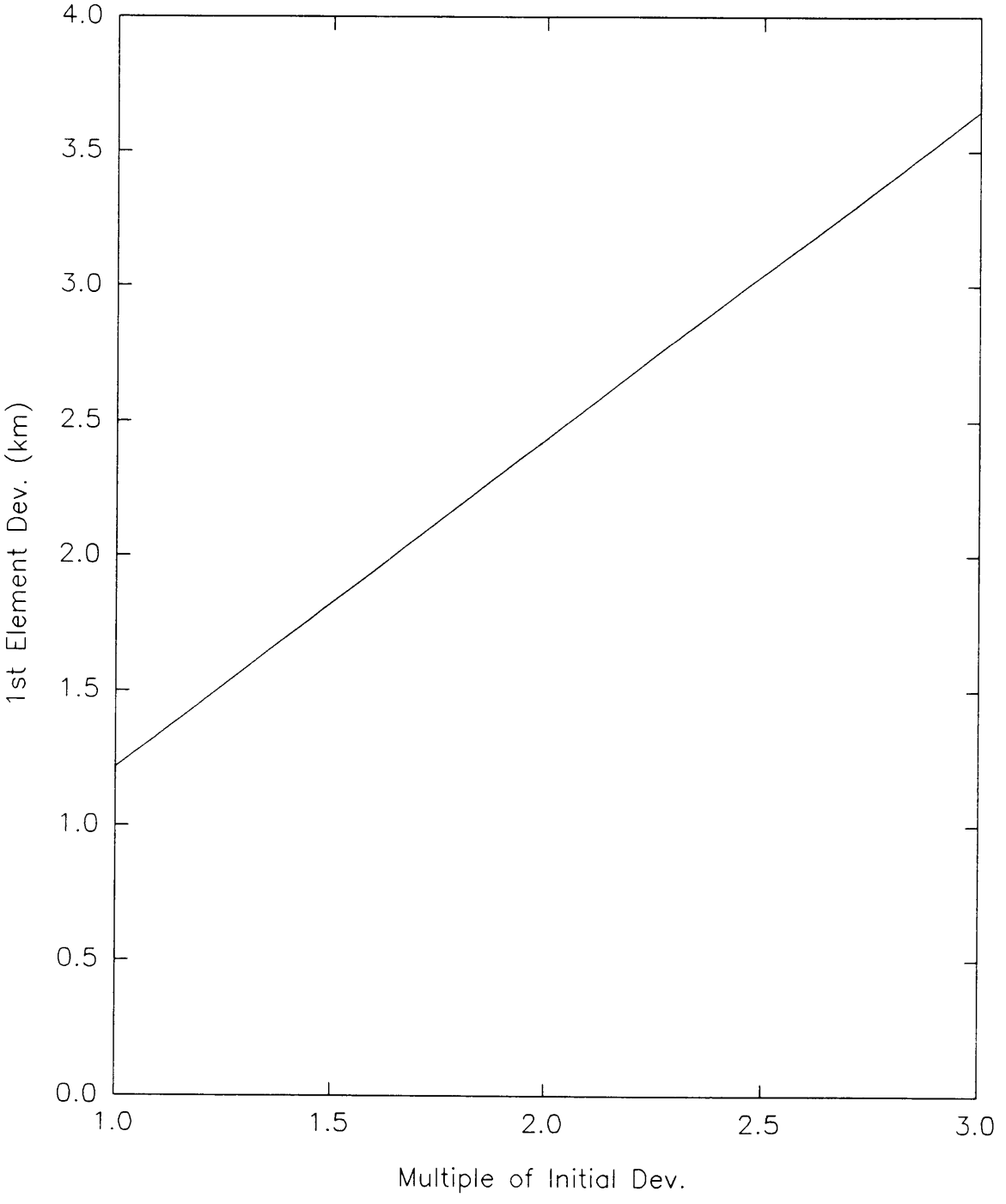

GRAPH 54

2nd Element Deviation vs. Multiple of Initial Deviations
(Gauss-Hermitian Quadrature Algorithm)

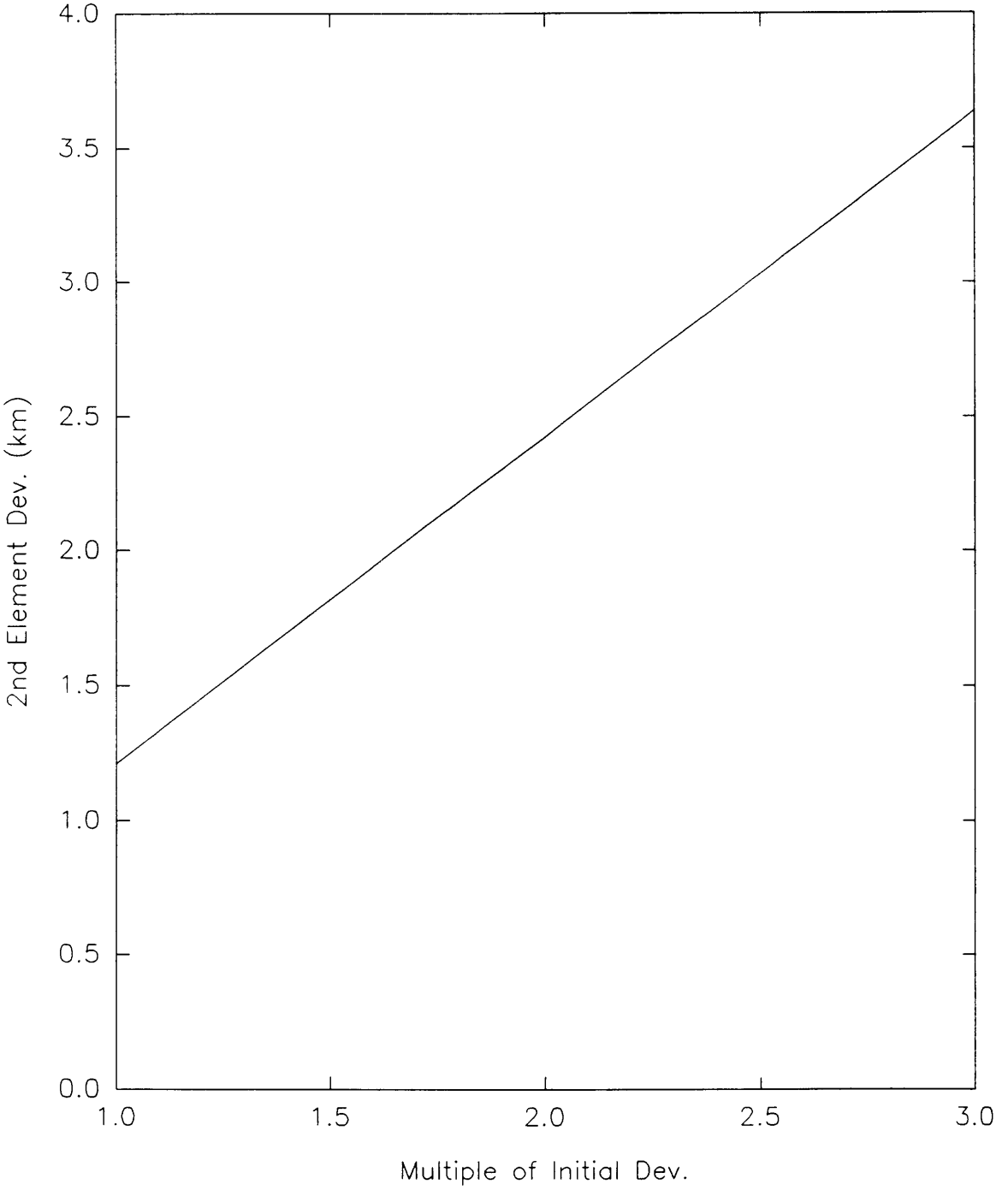

GRAPH 55

3rd Element Deviation vs. Multiple of Initial Deviations
(Gauss-Hermitian Quadrature Algorithm)

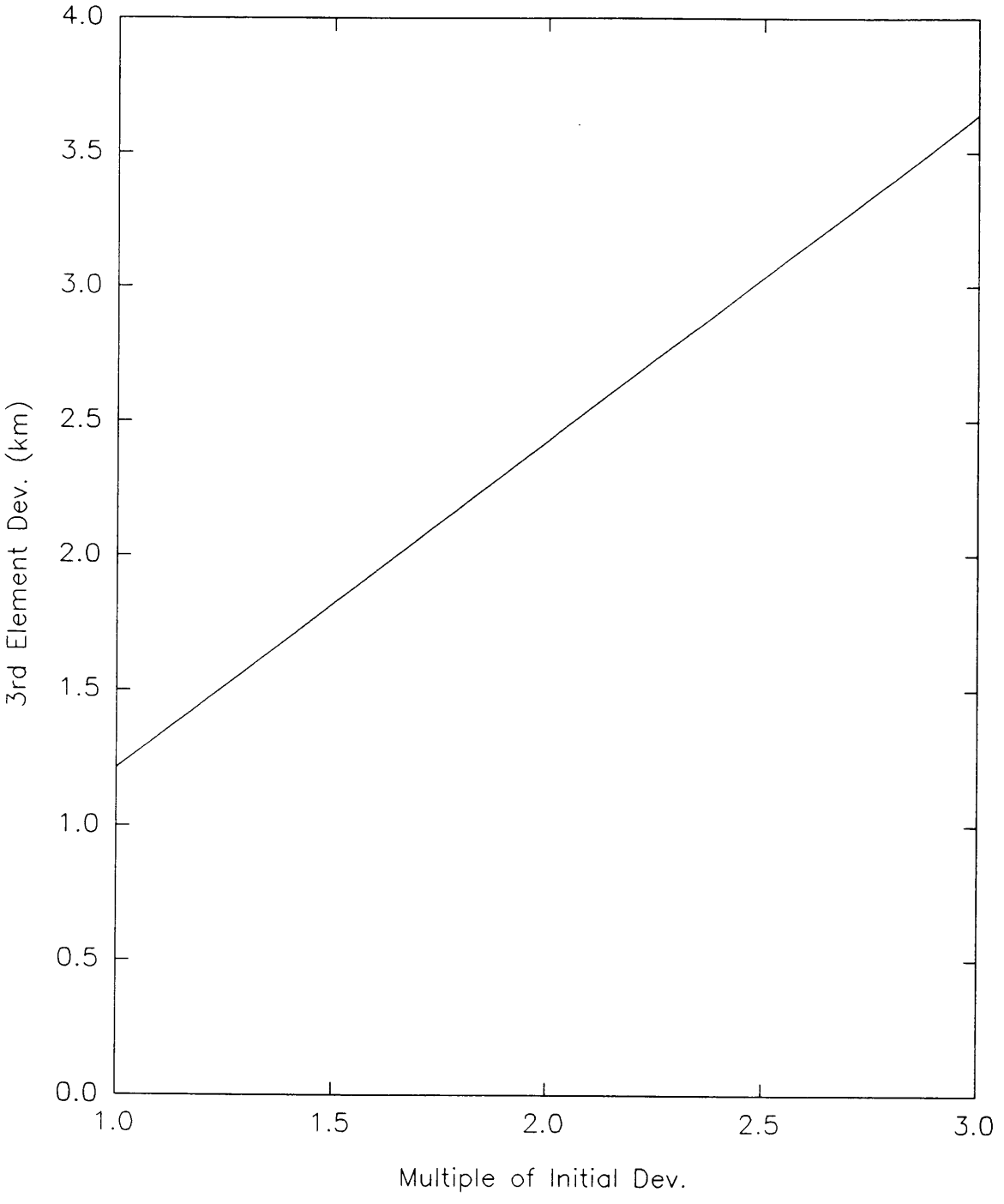

GRAPH 56

4th Element Deviation vs. Multiple of Initial Deviations
(Gauss-Hermitian Quadrature Algorithm)

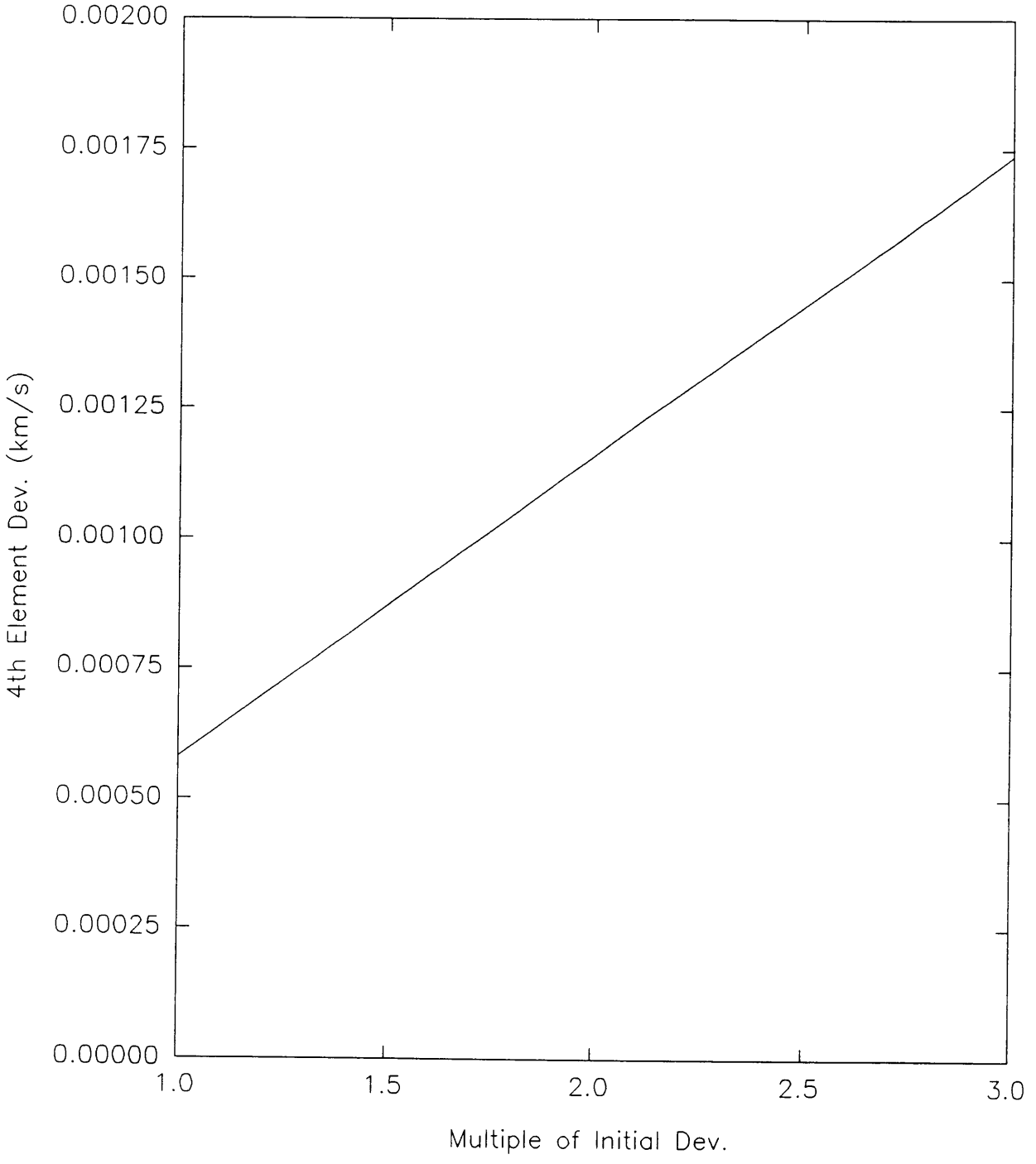

GRAPH 57

5th Element Deviation vs. Multiple of Initial Deviations
(Gauss-Hermitian Quadrature Algorithm)

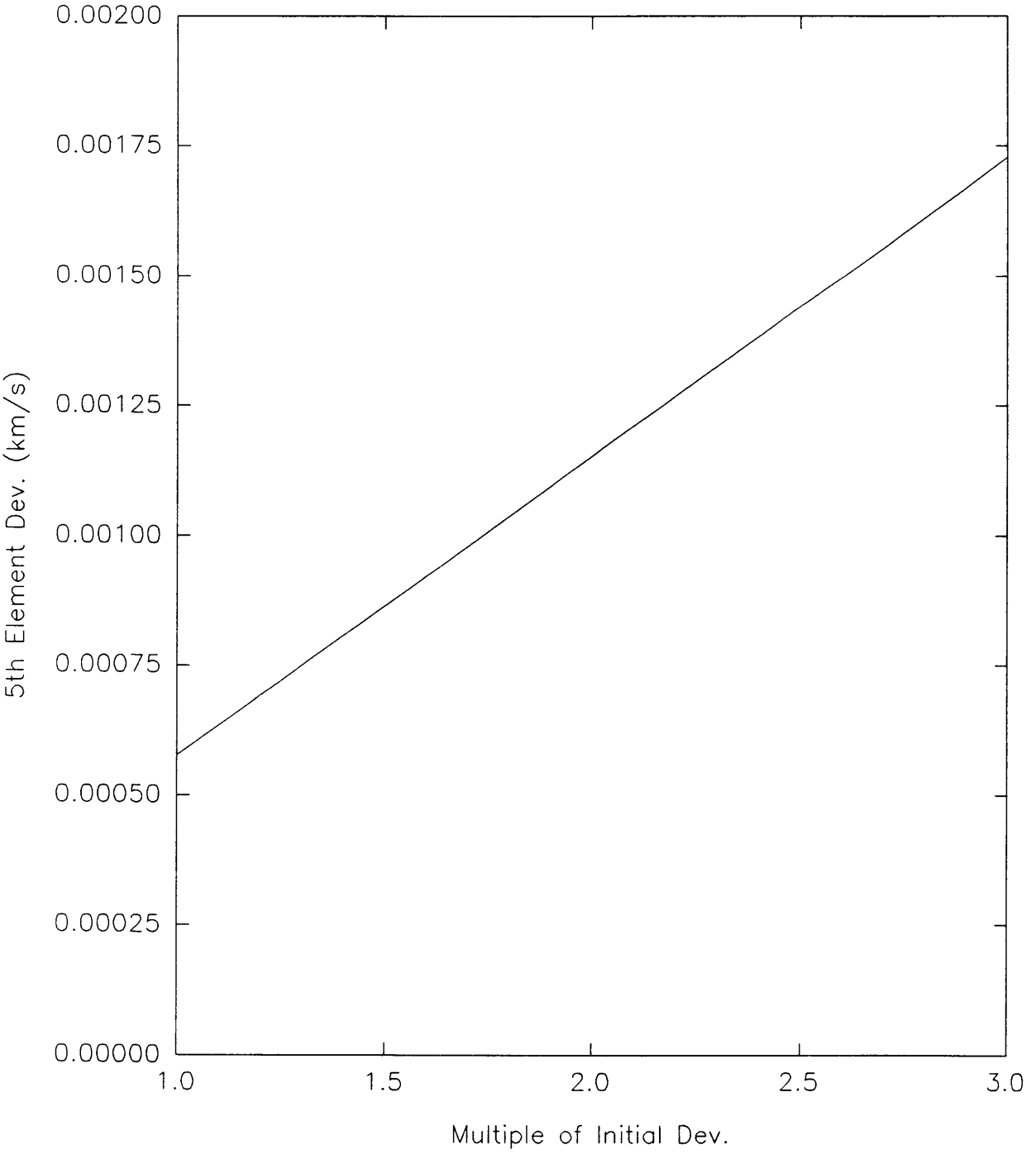

GRAPH 58

6th Element Deviation vs. Multiple of Initial Deviations
(Gauss-Hermitian Quadrature Algorithm)

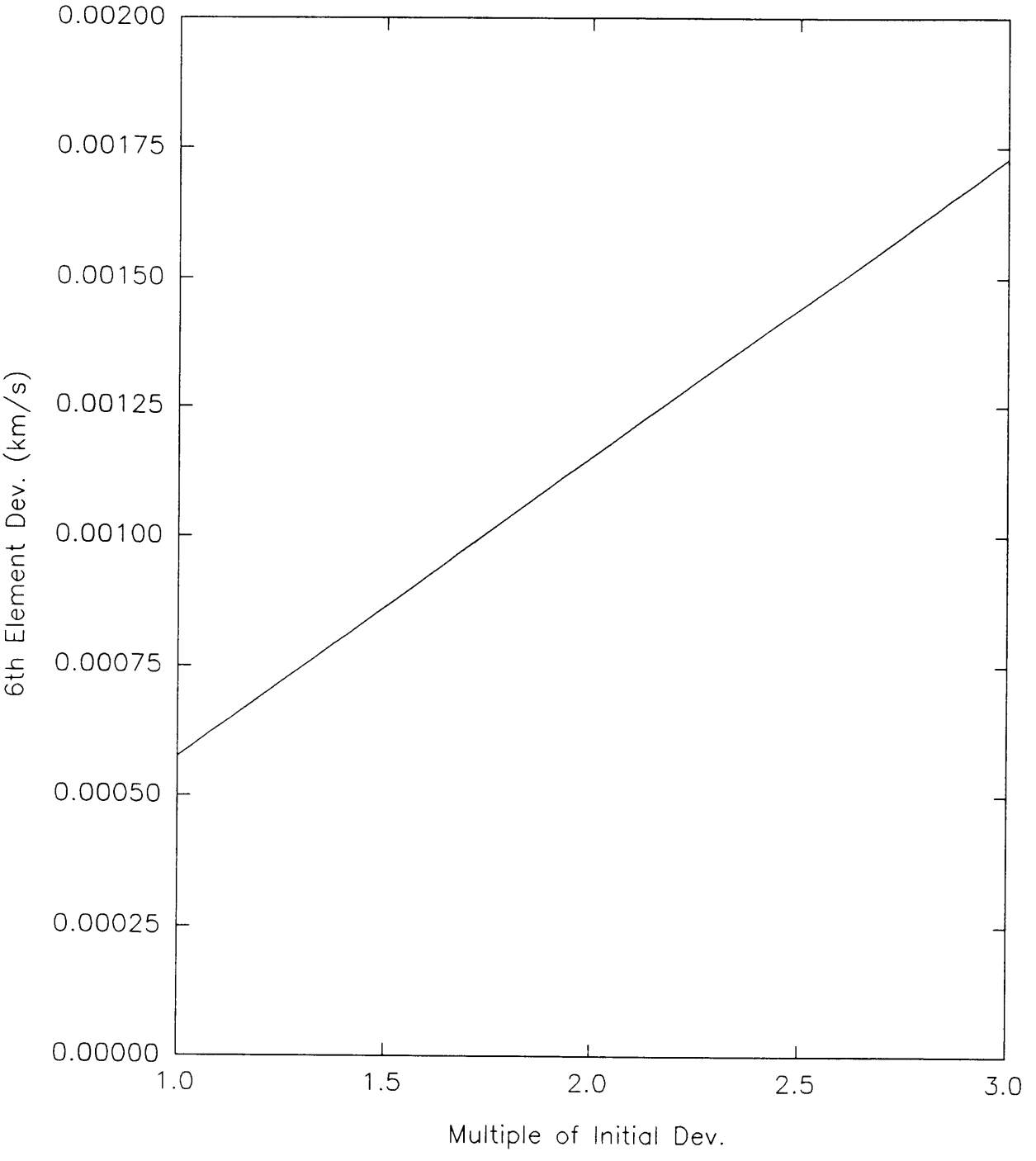

GRAPH 59

1st Element Deviation vs. Multiple of Initial Deviations
(Linear Approximation Algorithm)

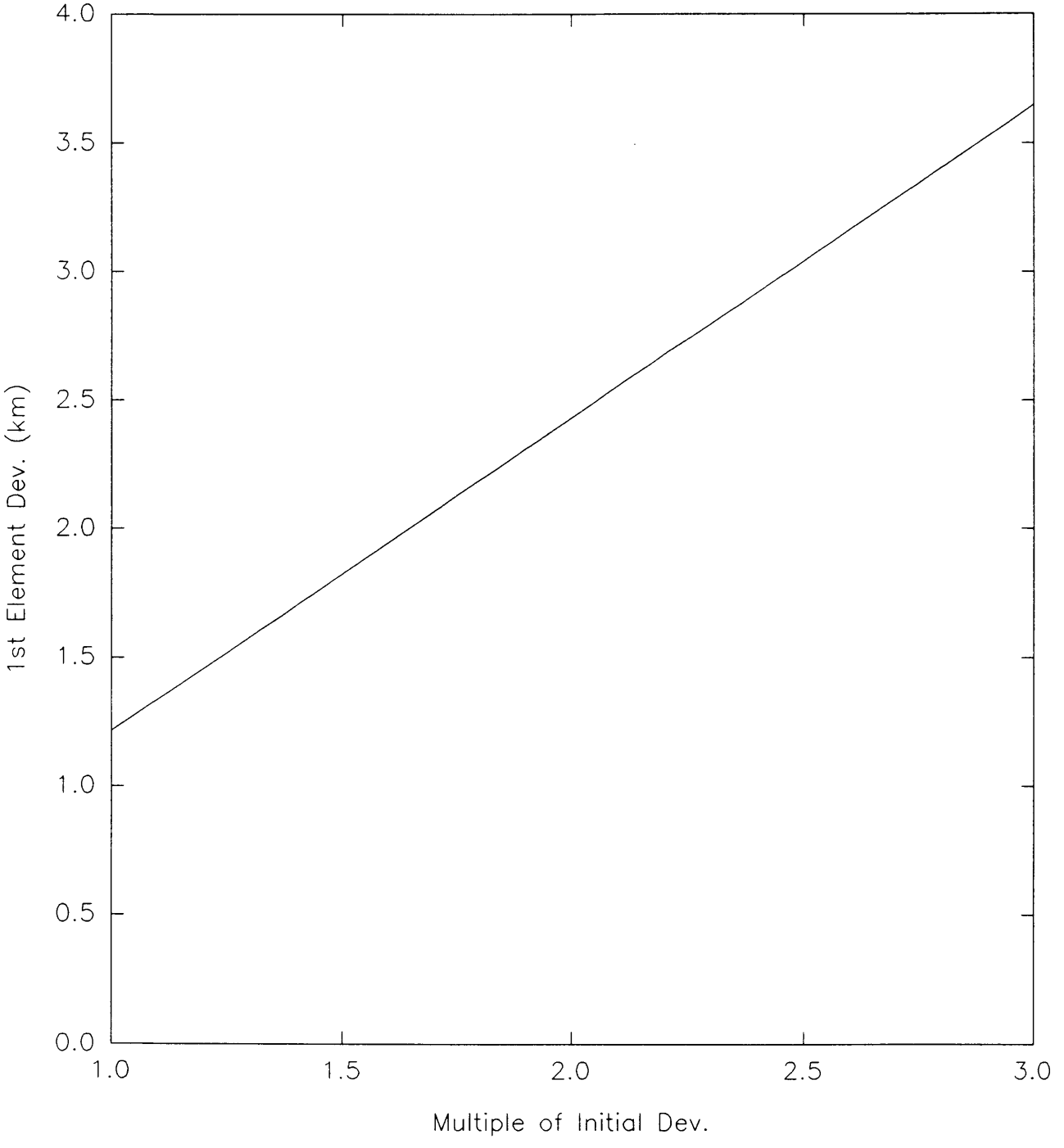

GRAPH 60

2nd Element Deviation vs. Multiple of Initial Deviations
(Linear Approximation Algorithm)

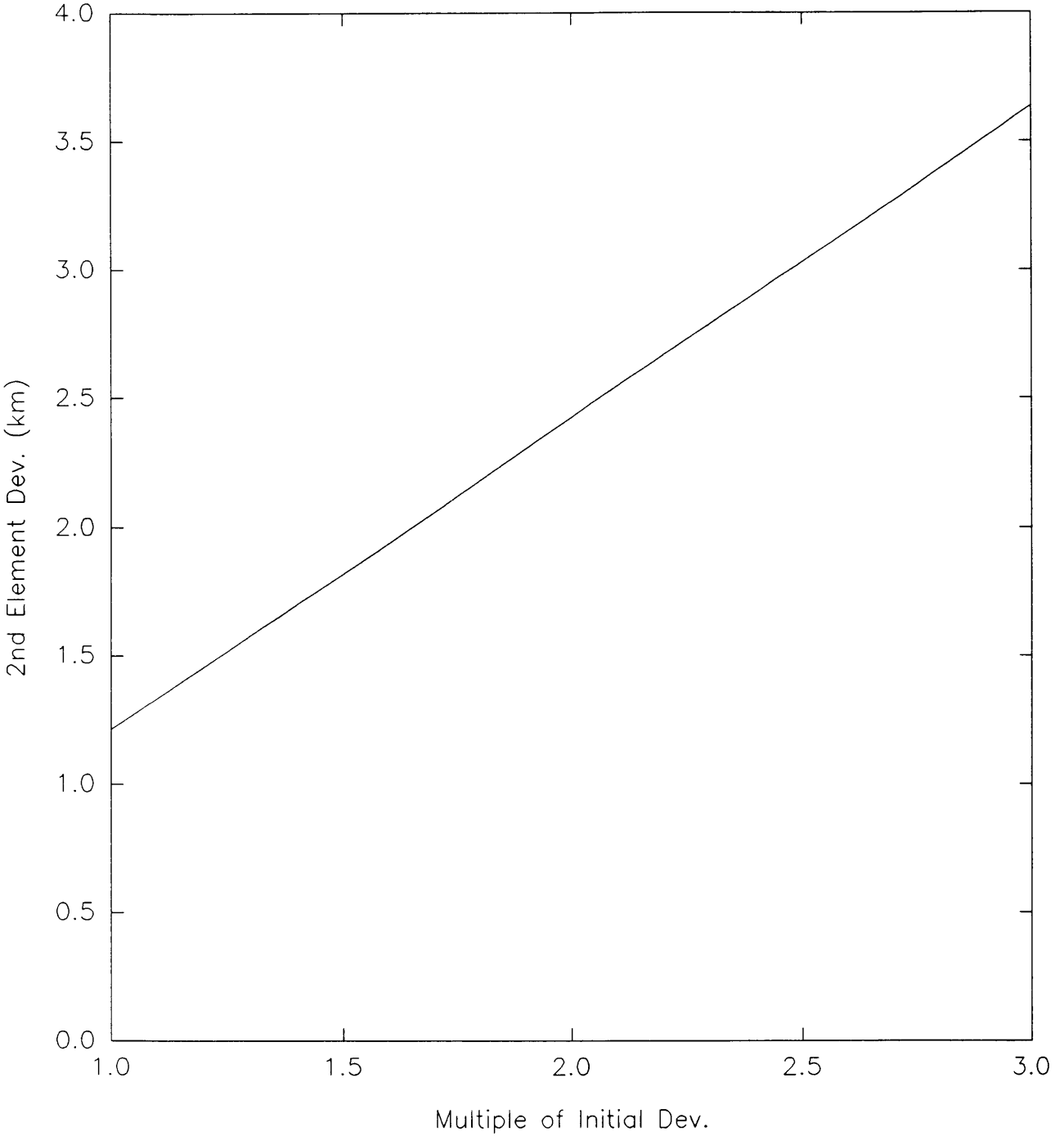

GRAPH 61

3rd Element Deviation vs. Multiple of Initial Deviations
(Linear Approximation Algorithm)

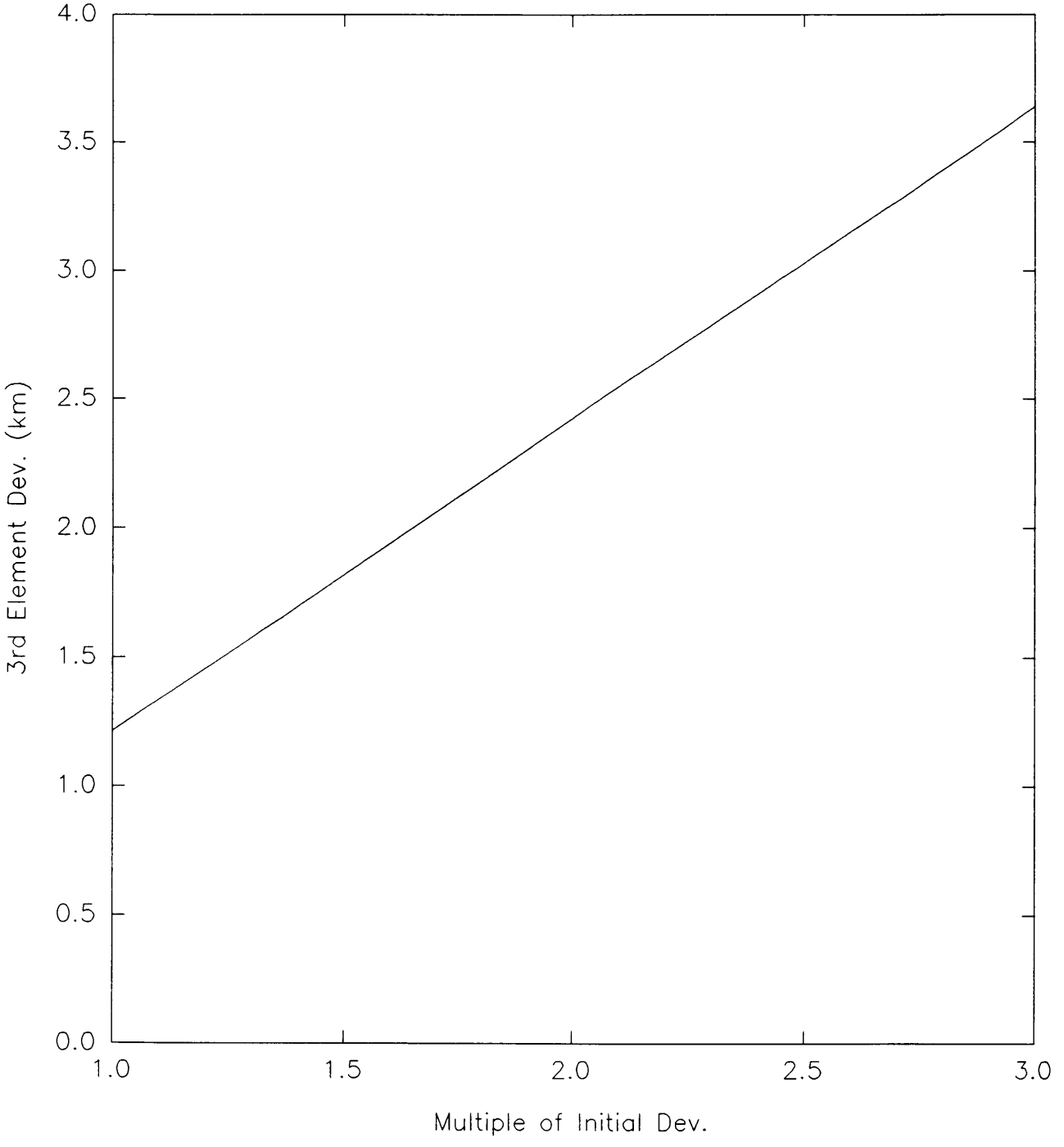

GRAPH 62

4th Element Deviation vs. Multiple of Initial Deviations
(Linear Approximation Algorithm)

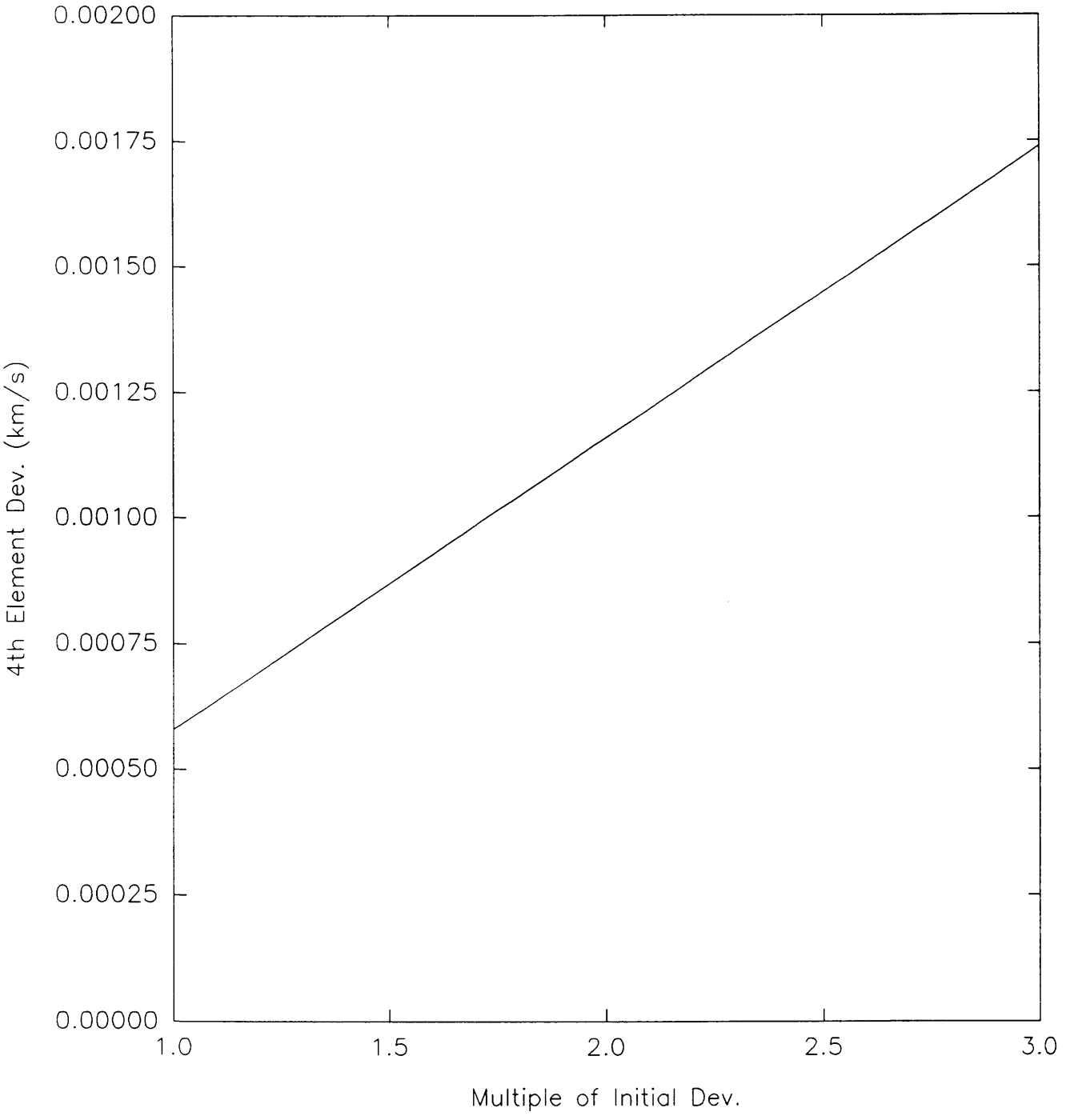

GRAPH 63

5th Element Deviation vs. Multiple of Initial Deviations
(Linear Approximation Algorithm)

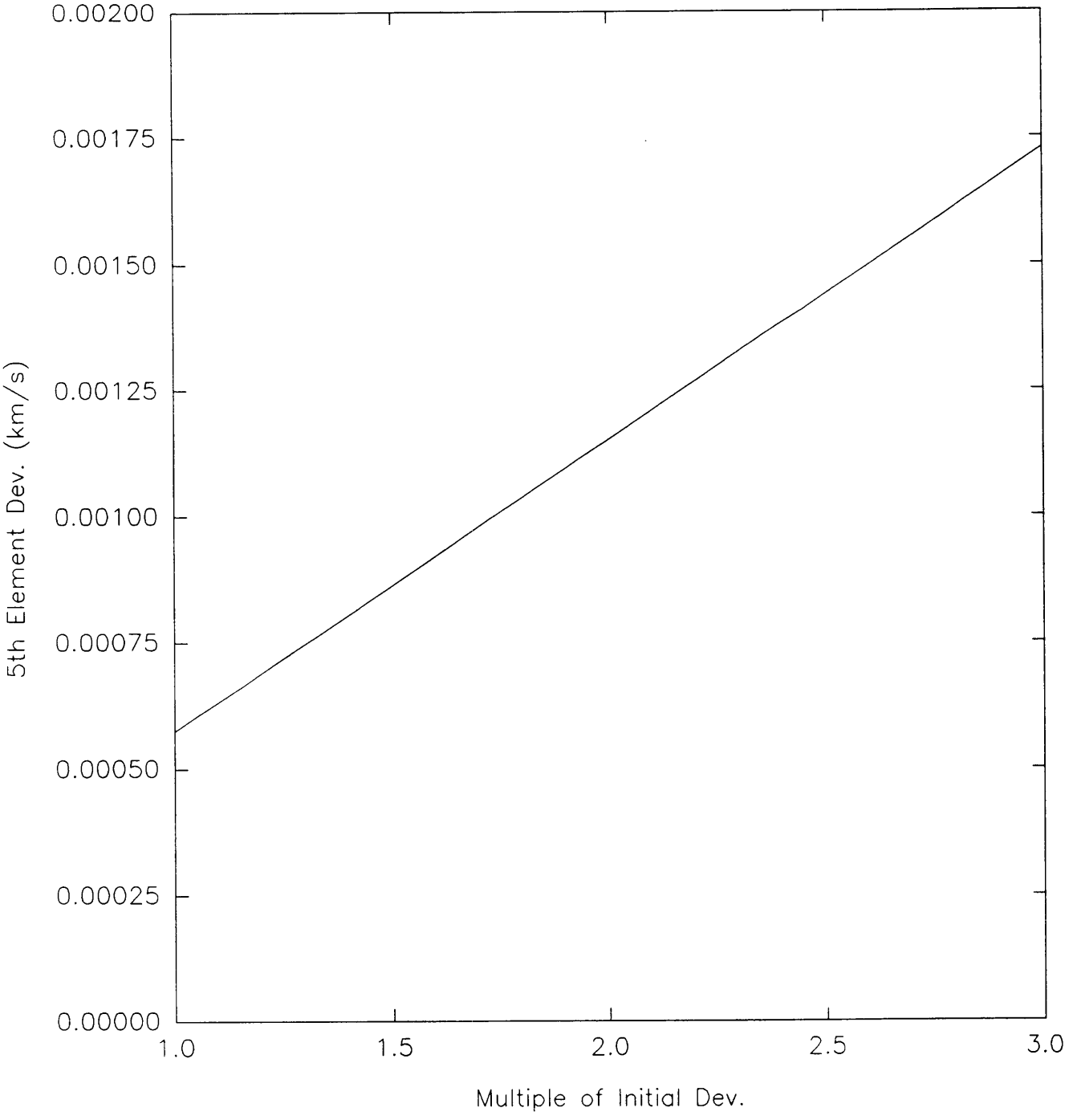

GRAPH 64

6th Element Deviation vs. Multiple of Initial Deviations
(Linear Approximation Algorithm)